LUND UNIVERSITY

Cloud Studies with the Droplet Aerosol Analyzer

Berghof, Maria

2015

Cloud Studies with the Droplet Aerosol Analyzer

Maria I. A. Berghof

Doctoral Thesis
2015

Organization	Document name
LUND UNIVERSITY	DOCTORAL DISSERTATION
	Date of issue
Division of Nuclear Physics	October 1st, 2015
Box 118, SE-22100, Lund	

Author(s)	Sponsoring organization
Maria I. A. Berghof	

Title and subtitle
Cloud Studies with the Droplet Aerosol Analyzer

Abstract

Climate change and atmospheric aerosols are a threat for human health and life. Reducing aerosol emissions would save human lives close to the aerosol source, but could lead to more death due to the implications of a warmer climate. Aerosol particles acting as cloud or ice nuclei can induce a change in cloud properties and thus indirectly induce a change in planetary albedo, which is considered the major reason of changes in planetary albedo associated with global warming.

Because of the complexity of the interaction between aerosols and clouds, uncertainties in cloud parametrization remain the major cause of discrepancies between cloud observations and simulations. Thus, improving the understanding of aerosol-cloud-interactions is one of the keys for reducing uncertainty in the estimate of the total anthropogenic radiative forcing and climate sensitivity. Climate sensitivity is important for quantifying risks and probabilities, and the development of adaption strategies.

The Droplet Aerosol Analyzer (DAA) was developed to study aerosol-cloud interaction and is unique in providing the number and the direct relationship between cloud droplet and residual particle size. For this purpose a more automatic version with better time resolution (10 min) and an improved and more automated inversion algorithm has been developed to better suit the needs of long-term measurements.

Between June and October 2010 aerosol-cloud interaction measurements have been performed at the summit of Mt. Brocken (51.80° N, 10.62° E, 1142 m a.s.l.) in central Germany. For this period the aerosol and cloud properties and the droplet activation regime regarding the ratio between updraft velocity and particle number concentration (w/N_{tot}), have been determined.

The relation between cloud droplet number concentration $N_{\mathrm{d,tot}}$ and total number concentration N_{tot}, updraft velocity w_{pred}, and size distribution shape $R_{0.1\ \mu\mathrm{m}}$ has been determined for three overlapping w/N_{tot}-intervals.

As expected, for increasing w/N_{tot}-ratio (from the transitional regime towards aerosol limited regime) the relative sensitivity of $N_{\mathrm{d,tot}}$ against w_{pred} decreases while the relative sensitivity of $N_{\mathrm{d,tot}}$ against N_{tot} increases. The influence of the size distribution shape $R_{0.1\ \mu\mathrm{m}}$ was examined and the absolute relative sensitivity of $N_{\mathrm{d,tot}}$ against $R_{0.1\ \mu\mathrm{m}}$ was observed to decrease from the transitional towards the aerosol limited regime.

The onset of 'roll-off', where an increase in N_{tot} does not lead to a proportional increase in $N_{\mathrm{d,tot}}$, shifted towards higher total number concentration for increasing w/N_{tot}-ratio.

Key words
Cloud, Aerosol, DAA

Classification system and/or index terms (if any)

Supplementary bibliographical information	Language
	English

ISSN and key title	ISBN
	978-91-7623-484-6 (print)
	978-91-7623-485-3 (pdf)

Recipient´s notes	Number of pages	Price
	Security classification	

Distribution by (name and address)

Signature _____ *M. Berghof* _____   Date _____ 01.10.2015 _____

THESIS FOR THE DEGREE OF DOCTOR OF PHILOSOPHY

CLOUD STUDIES WITH THE DROPLET AEROSOL ANALYZER

MARIA I. A. BERGHOF

DIVISION OF NUCLEAR PHYSICS
DEPARTMENT OF PHYSICS
LUND UNIVERSITY
SWEDEN

FACULTY OPPONENT: ANNELE VIRTANEN
UNIVERSITY OF EASTERN FINLAND
DEPARTMENT OF APPLIED PHYSICS
KUOPIO, FINLAND

DOCTORAL THESIS

WHICH, BY DUE PERMISSION OF THE FACULTY OF ENGINEERING AT LUND UNIVERSITY, WILL BE PUBLICLY DEFENDED ON FRIDAY, NOVEMBER 13TH, 2015, AT 9:00 IN RYDBERG HALL AT THE DEPARTMENT OF PHYSICS, SÖLVEGATAN 14C, LUND.

Cloud Studies with the Droplet Aerosol Analyzer
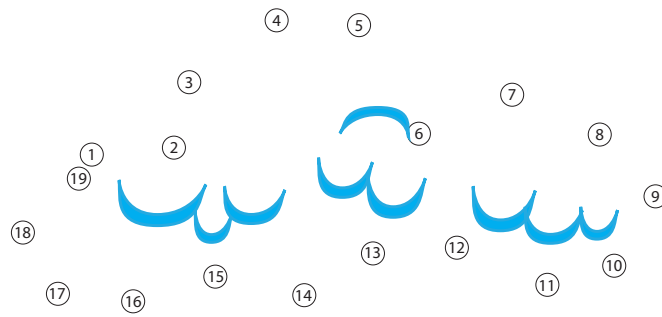Thesis for the Degree of Doctor of Philosophy in Engineering

Typeset by the author using LaTeX 2_ε, version 2015/01/01

④ ⑤

③

⑦

⑥

② ⑧

① ⑨

⑲

⑱

⑬ ⑫

⑰ ⑯ ⑮ ⑭ ⑪ ⑩

Meinen lieben Großeltern
Eva und Friedrich Beleites

Abstract

Climate change and atmospheric aerosols are a threat for human health and life. Reducing aerosol emissions would save human lives close to the aerosol source, but could lead to more death due to the implications of a warmer climate. Aerosol particles acting as cloud or ice nuclei can induce a change in cloud properties and thus indirectly induce a change in planetary albedo, which is considered the major reason of changes in planetary albedo associated with global warming.

Because of the complexity of the interaction between aerosols and clouds, uncertainties in cloud parametrization remain the major cause of discrepancies between cloud observations and simulations. Thus, improving the understanding of aerosol-cloud-interactions is one of the keys for reducing uncertainty in the estimate of the total anthropogenic radiative forcing and climate sensitivity. Climate sensitivity is important for quantifying risks and probabilities, and the development of adaption strategies.

The Droplet Aerosol Analyzer (DAA) was developed to study aerosol-cloud interaction and is unique in providing the number and the direct relationship between cloud droplet and residual particle size. For this purpose a more automatic version with better time resolution (10 min) and an improved and more automated inversion algorithm has been developed to better suit the needs of long-term measurements.

Between June and October 2010 aerosol-cloud interaction measurements have been performed at the summit of Mt. Brocken ($51.80°$ N, $10.62°$ E, 1142 m a.s.l.) in central Germany. For this period the aerosol and cloud properties and the droplet activation regime regarding the ratio between updraft velocity and particle number concentration (w/N_{tot}), have been determined.

The relation between cloud droplet number concentration $N_{\text{d,tot}}$ and total number concentration N_{tot}, updraft velocity w_{pred}, and size distribution shape $R_{0.1\ \mu\text{m}}$ has been determined for three overlapping w/N_{tot}-intervals.

As expected, for increasing w/N_{tot}-ratio (from the transitional regime towards aerosol limited regime) the relative sensitivity of $N_{\text{d,tot}}$ against w decreases while the relative sensitivity of $N_{\text{d,tot}}$ against N_{tot} increases. The influence of the size distribution shape $R_{0.1\ \mu\text{m}}$ was examined and the absolute relative sensitivity of $N_{\text{d,tot}}$ against $R_{0.1\ \mu\text{m}}$ was observed to decrease from the transitional towards the aerosol limited regime.

The onset of 'roll-off', where an increase in N_{tot} does not lead to a proportional increase in $N_{\text{d,tot}}$, shifted towards higher total number concentration for increasing w/N_{tot}-ratio.

Populärvetenskaplig sammanfattning

Det är väldigt tyst. Vägen framför är nästan osynligt. Du befinner dig i mitten av ett forskningsområde - ett moln. Redan som små barn vet vi hur ett moln ser ut. Men vad vet vi egentligen om moln? På Lunds Universitet forskar man sedan 1990-talet om moln. Det finns fortfarande mycket att forska om hur vi människor påverkar moln.

Vi alla känner igen situationen: trots att vädertjänsten har lovat solsken börjar det att ösregna. Moln påverkar oss nästan varje dag men vi vet ändå ganska lite om dem. Därför är det svårt att göra en säker prognos om molntäcket och regn för i morgon.

Moln påverkar vårt klimat

Förutom väder påverkar moln också jordens klimat. De kan till exempel kyla jordytan genom att spegla tillbaka solstrålning ut i rymden. Men de kan också skydda jordytan från att kylas ner genom att agera som ett täcke på natten. Satellitmätningar visar att omkring sextio procent av jorden är täckt av moln. Skulle molnens egenskaper och mängd ändras kommer det att påverka vårt klimat. Med hjälp av klimatmodeller kan man uppskatta hur mycket moln kan kyla eller värma vårt klimat. Men det finns stora osäkerheter i den teoretiska beskrivningen av moln i väder- och klimatmodeller. För oss är säkra prognoser över framtidens klimatförändringar viktiga för att kunna agera på rätt sätt.

Klimatförändringar påverkar moln

FN:s klimatpanel (Intergovernmental Panel on Climate Change, IPCC) ska uppskatta och bedöma riskerna i förändringar av vårt klimat. Målet är att hitta strategier för att förebygga och anpassa oss, deras sammanfattning kommer ut i en stor rapport. Den senaste rapporten från IPCC 2014 beskriver att olika klimatmodeller skiljer sig mycket i klimatkänslighet. Klimatkänslighet är ett mått på hur mycket jordens medeltemperatur skulle öka vid en fördubbling av växthusgasen koldioxid.

Raporten visar att dels har klimatmodellerna för liten uplösning för att kunna beskriva moln. Det saknas också kunskap om hur molns egenskaper motverkar eller förstärker temperaturförändringar. Det kallas molns återkopplingseffekt. Till exempel medför en ökning av jordens medeltemperatur att mer vatten förångas, vilket i sin tur kan leda till ökad molnbildning. Å andra sidan behövs i den varmare luften en större mängd vattenånga för att bilda ett moln, vilket kan leda till en minskad molnbildning.

Skulle det blir fler moln, så skulle mer solstrålning blir reflekterad och det skulle blir kallare igen. Då sulle molnen på så vis ha en negativ återkopplingsef-

fekt, de kan altså motverka en temperaturökning, vilket är positivt för oss. Men det kan vara åt andra hållet också, med färre moln som leder till temperaturökning och positiv återkopplingseffekt. För att kunna agera rätt är det viktig att veta hur mycket och på vilket sätt vi mäniskor påverkar jordens klimat.

Partiklar och molndroppar

Det finns fortfarande en stor okunskap om hur ett enskilt moln bildas och hur vi människor påverkar molns mikrostruktur.

Ett moln består till stora delar av vatten i form av några mikrometer stora molndroppar. Sådana små droppar kan vi bara se när de är väldigt många, som i ett moln. Förutom mycket vatten består en molndroppe av en några hundra till några tiotals gånger mindre partikel. Partiklar i varierande storlek finns överallt i luften. Till exempel bildas stora saltpartiklar när vågor bryts och mindre partiklar när det brinner och ryker. Partiklarnas storlek, antal och sammansättning har stor effekt på hur molndroppar bildas och därmed på molnets egenskaper. Vid berg bildas ofta moln eftersom luften tvingas att stiga upp och då stiger också den relativa luftfuktigheten (RH). RH är ett mått på hur mycket av den maximalt möjliga mängden vattenånga luften innehåller och räknas i procent. Är RH större än 100 procent är det mycket sannolikt att vattenånga bildar imma på en yta, på samma sätt som när vattenånga kondenserar på badrumsspegeln efter vi har duschat länge.

Teorin om molns beskrevs redan 1921

Vanligtvis finns det inga badrumsspeglar i atmosfären, men ofta finns det partiklar som kan agera på samma sätt. När vattenånga kondenserar på partiklarna växer de sig större. Hur mycket de växer beror på deras storlek och kemiska sammansättning. Detta beskrevs av den svenska meteorologen Hilding Köhler 1921.

Köhlerteorin förklarar till exempel att molndroppar växer när RH stiger och de inte krymper när RH sjunker när de väl blivit tillräckligt stora. Men Köhlerteorin beskriver molndroppar i jämviktsläge, vilket de inte är i verkligheten. Oftast är det mycket rörelser i luften, både vindhastighet och rikning varierar och därmed också partiklarnas storlek, antal och sammansättning, det råder inget jämviktsläge.

Att mäta direkt inuti ett moln

Att partiklarna spelar stor roll vid bildandet av moln är klarlagt. Men för att få veta i detalj hur de påverkar krävs det mer forskning. Att studera hur partiklar påverkar molnbildning i realiteten kan man göra på olika sätt.

1996 utvecklades ett instrument på Lunds Universitet speciellt för att studera moln och dimma. Instrumentet heter DAA (Droplet Aerosol Analyzer) och mäter på moln genom att suga in och torka ut dropparna.

2010 åkte molnforskarna med DAA:n till ett ställe där det finns många moln, till Mt. Brocken, ett berg som ligger i Harz-region i centrala Tyskland.

Mätmetoden kan beskrivas i fyra steg. Först suger instrumentet in luft som inehåller molndroppar men också partiklar. Sen mäter instrumentet droparnas storlek som dom har haft i molnet, dem kan vara mellan tjugo mikrometer och några tiotals nanometer. För att veta vad molndroppar består av torkar man bort allt vatten och mäter strorleken på dem partiklar som molndropparna har bildats av. I sista steget räknar man antalet av molndroppar eller partiklar.

Vi männikor påverkar moln

Vi kan altså mäta vilka partiklar som har deltagit i molnbildning genom att växa sig till molndroppar och vilka som inte har gjort det. Vi kan också undersöka hur mycket vi människor påverkar detta genom att jämföra luft som kommer från olika ställen. Från havet kommer det oftast ren luft som inhåller få partiklar. Där det finns mycket industrier är luften mindre ren och innehåller fler partiklar.

Eftersom partiklar påverkar molnbildning blir det väldigt intressant att studera molnbildning beroende på partiklarnas egenskaper och från vilket håll luften kommer.

Denna avhandling presenterar resultat från molmätningarna på Mt. Brocken. Här presenteras matamatiska sammanband, så kallade parametriseringar, som beskriver aerosol partiklarnas effekt på molndroppsbildningen. Det har visat sig, att det finns olika lägen där upvindhastigheten påverkar molnbildning mer eller mindre. För att kunna jämföra molnmätningarna och olika parametriseringar bättre, så behöver man känna till i vilket läge molnet befinner sig.

I framtiden kan molnmätningar på så vis förbättra den teoretiska beskrivningen av molnbildning och ge en säkrare prognos av framtidens klimatförändringar. Eller ge en säkrare regnprognos och på så vis påverka vardagslivet väldigt mycket.

List of Publications

This thesis is based on the work presented in the following publications and submitted manuscripts. The papers are referenced in the text using the indicated labels.

PAPER I: **Continuous stand-alone controllable aerosol/cloud droplet dryer for atmospheric sampling**
Atmospheric Measurement Techniques **6** *(2013) 349–357.*
S. Sjogren, G. P. Frank, M. I. A. Berghof and B. G. Martinsson

I assisted with the data analysis of the longtime performance of the dryer, I contributed to the discussion of the manuscript.

PAPER II: **Inversion of droplet aerosol analyzer data for long-term aerosol-cloud interaction measurements**
Atmospheric Measurement Techniques **7** *(2014) 349–357.*
M. I. A. Berghof, G. P. Frank, S. Sjogren and B. G. Martinsson

I translated the inversion routine from Quattro Pro into Matlab and developed it further, in order to meet the requirements of the improved version of the Droplet Aersol Analyser (DAA). I wrote the paper with comments of the co-authors.

PAPER III: **Development of the Droplet Aerosol Analyser for long-term unattended in-cloud measurements of aerosol-cloud interactions**
Unpublished Manuscript
G. P. Frank, M. I. A. Berghof, S. Sjogren and B. G. Martinsson

I performed the data analysis and evaluation of the calibration of major parts of the DAA (DMA, CPC, High Voltage Power supply, Bipolar charger, temperature and pressure sensors, mass flow meters, differential pressure meters). I wrote minor parts of the paper.

PAPER IV: **DAA Field Study on Cloud Droplet Activation Related to Aerosol Updraft Regimes**
Unpublished Manuscript
M. I. A. Berghof, B. Svenningsson, G. P. Frank, S. Sjogren and

B. G. Martinsson

I assisted in the realization of the experiment. I developed a method to estimate the change in the calibration curve of the unipolar charger due to the aging of the radioactive source. I performed the data analysis and evaluation of the DAA data and wrote the article with comments of the co-authors.

Related publications not included in this thesis

Size-resolved measurement of the mixing state of soot in the megacity Beijing, China: diurnal cycle, aging and parameterization.
Atmospheric Chemistry and Physics **12(10)** *(2012) 4477-4491.*
Y. F.Cheng, H. Su, D. Rose, S. S. Gunthe, M. I. A. Berghof, B. Wehner, P. Achtert et al.

Cloud condensation nuclei in polluted air and biomass burning smoke near the mega-city Guangzhou, China–Part 2: Size-resolved aerosol chemical composition, diurnal cycles, and externally mixed weakly CCN-active soot particles.
Atmospheric Chemistry and Physics **11(6)** *(2011) 2817-2836.*
Rose, D., S. S. Gunthe, H. Su, R. M. Garland, H. Yang, M. I. A. Berghof, Y. F. Cheng et al.

Contents

Contents

Chapter 1

Introduction

"Würdest Du mir bitte sagen, welchen Weg ich einschlagen muss?"
"Das hängt in beärächtlichem Maße davon ab, wohin du gehen willst",
    antwortete die Katze.
"Oh, das ist mir ziemlich gleichgültig", sagte Alice.
"Dann ist es auch einerlei, welchen Weg du einschlägst", meinte die Katze.
"Hauptsache, ich komme irgendwohin", ergänzte sich Alice.
"Das wirst du sicher, wenn du lange genug gehst", sagte die Katze.
                                                            Lewis Carroll

1.1 The Earth's Climate and the Human Influence

The Earth's energy balance (see Fig. 1.1) accounts for the incoming radiation
from the sun and outgoing radiation to space. When in balance, the amount
of incoming radiation is equal the amount of outgoing radiation. The Earth's
energy balance can be disturbed by changing any of the following properties,

- the amount of incoming radiation from the sun,

- the amount of shortwave radiation reflected by the Earth,

- the amount of infrared radiation from the atmosphere to the Earth's surface,

which leads to an initial temperature change of the Earth-atmosphere system.
A change in the global mean temperature leads to feedback mechanisms with
varying timescales and which are difficult to quantify. These mechanisms can
feed back on the radiative properties of the atmosphere and the Earth's surface
and thus the amount of radiation that reaches the Earth's surface.

The fraction of incoming radiation from the sun that is reflected by clouds,
aerosols and atmospheric gases is expressed by the albedo of the Earth. A
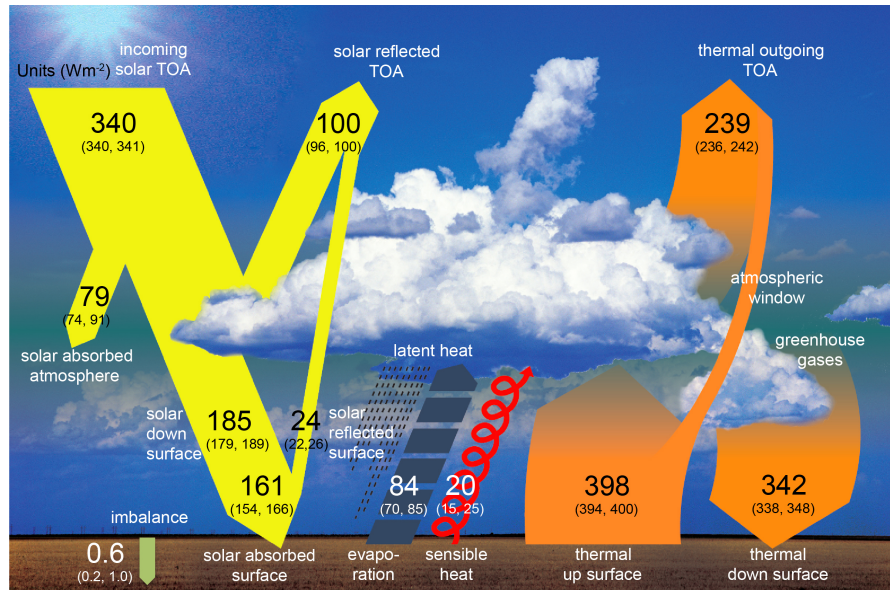
Figure 1.1: Estimate of the Earth's annual and global mean energy balance. Over the long term, the amount of incoming solar radiation absorbed by the Earth and atmosphere is balanced by the Earth and atmosphere releasing the same amount of outgoing longwave radiation. [1]

change in the global albedo would induce a change in the energy balance and thus the Earths climate. Clouds have a strong influence on the global albedo since they cover about $68\pm3\,\%$ of the Earth's surface (for cloud optical depth $\tau > 0.1$ [2]). Changes in cloud albedo are the major reason of changes in planetary albedo associated with global warming [3]. The global cloud albedo depends both on cloud amount but also on cloud optical properties. Aerosols can induce a change in cloud properties and can thus indirectly induce a change in planetary albedo and thereby affect Earth's climate [4, 5].

It is very likely that we humans have influenced the Earth energy balance by the release of gases like carbon dioxide (CO_2) and aerosol particles, but also by changing the surface albedo due to land use (urbanization, agriculture, deforestation,etc.). In order to quantify the impact of a perturbation, i.e. a change of the amount of aerosols, on earth climate, two kinds of measures were introduced. Radiative forcing (RF) quantifies the energy imbalance at the top of the atmosphere (TOA) and is expressed in watts per square meter averaged over a particular period of time. Effective radiative forcing (ERF) is the same as radiative forcing, but allows for rapid adjustments. Atmospheric temperatures, water vapor and clouds are allowed to change, but with global mean surface

temperature or a portion of surface conditions unchanged. With both RF and ERF the human influence on the earth energy budget, the global RF and ERF can be estimated for various species.

Figure 1.2 presents estimates and ranges in 2011 relative to 1750 and the net changes of the planetary energy balance. The positive radiative forcing due to an increase in greenhouse gases is partly offset by the cooling effect of the aerosols. However, while there is a high to very high confidence and a small uncertainty for long-lived greenhouse gases, the confidence for aerosol effects on clouds is low and highly uncertain. One explanation is the complex interaction between aerosols, clouds and atmospheric gases making it difficult to estimate the radiative forcing.

Thus improving the understanding of aerosol-cloud-interactions is one of the keys for reducing uncertainty in the estimate of the total anthropogenic RF.

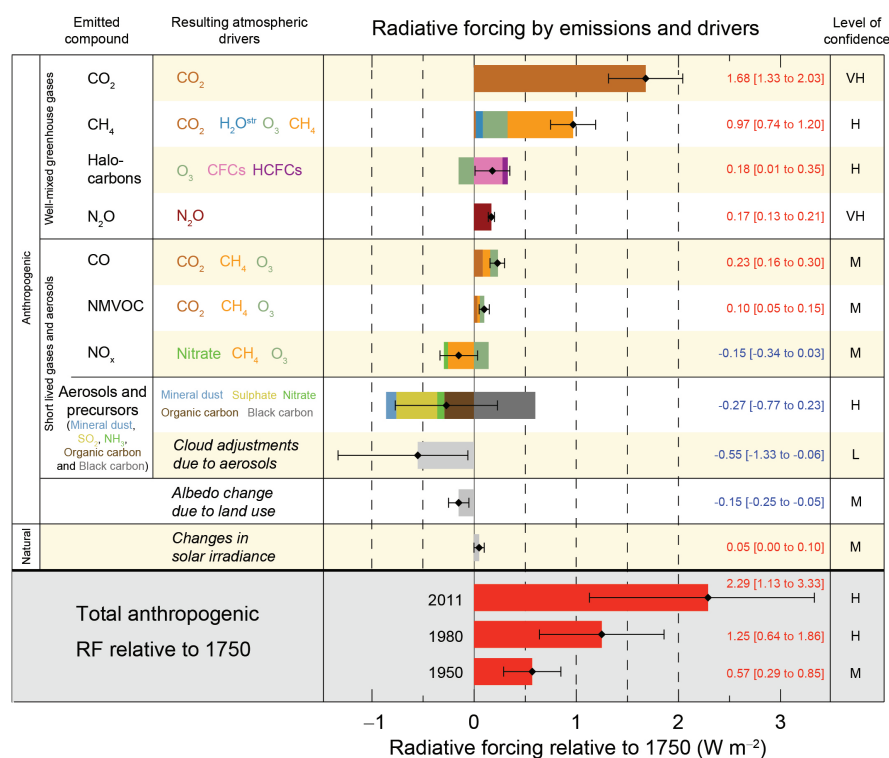*Figure 1.2:* Global average radiative forcing (RF) estimates and ranges in 2011 for greenhouse gases, short lived gases, aerosols and other important agents and mechanisms, together with level of confidence. The total anthropogenic radiative forcing and its range are shown for three different years relative to 1750. [6]

1.2 Climate Sensitivity

The magnitude of the estimate of the anthropogenic aerosol RF is important for estimating the climate sensitivity. The equilibrium climate sensitivity is defined as the temperature (global-mean, near-surface) response to radiative forcing from a doubling of the atmospheric CO_2 concentration from preindustrial levels. Thus, a more negative aerosol forcing would correspond to a higher climate sensitivity, which would partly or completely offset the climate impact of CO_2. Depending on climate sensitivity the reduction of aerosols would impact differently on Climate. Climate change and atmospheric aerosols are both a threat for human health and life [7, 8]. The reduction of aerosol emissions would save human lives close to the aerosol source on one hand, but could lead to more death due to the implications of a warmer climate. Thus, climate sensitivity is important for quantifying risks and probabilities and the development of adaption strategies.

1.3 Aerosol-Cloud Interaction

Aerosols affect the energy balance of the earth directly by changing reflectivity and absorption of the atmosphere (direct radiative effect). The prediction of the direct aerosol forcing between 2011 and the pre-industrial era (1750) requires knowledge of the distribution, chemical composition and optical properties at both times. Due to emissions of aerosol particles in 2011 compared with pre-industrial era less solar radiation reaches the Earth's surface. The TOA global-mean net direct effect is estimated to $RF = -0.35$ (-0.85 to $+0.15$) W/m^2 for 2011. When allowing for rapid adjustments in the atmosphere, the effective radiative forcing is slightly lower ($ERF = -0.45$ (-0.95 to $+0.05$) W/m^2 [9]). This means that when considering the direct effect only, in general the aerosols have a cooling effect. Since aerosol particles can act as cloud condensation nuclei (CCN) or ice nuclei (IN) they can influence cloud properties and thus indirect affect the energy balance of the earth. But the interaction between aerosols and clouds is very complex.

   As an example how aerosols indirectly influence clouds is by increasing the number of cloud active aerosol particles. This would lead to an increase in cloud droplet number concentration. When assuming a constant liquid water content, this increase would lead to smaller, more numerous, cloud droplets with an increased total droplet surface area, and thus an increased cloud albedo. For a constant cloud amount this would have a global cooling effect. This effect was discovered first by Twomey in 1974, who suggested that air pollution gives rise to brighter clouds by increasing the droplet concentrations and thereby the op-

tical thickness (and cloud albedo) of the clouds (first indirect or Twomey effect, [10]). The Twomey effect can trigger multiple adjustments that even can interact with each other. As an impact on cloud microphysics the formation of precipitation for smaller droplets may take longer or might be completely suppressed, since their coagulation into raindrops is less efficient [11]. This could enhance the cloud lifetime and hence the cloud reflectivity [12]. It can also enhance entrainment of dry air into the cloud and thus increase cloud evaporation and thus decrease cloud lifetime [13]. Smaller more numerous cloud droplets can also influence cloud macrophysics. A delayed freezing of cloud droplets into ice crystals could suppress or delay downdrafts and warm rain in convective clouds [14]. This could lead to stronger updrafts and the release of latent heat from condensation and an increase of the convection and thus cloud height. Since the adjustments do not have the same direction in relation to radiative forcing, the calculation of the overall effect is difficult.

As another example, an increase in the number of absorbing aerosol particles can lead to a more stable atmosphere by cooling the surface and heating the atmosphere. This can suppress convection and thus the formation of convective clouds. Also the capacity of the atmosphere to hold water vapor increases and may decrease the probability to reach supersaturations needed to form clouds [15].

Thus, the many ways of possible interaction mechanisms make it difficult to estimate the global radiative forcing of the interaction between aerosols and clouds, however it is estimated to $RF = -0.45(-1.2 \text{ to } +0.0)$ W/m^2 [9]. Despite the high uncertainty in aerosol effective forcing estimates, there is a high confidence that aerosols have offset the warming due to the increase in greenhouse gas concentration.

1.4 Aerosol-Cloud-Interaction Measurement Techniques

There exist many different instruments for studying the interaction between atmospheric aerosol particles and cloud properties. There are many processes that are of interest, such as cloud formation, cloud evolution, precipitation initiation and cloud radiative properties.

The Particle Volume Monitor (PVM) can detect the integrated Particle Volume (liquid water content, LWC) of a cloud/fog. Scanning Mobility Particles Spectrometer (SMPS) can be used to measure the dry size distribution in the range from several nanometers up to several hundred nanometers. With a Forward Scattering Spectrometer Probe (FSSP, [16]) the ambient size distribution in the

range between $2\,\mathrm{nm}$ to $47\,\mathrm{nm}$ a can be obtained. Although SMPS and FSSP both provide information over a large size range about dry aerosol particle and ambient droplet size distribution respectively, it is not possible to get information about their relation.

The Droplet Aerosol Analyzer (DAA, [17]) can obtain the relation between both aerosol distribution in the range between $50\,\mathrm{nm}$ to $750\,\mathrm{nm}$ and ambient aerosol distribution in the range between $0.12\,\mathrm{\mu m}$ to $17\,\mathrm{\mu m}$ and was especially developed to study aerosol-cloud/fog interaction. The relation can be obtained, since the DAA measures the ambient size of individual droplets and interstitial particles, the size of the dry residual particles after evaporation of the water vapor, and the number concentration of the dry residual particles. This gives a unique three-parameter data-set (ambient diameter, dry residual particle diameter and number concentration). The results obtained in former field campaigns show the potential of the DAA to study the interaction between atmospheric aerosol properties and cloud properties in detail. A strong relation between aerosol and cloud properties was obtained, which is important for the radiative properties of the cloud (Po Vallery, Italy, 1994 [18]; Great Dun Fell, Cumbria, UK, 1995 [19]; Tenerife, Spain, 1997 (ACE-2 HILLCLOUD experiment, [20])). In order to obtain measurements results with higher statistical confidence and a higher time resolution a second generation of the DAA has been developed in 2008/2009. With and more automated measurement process, it is possible to perform longterm measurements over several month.

1.5 Droplet Formation Regimes

Field observations of aerosols and clouds are local field studies for a specific mix of aerosol types under specific meteorological conditions. It is necessary to identify these meteorological conditions, in order to be able to apply the results of field observations in Numerical models of the global climate (General Circulation Model, GCM). Reutter et al. [21] suggests three distinctly different regimes of cloud condensation nucleus (CCN) activation and droplet formation depending on the ratio between updraft velocity w [m/s] and aerosol number concentration N_{tot} [cm^{-3}] at cloud base:

- In the aerosol-limited regime ($w/N_{\mathrm{tot}} \gtrsim 10^{-3}\,\mathrm{m\,s^{-1}\,cm^{-3}}$) droplet activation is limited by the number of aerosol particles, the number of cloud droplets $N_{\mathrm{d,tot}}$ is directly proportional to N_{tot} and independent to w

- In the transitional regime ($10^{-4}\,\mathrm{m\,s^{-1}\,cm^{-3}} \lesssim w/N_{\mathrm{tot}} \lesssim 10^{-3}\,\mathrm{m\,s^{-1}\,cm^{-3}}$), $N_{\mathrm{d,tot}}$ is non-linear proportional to both w and N_{tot}

- In the updraft-limited regime ($w/N_{\text{tot}} \lesssim 10^{-4}\,\text{m}\,\text{s}^{-1}\,\text{cm}^{-3}$) updraft velocity is limiting droplet activation and $N_{\text{d,tot}}$ is directly proportional to w and independent to N_{tot}.

Previous results have shown a 'roll-off', where an increase in aerosol number concentration N_{tot} does not lead to a proportional increase in number of cloud droplets $N_{\text{d,tot}}$. The 'roll-off" onset happens at different aerosol number concentration levels [22–24]. Other studies have not observed roll-off [25]. According to Modini et al. [26] is the relation between cloud droplet number and total aerosol dependent on cloud dynamics and the size and composition of the aerosol.

The main objective of this thesis is to determine the droplet activation regime of the performed measurements and to parameterize the relation between aerosol number concentration and cloud droplet number concentration depending on the regime.

1.6 Thesis Outline

One objective was to implement improvements and changes to the DAA, the central instrument of the thesis, in order to reach a higher time resolution and a more automate measurement process. Another objective was to further develop the inversion routine of the DAA data in order to meet the requirements of the instrument. Both measurement technique and data inversion routine of the Droplet Aerosol Analyzer (DAA) are presented in chapter 2.

The experimental data behind this thesis have been measured in 2010 at the summit of Mt. Brocken ($51.80°$ N, $10.62°$ E, 1142 m a.s.l.) which is the highest peak of the Harz mountain range in central Germany. With its high occurrence of clouds (30 % to 60 % between June and October, [27]) Mt. Brocken has been location for ground-based studies of physical and chemical processes occurring in ground-based clouds [27–30]. A detailed description of the measurement location at Mt. Brocken and its instrumentation is presented in chapter 3.

The main objective of this thesis was to parameterize the relation between aerosol number concentration and cloud droplet number concentration depending on the droplet activation regime. The overview of the resulting dataset, parameterizations and interpretation are presented in Chapter 4.

Chapter 5 concerns the conclusion and outlook of this thesis.

Chapter 2

The Droplet Aerosol Analyzer (DAA)

This chapter describes the basic measurement principle of the Droplet Aerosol Analyzer (DAA, **PAPER III**, [31]), and the data analysis process. Since the measurements were performed continuous for several months (see Chapter 3), only cloud data of restricted quality are selected for further evaluation. The selected DAA data are corrected for losses and multiple charging before applying the inversion algorithm (**PAPER II**, [32]). Using the resulting three-parameter dataset, further variables describing cloud microphysics can be derived (see Section 2.2.4).

2.1 Basic DAA Measurement Technique

The DAA consists of an outdoor and an indoor part (see Fig. 2.1). In the outdoor part cloud droplets and interstitial particles are collected by an inlet, which is directed towards the wind by a wind vane. To reach a well defined charge state, the collected aerosol passes through a bipolar charger (BiCh). The unipolar charger (UniCh) charges the aerosol, still at ambient conditions, according to size and makes it possible to relate ambient droplet diameter and dry residual diameter. In the following drying unit (Dryer, **PAPER I** [33]) the water is evaporated and the dry, charged residual particles enter the indoor part. Having a number of charges related to ambient size [34], the particles are now selected according to their electrical mobility in the first DMA (DMA 1a and 1b). The following combination of BiCh, Differential Mobility Analyzer (DMA) and Condensation Particle Counter (CPC) gives the size distribution of the droplet residuals for a certain dry diameter size.

By knowing the dry diameter and the electric mobility of the unipolar charged residual particles, their charge state can be calculated. With the calibration of
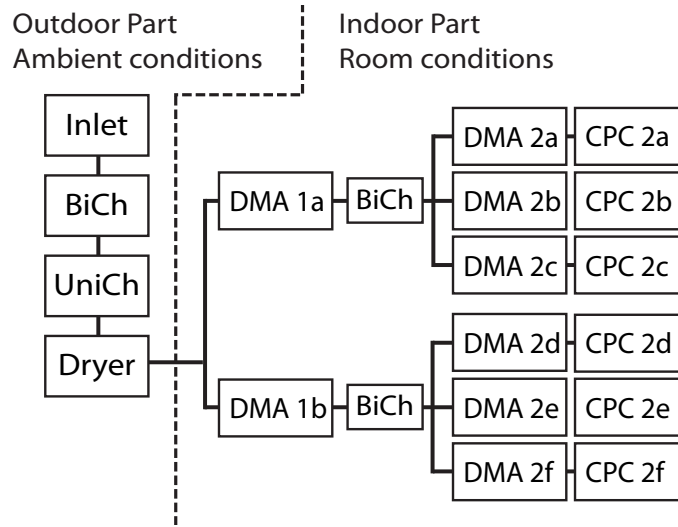
Figure 2.1: The DAA is based on a concept where the aerosol is processed in several steps: by aerosol charging mechanisms (BiCh, UniCh), diffusion drying (Dryer), electrostatic aerosol spectrometry (DMA), and counting (CPC) the desired relationships are obtained. (**Paper II**,[32])

the unipolar charger, the arithmetic mean charge can be related to the ambient diameter in the ambient size range between 0.12 μm and 17 μm.

The DAA measuring technique makes it possible to relate ambient diameter, dry residual particle diameter and number concentration and to calculate

- the dry aerosol size distribution $dN/d\ln D_{\mathrm{p}}$
- the ambient aerosol size D_{d} for each dry size D_{p} measured
- the number of interstitial aerosol particles and droplets for a dry diameter size interval
- the liquid water content LWC for an ambient diameter size interval
- the activated fraction for the total measured dry size interval f_{act} and the critical dry diameter of 50 % activation D_{50}

with a time resolution of around 10 minutes for one scan The dry diameter size interval was shifting every other scan, as shown in Table 2.1.

	D_{p} [nm]					
Set	DMA 2a	DMA 2b	DMA 2c	DMA 2d	DMA 2e	DMA 2f
1	776	427	272	170	112	78
2	548	313	205	131	88	61

Table 2.1: Campaign average of the measured DAA dry residue diameters for set 1 and 2 respectively.

2.1.1 DMA Calibration

(a)   (b)
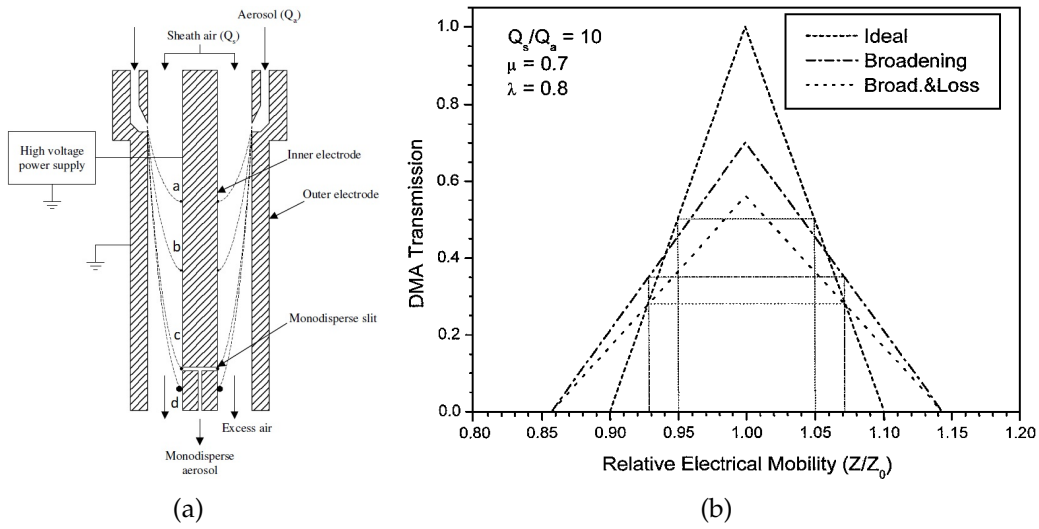
Figure 2.2: (a) Basic principle of a differential mobility analyzer (DMA). Adapted from [35]. (b) Ideal transfer function and influence of broadening and loss on width and transmission after [36].

The DAA consists of eight differential mobility analyzer (DMAs) which have been characterized [36].

A DMA is used to classify aerosol particles. It consists of two concentrically cylindrical electrodes with an electric field applied in between. Dry, clean air (sheath air flow, Q_{sh}) and the charged aerosol (aerosol flow, Q_{ae}) pass between the cylinders and particles having a specific electrical mobility can be selected depending on the electrical field strength and flow settings.

The transfer function is used to describe the particle penetration through a DMA as a function of electrical mobility and flow settings. The ideal transfer function is triangular (see Fig. 2.2(b)). Due to imperfections in the DMA the

transfer function may broaden or particles may be lost [36]. Thus, even nominally identical DMAs can perform different and the transfer function of each DMA needs to be determined depending on its settings and the measured particle size.

Two factors are used to describe the deviation from the ideal transfer function. The loss factor λ describes the decrease in area A of the transfer function due to loss of particles in the DMA

$$A = \lambda \frac{Q_{ae}}{Q_{sh}} Z_0, \ \lambda \leq 1 \tag{2.1}$$

The broadening factor $\mu (\leq 1)$ describes the change in width (full-width at half-maximum, FWHM) while preserving the area of the transfer function

$$FWHM = \beta \, Z_0 = \frac{Q_{ae}}{\mu \, Q_{sh}} Z_0, \ \mu \leq 1 \tag{2.2}$$

Both parameters are specific for each DMA and depend on the ratio of sheath air flow Q_{sh} to aerosol flow Q_{ae} and the particle diameter measured D_{p} and have been determined for 180 nm and 230 nm according to Table 2.2. The dependence of the broadening and loss factor on the particle diameter used for the specific DMA was estimated according to Karlsson and Martinsson [37] and was less than $3 \, \%$.

DMA	Length [m]	Q_{ae} [lpm]	Q_{sh} [lpm]	D_{p} [nm]	λ	μ
1a	0.274	3.2	14.3	180	0.955	0.869
				230	0.999	0.873
1b	0.1075	2.4	10.7	180	0.989	0.892
2a	0.475	1.3	5.2	180	0.965	1
				230	0.973	1
2b	0.492	1.1	4.4	230	0.992	0.895
2c	0.11	0.8	3.2	230	0.947	0.938
2d	0.11	0.8	3.2	230	0.816	1
2e	0.109	0.8	3.2	230	0.932	1
2f	0.11	0.8	3.2	230	0.940	1

Table 2.2: Characteristics of the DMAs used in the DAA and experimental results of their broadening (μ) and loss factor (λ).

2.1.2 The Unipolar Charger

The Aerosol entering the DAA passes the unipolar charging unit (bipolar charger and unipolar charger) and gets positively charged. The resulting charge distribution depends on the size of the incoming particles and the ion concentration in the charging region. The ion source in the unipolar charger is an α-source (Cm-244, 75 MBq) with a half-life of 18.1 years. Since the last calibration in 2000 by Frank et al. [34] the ion concentration has decreased due to radioactive decay. Thus the relation between arithmetic mean charge level q_a and mean ambient diameter D_d [µm] has changed. By knowing the half-life of the α-source and previous measured relation between q_a and D_d it is possible to estimate a new calibration curve.

2.1.2.1 The Unipolar Charger Model

The change in the relation between arithmetic mean charge level q_a and mean ambient diameter D_d with time is performed in three steps.

In a first step the dimensionless charging time of the calibration data (q_a, D_d) from 1996 τ_{1996} and 2000 τ_{2000} was estimated by solving the field-diffusion charging model for the continuum regime by Lawless [38]

$$\frac{\mathrm{d}v}{\mathrm{d}\tau} = \mathbf{M}(v, w_F) = \begin{cases} \mathbf{F}(v, w_F) + \boldsymbol{f}(w_F)\boldsymbol{Be}(0) & -q_{sat} \leqslant v \leqslant q_{sat} \\ \boldsymbol{f}(w_F)\boldsymbol{Be}(v - 3w_F) & (v > q_{sat}) \\ -v + \boldsymbol{f}(w_F)\boldsymbol{Be}(-v - q_{sat}) & (v < -q_{sat}) \end{cases} \tag{2.3}$$

with the field charging rate $\mathbf{F}$, diffusion charging rate $\mathbf{Be}$, the area of the particle that recieves the full diffusion current (fractional area, f), and the saturation charge q_{sat}:

$$\mathbf{F}(v, w_F) = Mw_F/4(1 - v/(Mw_F))^2 \tag{2.4}$$

$$\boldsymbol{Be} = \frac{v}{exp(v) - 1} \tag{2.5}$$

$$\boldsymbol{f}(w_F) = \begin{cases} 1/(w_F + 0.475)^{0.575} & (w_F \geqslant 0.525) \\ 1 & (w_F < 0.525) \end{cases} \tag{2.6}$$

$$q_{sat} = 1 + 2(\epsilon_r - 1)/(\epsilon_r + 1). \tag{2.7}$$

and using the dimensionless particle charge v, the dimensionless electric field

strength w_F and dimensionless charging time τ for ambient diameter D_d:

$$v = \frac{q\mathrm{e}^2}{2\pi\epsilon_0 D_d \mathrm{k}T} \tag{2.8}$$

$$w_F = \frac{\mathrm{e}E_c D_d}{2\mathrm{k}T} \tag{2.9}$$

$$\tau = \frac{Z^+ \mathrm{e}Nt}{4\epsilon_0}. \tag{2.10}$$

Here e is the electric elementary charge, ϵ_0 is the absolute permittivity of free space, k is the Boltzmans constant, T is the temperature, E_c is the electric field strength in the charging region ($20.75\ 10^2$ V/m), Z^+ is the ion mobility of positive ions ($1.4\ 10^{-4}$ m^2/Vs Hinds [39]), N is the total number of positive ions in the ion production region, t is the charging time.

The differential equation (eqn. 2.3) for a particle with ambient diameter D_d can be solved numerically using the mean charge of the bipolar charge distribution q_{bip} [40] as initial charge level. The charge acquired in the unipolar charger depends on the time-interval over which the differential equation is solved and this is the dimensionless charging time τ. Here measurements of mean drop diameter D_d and and arithmetic mean charge level q_a performed in 1996 and 2000 are used to estimate τ. As expected, τ decreases with time (see solid lines in Fig. 2.3(b)).

In a second step, the decrease in τ due to the radioactive decay of the of the α-source is estimated for 2010 (τ_{2010}). The decay leads to a decrease in total number of positive ions N and thus the ion current I and τ in the ion production region.

The ion current I in the production region of the unipolar charger can be estimated by a model developed by Frank et al. [34]. It describes the rate of change in number of ions (N) in respect to time (t) in the production region for a production rate P, geometric factor $G=0.77$, recombination rate R and transport to the perforated electrode T:

$$\frac{\mathrm{d}N}{\mathrm{d}t} = GP - RN^2 - TN \tag{2.11}$$

$$P = A_\alpha \exp(-\lambda t_\alpha)\frac{W_\alpha \omega}{W_i \mathrm{p} 4\pi} \tag{2.12}$$

$$R = \frac{\alpha_r}{V} \tag{2.13}$$

$$T = Z^+(U_{ce} - U_{pe})\frac{2\pi l}{V\ln\frac{r_{pe}}{r_{ce}}} \tag{2.14}$$

Here A_α is the activity of the ion source (α-source, Cm-244, 75 MBq, 1989), λ
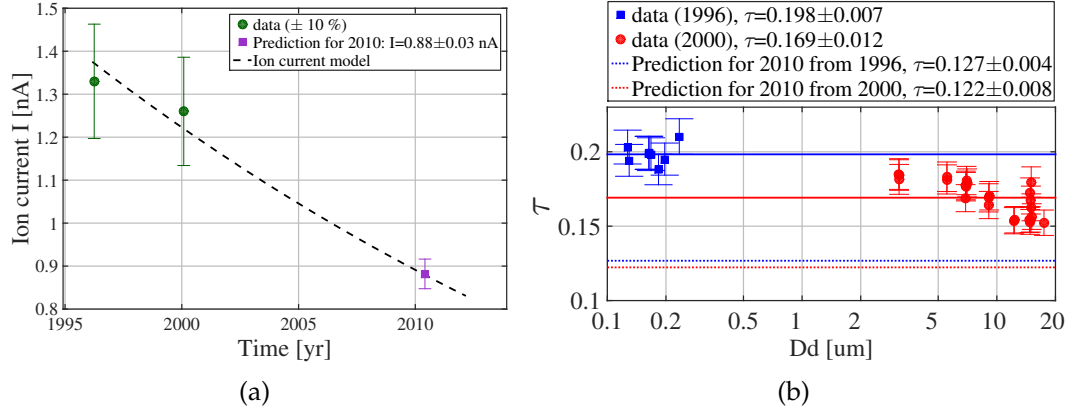
Figure 2.3: (a) Measured ion current (green circles) with 10 % errorbars, prediction according to the model developed by Frank et al. [34], see below, (broken line) and predicted ion current for 2010 (purple square) with observational errorbars (3 %). (b) Dimensionless time τ calculated according to Lawless [38] for data from 1996 (blue squares) and 2000 (red circles). Averages (solid line) and predicted τ (broken lines) estimated using the predicted ion current according to Frank et al. [34].

is the decay constant of the ion source ($\lambda = ln(2)/t_{1/2}$, with the half-life $t_{1/2}$ of 18.1 years). t_α is the time in years past since 1989, W_α is the energy of one α-particle from the ion source (5.8 MeV), $W_i p$ is the mean energy required to produce one ion-electron pair (34 eV), ω is the solid angle (0.27 srad, estimated), l and V are height of and active volume in the ion production region ($1.5 \ 10^{-4}$ m and $1.6 \ 10^{-5}$ m^3 respectively), α_r is the recombination effect ($1.6 \ 10^{-12}$, [41]), U_{ce} and U_{pe} are the voltage of the central and perforated electrodes (707 V and 41.3 V respectively), r_{ce} and r_{pe} are the radii of the central and perforated electrodes ($1.5 \ 10^{-3}$ m and $20.1 \ 10^{-3}$ m respectively).

The electric current resulting from motion of the ions, I depends on the number of ions transported to the perforated electrode:

$$I = NT e. \tag{2.15}$$

In order to describe the change in ion current in the charging region due to the radioactive decay of the α-source equation 2.11 can be solved. For steady state conditions ($\frac{dN}{dt} = 0$) solving the quadratic equation for N gives together with

15

equation 2.15

$$I_{\mathrm{rel}} = \frac{I}{I(t=0)} = \frac{T\mathrm{e}}{I(t=0)} \left(-\frac{T}{2R} + \sqrt{T^2 + 4RP} \right). \tag{2.16}$$

The ion current is estimated for 2010 I_{2010} from measurements performed in 1996 and 2000, see Figure 2.3(a). Using the relative change in I, the relative change in dimensionless charging time between 2000 to 2010 can be estimated using equation 2.10, 2.14 and 2.15

$$\frac{\tau_{2010}}{\tau_{2000}} = \frac{N_{2010}}{N_{2000}} = \frac{I_{2010}}{I_{2000}}. \tag{2.17}$$

2.1.2.2 The Ambient Diameter $\mathrm{D_d}$

In the last step the relation between arithmetic mean charge q_{a} and ambient particle diameter D_{d} (see Fig. 2.4) is estimated using the predicted τ and equation 2.3. The relation is estimated both for standard laboratory conditions as well as for average temperature and pressure during the measurement campaign 2010 at Mt. Brocken (June-October) using a pressure reduced ion mobility [42]. A fit to the modeled relation between q_{a} and D_{d} for standard pressure (p=1013.15 hPa) and temperature (T= 298 K) gives

$$D_{\mathrm{d}}(q_{\mathrm{a}}) = -4.25 + (7.54 + 0.82q_{\mathrm{a}})^{0.72}, \tag{2.18}$$

and for average pressure (p= 873.5 hPa) and temperature (T= 279.8 K) at Mt. Brocken during the campaign

$$D_{\mathrm{d}}(q_{\mathrm{a}}) = -3.91 + (6.59 + 0.67q_{\mathrm{a}})^{0.72}. \tag{2.19}$$

Because ten years passed between the last calibration of the unipolar charger and the measurements presented here (see ch. 4), the estimated mean ambient diameter D_{d} of this dataset has to be treated with care. Previous results obtained with the DAA show good agreement when comparing interstitial and residue size distribution, total cloud droplet number concentration, cloud droplet size distribution and cloud liquid water content LWC with other instruments (Differential Mobility Spectrometer (DMPS), Fast Forward Scattering Probe (FSSP) and Particulate Volume Monitor (PVM), [43]). In this dataset the estimated LWC is not well reproduced suggesting that the ambient diameter is underestimated by a factor of 1.5 to 2.
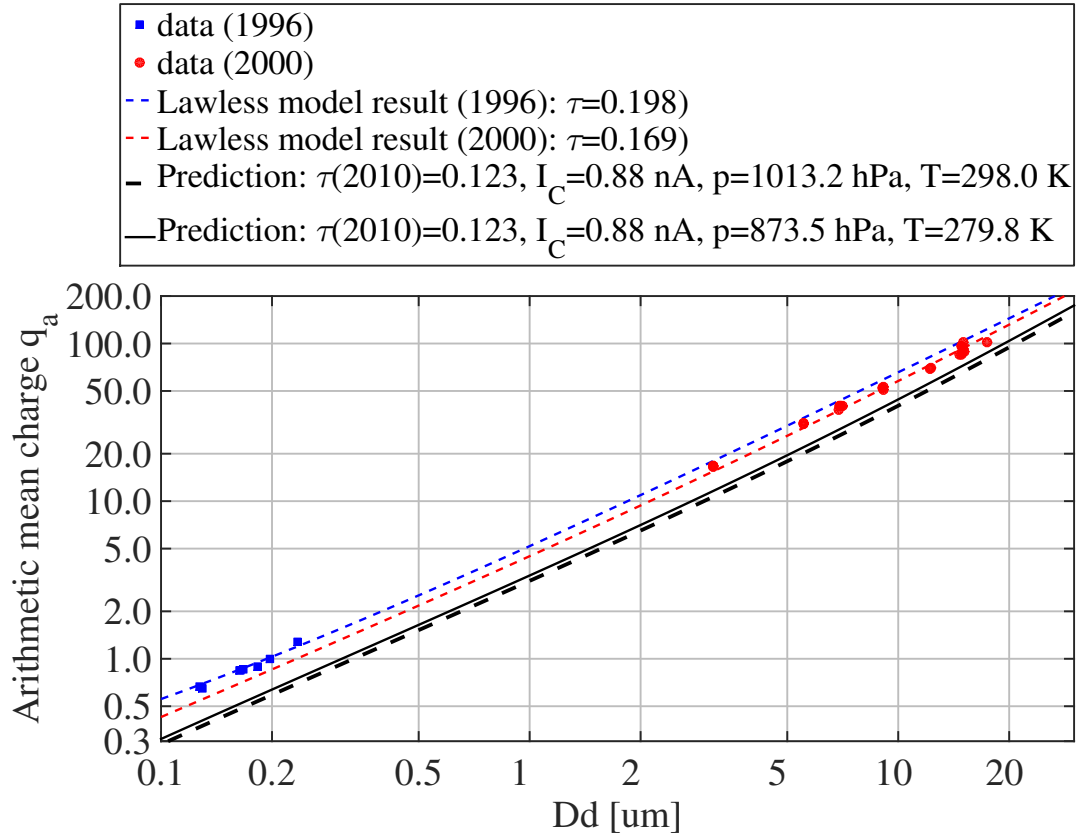
Figure 2.4: Measured arithmetic mean charge q_a and diameter D_d from 1996 (blue squares) and 2000 (red circles) and average relation modeled according to Lawless [38] (broken blue and red lines). For the predictions (black lines) the dimensionless time τ was estimated using the ion current modeled according to Frank et al. [34].

2.2 Data Inversion Routine

2.2.1 Data Preparation

Before evaluation the DAA data are checked for instrument performance, cloud conditions and influence of local sources.

The central part of the DAA are the eight DMAs. To ensure good data quality the variation of aerosol and sheath air flow, high voltage and pressure of each DMA during one scan (10 min) is restricted to be within four standard deviations of the whole measurement campaign. Also the relative humidity of the aerosol flow is restricted to be lower than 20 %.

To select data with cloud conditions, the liquid water content (LWC) measured by a PVM 100 (see Section 3.2.2) at the same location as the DAA was used. For LWC higher than the detection limit (LWC>0.002 g/cm^3) it is assumed to be cloudy at Mt. Brocken. Since high variation of LWC during one scan makes the data interpretation difficult, the standard deviation during one scan was restricted to be smaller than 1.7 % of the average during one scan. In order to include the beginning and end of each cloud, before and after the first and last DAA scan during cloud, additionally 40 min (4 scans) that are cloud free are selected.

In close proximity of the hut on Mt. Brocken plateau, there is a meteorological station (distance d=96 m, direction 114°), a hotel (d=140 m, 296° to 334°) and a trainstation building (d=80 m, 10° to 58°) with tracks (d≳90 m, 10° to 85°) of the steam train bringing tourists up and down the Mountain during day time (see ch. 3.1, Fig. 3.1(b)). To avoid contamination by local sources during day time (7 to 19 UTC) data are only selected for further evaluation if during the complete scan no wind direction from hotel, train station and train tracks was measured. During night time (19 to 7 UTC), with no trains going, only hotel and train station were restricted wind directions.

2.2.2 Raw Data and Corrections

The charge distribution downstream of the unipolar charger is measured by two different sets of six dry diameters D_{p} (59 nm to 545 nm and 75 nm to 776 nm). During a measurement scan the voltage of DMA 2a-f is fixed representing one set of six diameters, whereas the voltage of DMA 1a and 1b is stepped over different charge levels to obtain the charge distribution. Each scan can be used independently giving a time resolution of 10 minutes, or with full size resolution of 20 minutes.

The DAA raw data of each scan consist of CPC counts (N_{count}), CPC counting time (t_{count}), and of each of the eight DMAs high voltage (U), sheath air flow

(Q_{sh}), aerosol flow (Q_{ae}), pressure (p_{DMA}) as well as aerosol flow temperature (T_{ae}), and atmospheric pressure (p).

The derived variables are dry particle diameter (D_{p}), electrical mobility (Z_{p}), electrical charge level (q_{DAA}), and raw number concentration.

Particle losses in each DMA due to losses and transfer function broadening are accounted for using the loss λ and broadening parameter μ according to Table 2.2 and a particle size dependent transfer function [37, 44].

In order to obtain the charge distribution $N^{\text{DAA}}(q_{\text{DAA}})$ downstream of the unipolar charger, the number of only singly charged particles downstream of the second bipolar charger is needed. But particles passing the second bipolar charger are multiply charged. Therefor, for each mobility level measured in the DMA 2 level, the fraction of multiply charged particles is calculated according to Wiedensohler [40]. The DMA 2a-f mobility step is set to two and by that doubly and quadruply charged particles are measured by the DMA 2 with the closest and second closest smaller dry particle diameter. For triply charged particles a linear relation is assumed between the concentration of the doubly and the quadruply charged particles. The obtained charge distributions $N^{\text{DAA}}(q_{\text{DAA}})$ for each of the measured dry diameters is corrected for laboratory pressure (1013.25 hPa) and temperature (293.15 K) (see Fig. 2.5).

2.2.3 Fit of the Charge Distribution

The shape of the charge distribution measured by the DAA $N^{\text{DAA}}(q_{\text{DAA}})$ depends on the ambient particle size D_{d}. It contains mainly two kinds of ambient particles:

- Droplets with a high number of charges obtained in the unipolar charger and a lognormal charge distribution (see blue fit-function in Fig. 2.5).

- Interstitial aerosol particles with a low number of charges (see red fitfunction in Fig. 2.5).

In order to estimate ambient particle size D_{d} and number concentration N^{UCh} of the aerosol entering the unipolar charger the measured charge distribution is compared with a modeled charge distribution $N^{\text{fit}(q_{\text{a}})}$. The modeled charge distribution describes the transmission of positively charged particles from the unipolar charger through the two DMAs. It uses ambient particle size D_{d} and number concentration N^{UCh} as coefficients and uses information about the unipolar charger and DMA as input parameter. Since N^{UCh} is the concentration of particles entering the unipolar charger, in a last step losses in the DAA inlet are accounted for according to Belyaev and Levin [45] to estimate the particle concentration ΔN entering the DAA for each measured dry size interval.
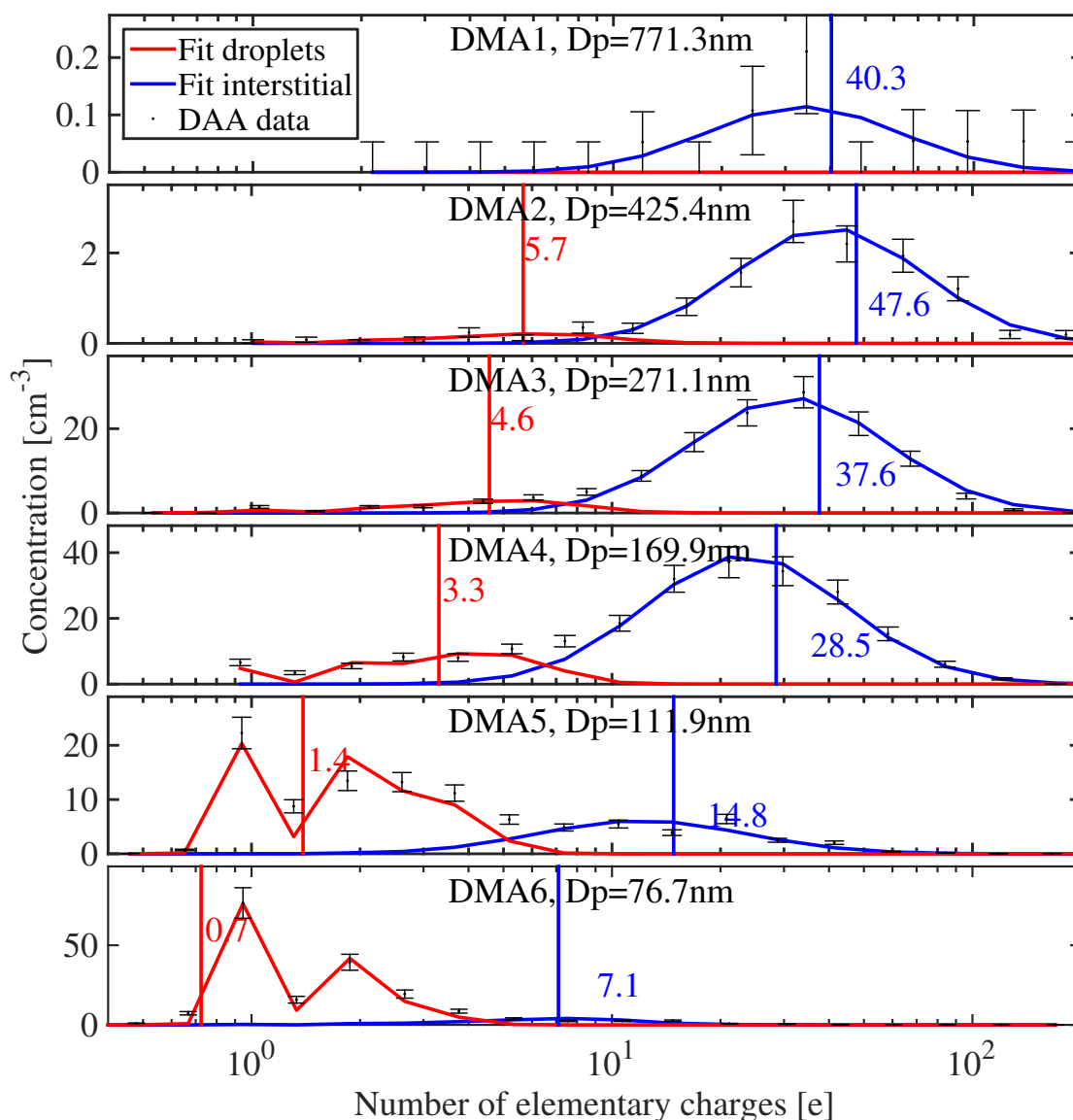
Figure 2.5: Example of results obtained from data collected at Mt. Brocken, during one scan from September 14, 2010, 02:05 to 2:15 UTC. The panels show charge distribution data from the DMA 2a-f, including the standard error for Poisson counting of the raw counts. In this example, fits were performed for each DMA 2a-f, which are used to classify the aerosol into interstitial particles and droplets. In the top panel, showing the results from DMA 2a for the largest dry particle diameter measured in this scan there were insufficient particles and droplets to allow a fit. Note the varying scale on the y-axes.

2.2.4 DAA Data set and derived variables

The DAA dataset relates directly between ambient particle diameter D_d, dry (residual) particle diameter D_p and number concentration ΔN per measured size interval. For a certain measured D_p, both concentration ΔN and ambient size D_d of the interstitial aerosol and the droplets can be estimated.

The separation between cloud droplets and residual particles is done in three steps. In the first step particles larger than the diameter of activation $D^*_{V(AS)=0.8}$ are assumed to be activated according to Köhler's theory and are regarded as droplets. $D^*_{V(AS)=0.8}$ is calculated assuming the particles to behave as if they consisted of insoluble material and an arbitrary volume fraction of ammonium sulfate of $V(AS)=0.8$. Since not all cloud droplets that formed on the largest dry particles might have been activated according to Köhler's theory, they would be mistaken as residual particles. In the second step all particles larger than the smallest activated droplet are regarded as droplets. In the third step it is assumed that the droplet diameter does not decrease with increasing dry diameter, while taking into account measurement uncertainty.

In order to show the capabilities of the DAA a cloud event from the September 14, 2010, 02:05 to 2:15 UTC was selected. As shown in Figure 2.6 a direct relation between ambient particle diameter, dry (residual) particle diameter and the number concentration is obtained. Interstitial particles (red) and droplets (blue) can be identified. As can be seen in the distribution of ambient particles (see a, D_d-ΔN plane in Fig. 2.6), there is a gap between interstitial aerosol and cloud droplets at around $2\,\mu m$. The size of the cloud droplets ranged from $3.5\,\mu m$ to $9.5\,\mu m$ and formed on dry particles in the size range between $0.11\,\mu m$ to $0.77\,\mu m$ (see c, D_p-D_d plane in Fig. 2.6). Even though the cloud droplets that formed on the largest dry particles might not have been activated according to Köhler's theory (indicated by the three black lines in the D_p-D_d plane), they are regarded as cloud droplets here (see above). It should be remembered also that the ambient diameter D_d is probably underestimated by a factor of between 1.5 to 2.

From the distribution of dry (residual) particles (right, D_p-ΔN plane in Fig. 2.6 and also Fig. 2.7) further parameters can be estimated, for example the activated fraction f and the critical dry diameter of $50\,\%$ activation (D_{50}), and the total number concentration of dry (residual) particles, cloud droplets and interstitial particles for a chosen dry particle size range and the fraction of activated cloud droplets f_{act}. Here the total number concentration N_{tot} and number concentration of interstitial particles $N_{i,tot}$ is estimated for the size range D_p=(0.1 to 0.7) μm. The total number of droplets $N_{d,tot}$ is estimated for the total measured dry diameter size range. For the example case the total number concentration of dry (residual) particles is estimated to N_{tot}=790 cm^{-3}, the total number con-
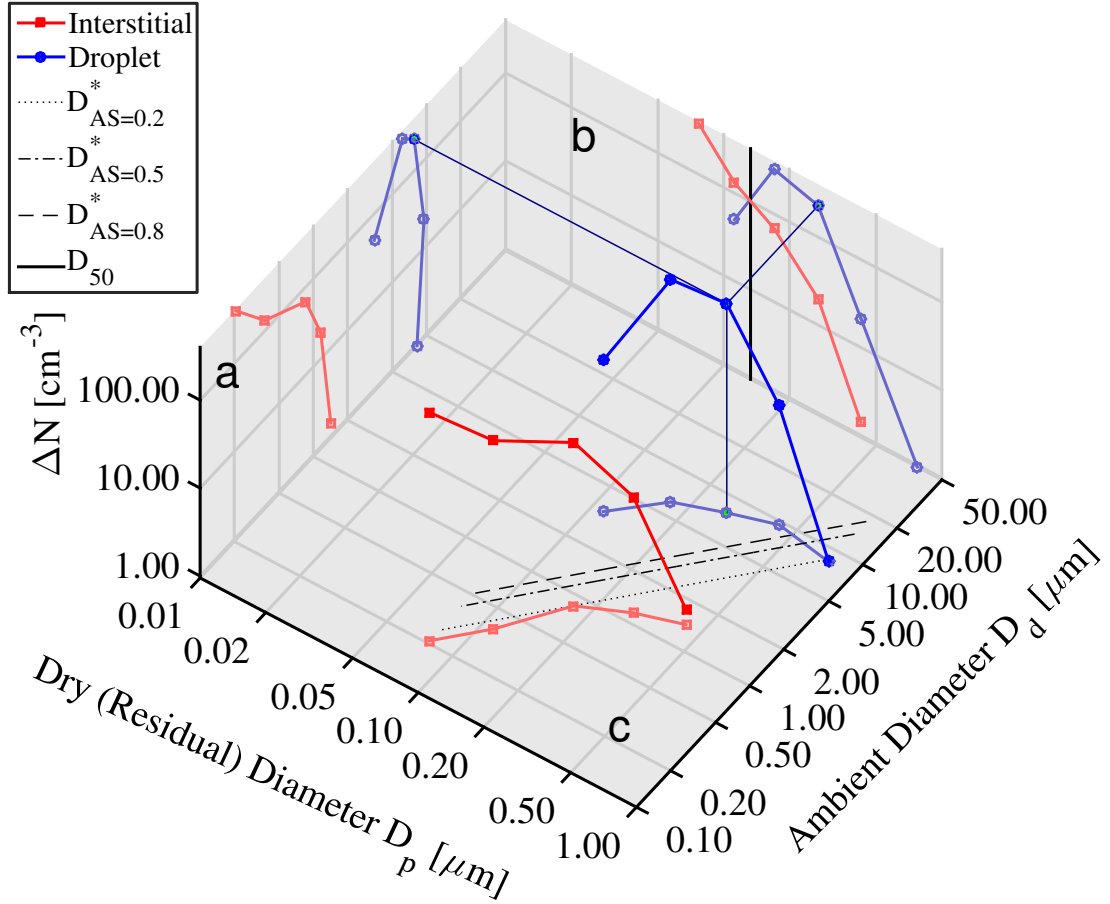
Figure 2.6: Concentration ΔN in each measured size interval of droplets and residual particles as a function of ambient particle and dry particle diameter on September 14, 2010, 02:05 to 2:15 UTC. The three black lines in the D_{p}-D_{d} plane indicate the critical ambient diameter of activation $D^*_{V(AS)}$ according to Köhler's theory as a function of D_{p} for different volume fractions of ammonium sulfate in the particles. The projections in paler colors show the distribution of ambient particles (left, D_{d}-ΔN plane), the distribution of dry (residual) particles (right, D_{p}-ΔN plane) and ambient particle diameter D_{d} as a function of dry (residual) particle diameter D_{p} (bottom, D_{p}-D_{d} plane).
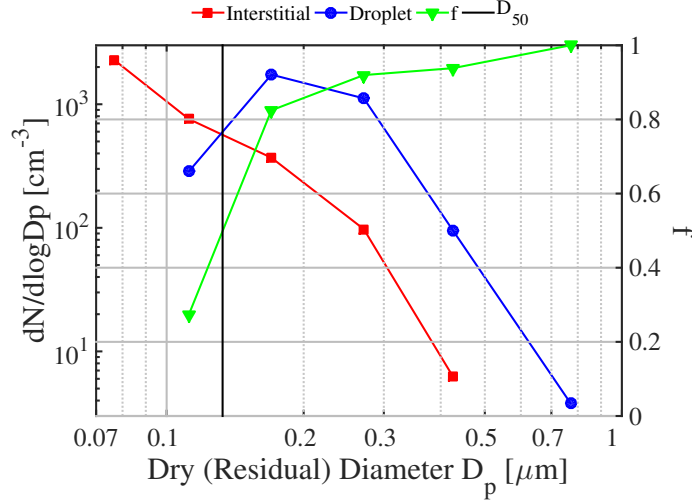
Figure 2.7: Dry residual interstitial and droplet distribution on September 14, 2010, 02:05 to 2:15 UTC (left y-axis). The critical dry diameter of 50 % activation D_{50} (black vertical line) is estimated for an activated fraction f (green) of 0.5.

centration of interstitial particles to $N_{i,tot}=168\ cm^{-3}$, and the total number concentration of droplets to $N_{tot}=622\ cm^{-3}$.

The shape of the aerosol number size distribution can be estimated by the number-to-volume concentration ratio R_{D_c} [46]. R_{D_c} is defined as the ratio between number concentration N_{tot} of particles with a dry diameter D_p larger than D_c and the total volume concentration V_{tot}

$$R_{D_c} = \frac{N_{tot}(D_p > D_c)}{V_{tot}}\ [\mu m^{-3}] \tag{2.20}$$

For high R_{D_c} the number size distribution is shifted towards smaller diameter. For the presented dataset R_{D_c} was calculated for $D_c=0.1$ μm.

Chapter 3

Mt. Brocken Measurement Campaign

Between June and October 2010 cloud investigations have been performed at Mt. Brocken. This chapter describes the measurement site and its instrumentation.

3.1 Measurement Site

Mt. Brocken ($51.80°$ N, $10.62°$ E, 1142 m a.s.l.) is the highest peak of the Harz mountain range in central Germany. At its summit there is a plateau (area approx. 0.25 km^2) that is very exposed to the wind due to the steep slope at all of its edges. The plateau lies above the treeline and is covered with grass and scrub. Hertel and Schöling [47] suggest that the tree-line at Mt. Brocken is climate driven and influenced by the thermal conditions which clouds may significantly contribute to. According to Acker et al. [27] the wind field at Mt. Brocken is relatively uninfluenced by the surrounding mountains. The plateau is dominated by westerly/southwesterly winds representing predominant low tropospheric wind [48]. It is most of the time situated in the upper planetary boundary layer (PBL), during daytime in the mixed layer and under weak winds and strong insolation the plateau can create a local, shallow convective boundary layer (CBL). During night-time the plateau is often located in the turbulence-free residual layer (remains of the mixing layer from the day before) or for subsiding of the PBL below the top of Mt. Brocken even in the free troposphere (FT) [49].

Mt. Brocken has been the location for ground-based studies of physical and chemical processes occurring in ground-based clouds [27–30]. It has a high occurrence of clouds (30 % to 60 % between June and October, [27]), of which stratucumulus (38 %) and stratocumulus and cumulus together (Sc/Cu, 32 %) are the most dominating cloud types[28]. For convective clouds the cloud base
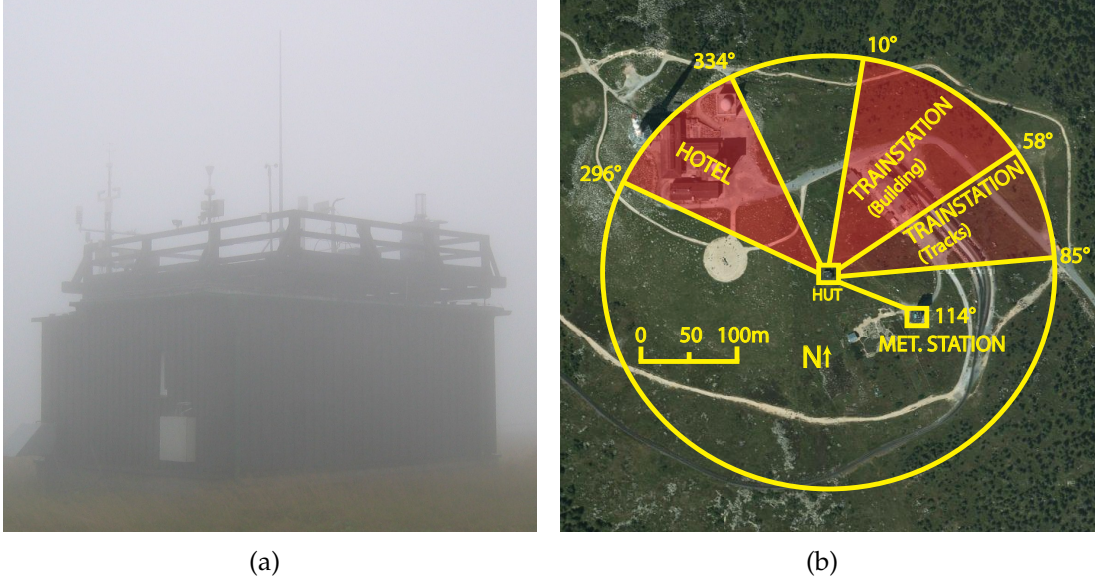
Figure 3.1: (a) Measurement hut at summit of Mt. Brocken. (b) Measurement site at summit of Mt. Brocken with meteorological station, hotel, train station and tracks marked. Due to possible contamination by local sources data with certain wind directions marked with red are not evaluated (see Section 2.2.1).

was often found between 900 m and 1200 m a.s.l. and stratiform clouds between 700 m and 900 m a.s.l. [28, 30]. However, all clouds studied at Mt. Brocken are influenced by the orography.

Since Mt. Brocken is also a tourist attraction with a steam train bringing tourists up and down the mountain during daytime, the measurement hut on top of the summit plateau is surrounded by several buildings (see Fig.3.1(b)). Situated on the Mt. Brocken plateau there is a meteorological station (distance d=96 m, direction 114°), a hotel (d=140 m, 296° to 334°) and a train station building (d=80 m, 10° to 58°) with tracks ($d\gtrsim$90 m, 10° to 85°) of the steam train.

3.2 Instrumentation

Instruments were placed at two locations. At the measurement hut at Mt. Brocken summit (see Fig. 3.1(a)) the Droplet-Aerosol-Analyser (DAA) together with the Particle Volume Monitor (PVM) monitored cloud microphysical properties. Also fundamental meteorological properties, such as horizontal wind speed (U), wind direction (α_U), relative humidity (RH), temperature (T) and atmospheric pressure (p) were measured at the roof top of the measurement hut. In Schierke (612 m a.s.l.), at the foot of Mt. Brocken located 4.44 km and 146°
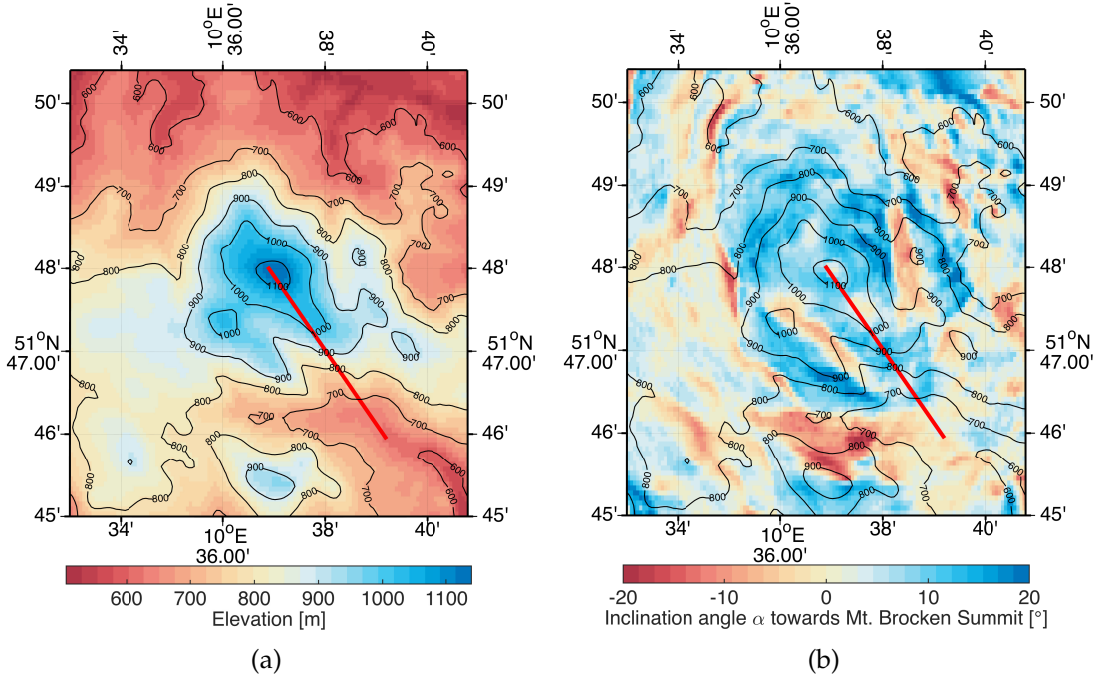
Figure 3.2: (a) Topographic map of Mt. Brocken with contour lines in 100 m intervals. The red line indicates the direction and distance between Mt. Brocken summit and the location of the Celiometer at the foot of Mt. Brocken. (b) Inclination angle α of Mt. Brocken slope.

in horizontal direction (southeast) and 530 m below of the measurement hut, a Ceilometer measured cloud base height (CBH).

3.2.1 The Droplet Aerosol Analyzer

A detailed description of the DAA instrument is presented in Chapter 2.

The DAA was especially developed for aerosol-cloud/fog interaction studies. The improved version has a better time resolution (10 min) and is more automated than the previous version of the instrument (**Paper III**, [31]). The dataset contains the three-parameter data-set consisting of ambient diameter D_{d}, dry residual particle diameter D_{p} and number concentration ΔN, for each size-bin measured.

3.2.2 The Particle Volume Monitor (PVM)

The Gerber Particle Volume Monitor (PVM 100) is a ground based instrument that monitors cloud microphysical properties. It uses laser light and measures

the forward-scattering by cloud droplets in the open air along a 40 cm long path. The PVM 100 estimates for example the the liquid water content (LWC) of the ambient air with a sampling rate of 5 s, a detection limit of $LWC > 0.002$ g/cm^3 and an uncertainty of less than $0.009 \frac{\text{g}}{\text{m}^3}$ [27].

However, the uncertainty of the LWC measured by the PVM 100 is probably much higher due to drift in the instrument as discussed by Cederfelt et al. [43].

3.2.3 The Ceilometer

The Ceilometer (Vaisala CT25K) is a ground based instrument monitoring Cloud base hight. It detects backscattering of laser light caused by clouds in vertical direction resulting in a backscatter profile. Up to three cloud bases can be detected with a time resolution of 15 s and a vertical resolution of 30 m [50]. In order to account for the horizontal distance between cloud base measurements in Schierke and Mt. Brocken summit (d=4.44 km) simple trigonometry using the wind direction α_U gives the difference in time Δt

$$\Delta x = \cos(\alpha_{\mathrm{U}} - 146°)d \tag{3.1}$$

$$\Delta t = \frac{\Delta x}{U}[s] \tag{3.2}$$

$$t_{\mathrm{Celio}} = t_{\mathrm{DAA}} - \Delta t. \tag{3.3}$$

The lowermost detected cloudbase height was averaged over one DAA scan for cloudbase height below Mt. Brocken summit ($\overline{CBH}_{<1142\ \mathrm{m}}$) and for all cloudbase heights ($\overline{CBH}_{\mathrm{tot}}$). The resulting data were divided into three groups by comparing the cloudbase detected below Mt. Brocken with CBH_{all}.

- Lowlevel clouds, unbroken: closed cloud layer detected below Mt. Brocken ($\overline{CBH}_{<1142\ \mathrm{m}} + \sigma(CBH_{<1142\ \mathrm{m}}) \leq CBH_{\mathrm{all}}$)

- Lowlevel clouds, broken: gaps in the cloud layer detected below Mt. Brocken ($\overline{CBH}_{<1142\ \mathrm{m}} + \sigma(CBH_{<1142\ \mathrm{m}}) < CBH_{\mathrm{all}}$)

- orographic clouds: no cloud layer detected below Mt. Brocken, but LWC data indicate cloud occurrence at Mt. Brocken

The Harz mountain range has a horizontal length between 40 km and 80 km and does affect the planetary boundary layer significantly [51]. Thus all clouds measured at the Mt. Brocken experience an orographic influence of the underlying terrain.
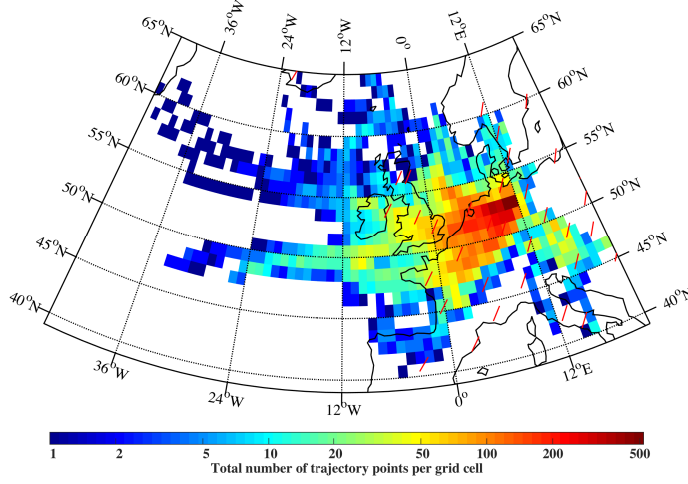
Figure 3.3: The total number of back-trajectory endpoints ($n_{i,j}$) for each cell shows the coverage of trajectories during cloud events.

3.3 Trajectories

In order to analyze source and transport of air masses arriving at Mt. Brocken summit ($51.80°$ N, $10.62°$ E, 1142 m a.s.l.), 48-h back trajectories have been computed for cloud periods using the NOAA HYSPLIT model [52]. The back trajectories started at 1242 m a.s.l. or 100 m over Mt. Brocken summit using the velocity field from archived meteorological data (GDAS1).

The Potential Source Contribution Function (**PSCF**, [53]) can be used to identify geographical regions that contribute to observed air pollution at a site. Here **PSCF** is calculated to identify sources that contribute to pollution and cloud properties observed at Mt. Brocken. A $1°x1°$ grid is used here for calculation of conditional probability for each grid cell $\textbf{PSCF}_{i,j}$ by relating the number of back trajectory endpoints corresponding to a set criterion $\textbf{m}_{i,j}$ to the total number of back trajectory endpoints $\textbf{n}_{i,j}$ in each cell

$$PSCF_{\textbf{i,j}} = \frac{m_{\textbf{i,j}}}{n_{\textbf{i,j}}}. \tag{3.4}$$

The total number of trajectory endpoints in all grid cells over Europe ($n_{i,j}$) shows the coverage of the trajectories during the campaign (see Fig. 3.3).

In order to account for overestimating of the $PSCF$ an arbitrary weight is used based on the standard error of counting. For a grid cell with a low number of trajectory endpoints the $PSCF$ might be overestimated, for example with $PSCF_{\textbf{i,j}} = \frac{m_{\textbf{i,j}}}{n_{\textbf{i,j}}} = \frac{1}{1}$ a high source contribution is estimated. For grid cells with an

error larger than w_{thresh} the weighting factor $\mathbf{w}_{i,j}$ is multiplied with **PSCF**

$$\mathbf{w}_{i,j} = \left(\frac{1}{w_{thresh} - 1} \right) \left(\frac{\sqrt{\mathbf{n}_{i,j}}}{\mathbf{n}_{i,j}} - 1 \right) + w_{min}. \tag{3.5}$$

Here an arbitrary error threshold of $w_{thresh}=0.2$ and a minimum weight of $w_{min}=0.2$ is used.

Chapter 4

Results and Discussion

4.1 Measurement Campaign Overview

The measurement campaign at Mt. Brocken was held from June until October 2010. Overall 23.4 days of cloud data meet the requirements presented in Section 2.2.1 and 77 % have been evaluated and are presented here.

The dominating wind direction for the evaluated data was between south and west, which is caused by restriction of certain wind sectors (see Fig. 3.1(b)) in order to avoid local contamination.

The total concentration of all particles N_{tot} and the interstitial aerosol $N_{\text{i,tot}}$ was calculated for a dry diameter range between D_{p}=0.1 − 0.7 µm. Droplets might formed on particles smaller than D_{p}=0.1, thus the total droplet number $N_{\text{d,tot}}$ was calculated for diameters lower than D_{p}=0.1 up to 0.7 µm. The variation of N_{tot}, $N_{\text{i,tot}}$, and $N_{\text{d,tot}}$ during the cloud events is presented in Figure 4.1(a). The average of N_{tot} was 337 ± 288 cm^{-3}.

An overview over meteorological variables, aerosol and cloud properties during the campaign are presented in Figure 4.1.

The variation of the shape of the dry size distribution $R_{0.1\ \mu\text{m}}$ and the diameter of 50 % activation D_{50} is presented in Figure 4.1(c). A higher $R_{0.1\ \mu\text{m}}$ indicates a shift in the size distribution towards smaller diameters, which can be identified in the last period of the evaluated data (14.09. to 15.09.2010). At the same time D_{50} is decreasing, leading to a high fraction of cloud droplets ($N_{i,tot}$<N_{tot} in Fig. 4.1(a)). During this time period the wind direction is stable around 220° with high windspeed, as can be seen in Figure 4.1(d). Figure 4.1(e) shows the variation of the height of the lowest cloudbase. Clouds with cloudbase below Mt. Brocken summit are mainly unbroken, which is consistent with previous results from Möller et al. [28] who detected stratiform clouds mainly between 700 m and 800 m.

In order to identify areas that contribute to high or low total number concen-

(a)

(b)

(c)

(d)

(e)
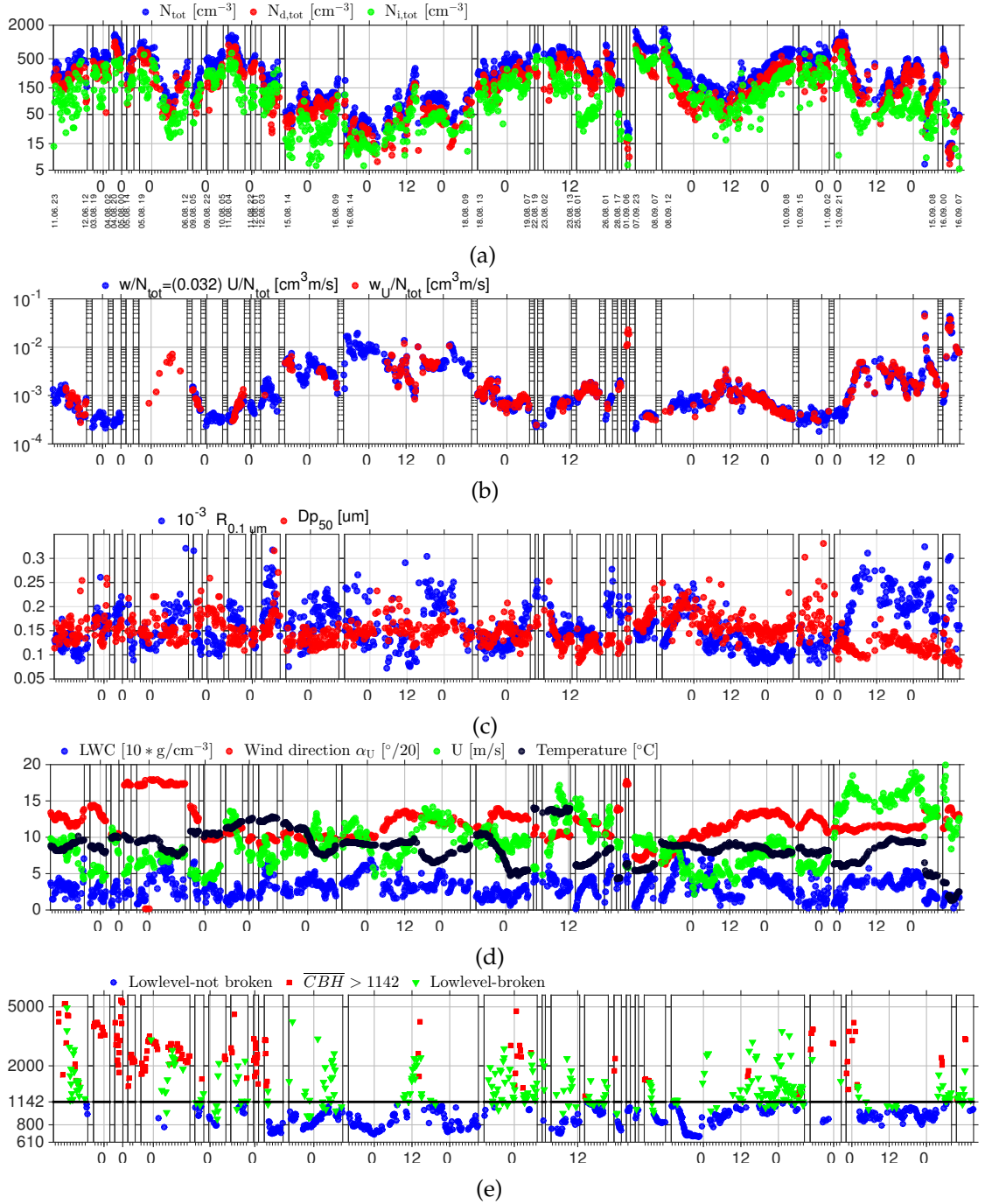
Figure 4.1: Measurement campaign overview from June 1 until September 16, 2010. Temporal variation of the (a) total aerosol number concentration N_{tot} (blue), total droplet number concentration $N_{\text{d,tot}}$ (red), and total interstitial aerosol number concentration $N_{i,tot}$ (green), with vertical start and end date (*dd.mm HH*) for each cloud event; (b) estimated w/N_{tot}-ratio (red) and prediction w/N_{tot} using horizontal wind speed for wind direction between $145°$ to $286°$ (blue); (c) aerosol size distribution shape $R_{0.1\ \mu\text{m}}$ (blue), and diameter of $50\ \%$ activation D_{50} (red); (d) liquid water content $LWC\ [\text{g}/\text{cm}^3]$ and meteorological parameters (horizontal wind speed U [m/s], wind direction, and temperature T); (e) average of the Lowest cloud base height over each DAA scan, as detected by the Ceilometer at the foot of Mt. Brocken. Note that in case of cloud measured at Mt. Brocken summit (1142 m a.s.l.) and broken cloud layer below Mt. Brocken, the average cloud base height can be higher than Mt. Brocken summit. (**PAPER IV**, [54])

Figure 4.2: (a) Potential Source Contribution Function for low N_{tot} ($N_{\text{tot}}<20^{\text{th}}$ percentile). (b) Potential Source Contribution Function for high N_{tot} ($N_{\text{tot}}>80^{\text{th}}$ percentile). (**PAPER IV**, [54])

trations observed at Mt. Brocken the Potential Source Contribution Function (**PSCF**; [53], [55]) was calculated using 48-h back trajectories arriving 100 m above Mt. Brocken summit (NOAA HYSPLIT model, [52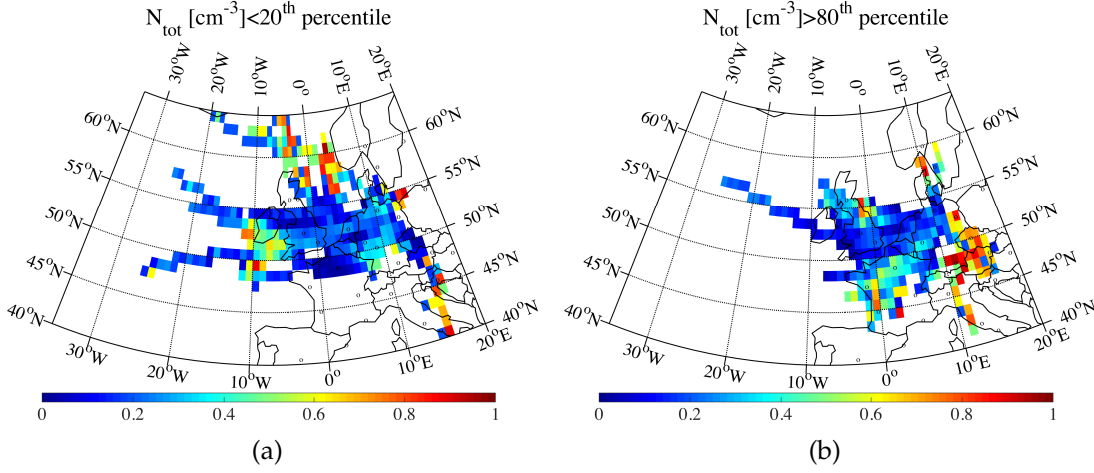]). During the measurement campaign low number concentration observed at Mt. Brocken occurs mainly under marine influenced air masses from west and north ($N_{\text{tot}}<20^{\text{th}}$ percentile, see Fig. 4.2(a)). The main source region for high number concentration levels are located southwest, south and east of Mt. Brocken (see Fig. 4.2(b)). These source regions are located in southern and eastern Germany, Czech Republic, Austria. Also air masses passing the Po Valley, which is renowned for its high air pollutant concentrations, lead to high number concentrations. Minor sources are located in northeast England and southwest France, and in the sea passage between Denmark and Norway.

4.2 Cloud Droplet Number Prediction

The fraction of aerosol particles activating into cloud droplets depends on the existence of aerosol particles suitable for activation under the existing meteorological conditions. The size and composition of the aerosol particles is important, but also the amount of water vapor that can contribute to supersaturation.

Reutter et al. [21] suggests three distinctly different regimes of cloud condensation nucleus (CCN) activation and droplet formation depending on the ratio between updraft velocity w [m/s] and aerosol number concentration N_{tot} [cm^{-3}]

at cloud base.

- In the aerosol-limited regime ($w/N_{\text{tot}} \gtrsim 10^{-3}\,\text{m}\,\text{s}^{-1}\,\text{cm}^{-3}$) droplet activation is limited by the number of aerosol particles. The number of cloud droplets is directly proportional to N_{tot} and independent of w.

- In the updraft-limited regime ($w/N_{\text{tot}} \lesssim 10^{-4}\,\text{m}\,\text{s}^{-1}\,\text{cm}^{-3}$) updraft velocity is limiting droplet activation and $N_{\text{d,tot}}$ is directly proportional to w and independent of N_{tot}.

- In the transitional regime, ($10^{-4}\,\text{m}\,\text{s}^{-1}\,\text{cm}^{-3} \lesssim w/N_{\text{tot}} \lesssim 10^{-3}\,\text{m}\,\text{s}^{-1}\,\text{cm}^{-3}$), $N_{\text{d,tot}}$ is non-linearly proportional to both w and N_{tot}.

In order to assess the droplet activation regime of the dataset the updraft velocity at cloud base is estimated using the same approach as Hoyle et al. [56].

Assuming that the flow lines for the updraft strictly follow the terrain with neither convergence or divergence the updraft velocity at cloud base w_U can be estimated using horizontal wind speed at Mt. Brocken summit U and the inclination angle of the hill slope α at cloud base:

$$w_U = \tan(\alpha)\,U. \qquad (4.1)$$

The inclination angle of the flow lines α at the cloud base is calculated by matching CBH and wind direction with topographical data. The inclination angle of the slope towards Mt. Brocken summit is up to 20° (see Fig. 3.2(b)), and even though there are surrounding subpeaks, they supposedly do not influence the wind field at Mt. Brocken [27].

There is a strong relation between the measured horizontal wind speed at Mt. Brocken U and the estimated updraft velocity w_U for wind directions between south and southwest (see Fig. 4.3(a)). There are cases for wind direction between 342° and 128°, where a given U induces a high updraft. This can have two reasons. The steeper slope towards the north can lead to higher updrafts w for the same vertical wind speed. The Ceilometer is located almost south of Mt. Brocken and it could be that Mt. Brocken and the surrounding subpeaks influence the cloud base height for northerly winds. From here on the updraft velocity w denotes the estimated updraft velocity for wind direction between 145° and 287° using the average relation $w = 0.032 \cdot U$ (see Fig. 4.3(a)).

With both approximate updraft velocity w and total number concentration N_{tot} the droplet activation can be characterized (see Fig. 4.3(b)). The major fraction of the measurements is located in the aerosol limited regime, but partly also in the transitional regime. In both regimes droplet number depends on N_{tot}, whereas the dependence on updraft is supposed to be weaker for the aerosol limited regime compared to the transitional regime.

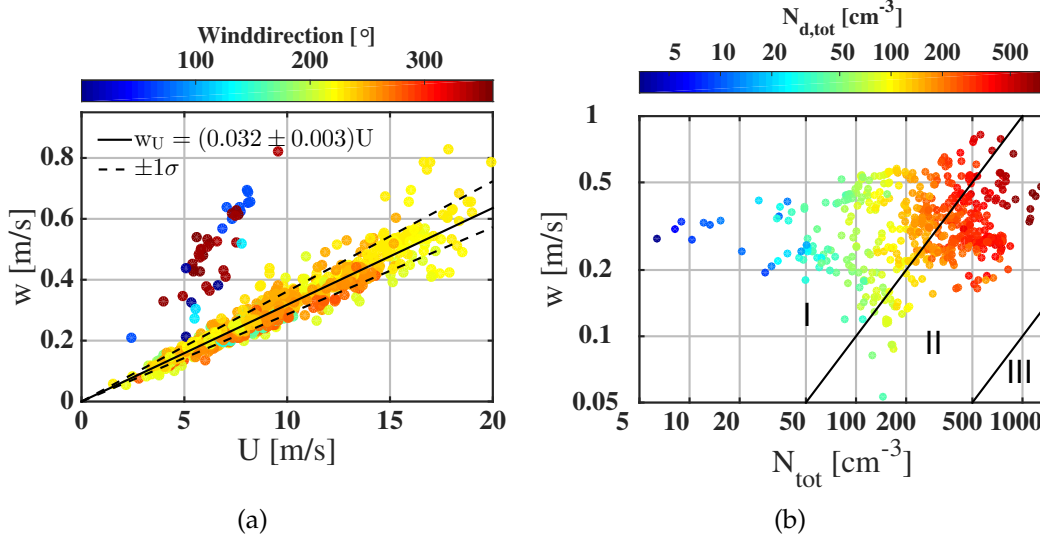(a)   (b)

Figure 4.3: (a) Relation between horizontal wind speed measured at top of Mt. Brocken U [m/s] and estimated updraft velocity w [m/s] at cloud base. Color indicates wind direction. (b) Relation between estimated updraft velocity at cloud base w [m/s] and N_{tot} [cm^{-3}] with cloud droplet number $N_{\text{d,tot}}$ [cm^{-3}] as color code. The black lines mark the approximate boarders between the three droplet activation regimes according to Reutter et al. [21] into (I) aerosol-limited regime ($w/N_{\text{tot}} \gtrsim 10^{-3} \, \text{m s}^{-1} \, \text{cm}^{-3}$), (II) transitional regime($10^{-4} \, \text{m s}^{-1} \, \text{cm}^{-3} \lesssim w/N_{\text{tot}} \lesssim 10^{-3} \, \text{m s}^{-1} \, \text{cm}^{-3}$), and (III) updraft-limited regime ($w/N_{\text{tot}} \lesssim 10^{-4} \, \text{m s}^{-1} \, \text{cm}^{-3}$). (**PAPER IV**, [54])

Therefore as non-linear approach a power-law for the prediction of total cloud droplet number concentration ($N_{\text{d,tot}}$) is used here. The relation includes total number concentration N_{tot}, predicted updraft velocity w [m/s], and in order to express the size distribution shape the number-to-volume concentration ratio $R_{0.1\,\mu\text{m}}$ [46]. A multiple linear regression model was run performing iteratively reweighted least squares multivariate regression. The estimated relation for the whole dataset is giving by

$$N_{\text{d,tot}}^{model} = 0.27 \, N_{\text{tot}}^{0.97} \, w^{0.37} \, R_{0.1\,\mu\text{m}}^{-0.17}. \tag{4.2}$$

The comparison between measured and predicted cloud droplet number gives a correlation coefficient of $R^2 = 0.89$. The standard deviation of the difference between modeled and measured $N_{\text{d,tot}}$ was $32\,\%$, with a maximum standard deviation of $54\,\%$. Even though no information about chemical composition of the particles is used in the model, the error in prediction of cloud droplet number is low. The obtained relation shows that the droplet number concentration is
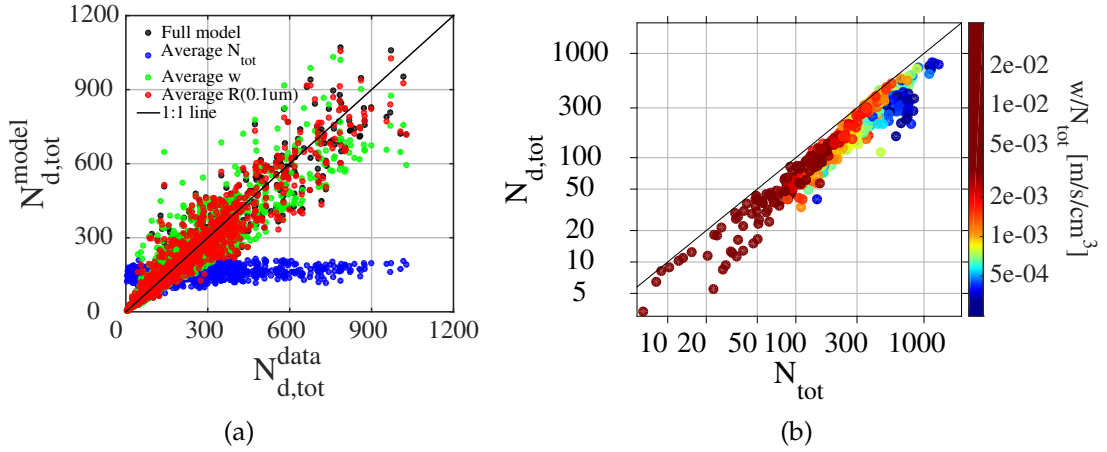
Figure 4.4: (a) Sensitivity of modeled droplet number concentration $N_{d,tot}^{model}$ when excluding the variation in aerosol properties (N_{tot}, U and $R_{0.1\ \mu m}$) and horizontal wind speed w measured at Mt. Brocken summit and using average instead. (b) Total number of cloud droplets $N_{d,tot}$ as function of total number number of particles N_{tot} with w/N_{tot}-ratio indicating cloud droplet activation regime according to Reutter et al. [21] as color code. (**PAPER IV**, [54])

most sensitive to the variation in total number concentration (Fig. 4.4(a)). When varying of the total number concentration in the model, but using the average w or $R_{0.1\ \mu m}$ respectively, the predicted cloud droplet number is still reasonable (green and red dots, respectively, in Fig. 4.4(a)). When neglecting the variability of N_{tot}, the predicted cloud droplet number differs strongly from the measured $N_{d,tot}$.

Assuming a constant wind speed U, and shape of the aerosol size distribution (R), the resulting model coefficients would indicate that a doubling of the total number concentration of aerosol particles would almost lead to a doubling of cloud droplet number (1.97$\pm$0.01) which is higher than suggested values by Feingold et al. [5] of 1.3 to 1.7 using linear regression of numerical model output. The power-law form used here (see eq. 4.2) suggests a 'roll-off', where an increase in N_{tot} does not lead to a proportional increase in $N_{d,tot}$, in case of an exponent of N_{tot} smaller than one.

Some previous results have shown a 'roll-off' of activated cloud droplet number at different total aerosol concentrations [22–24]. Other studies have not observed roll-off [25]. The relation between cloud droplet number and total aerosol depends on cloud dynamics and the size and composition of the aerosol [26]. When the droplet activation regime (w/N_{tot}) is examined (see Fig. 4.4(b)), the observed 'roll-off' could be due to a stronger dependence on the updraft
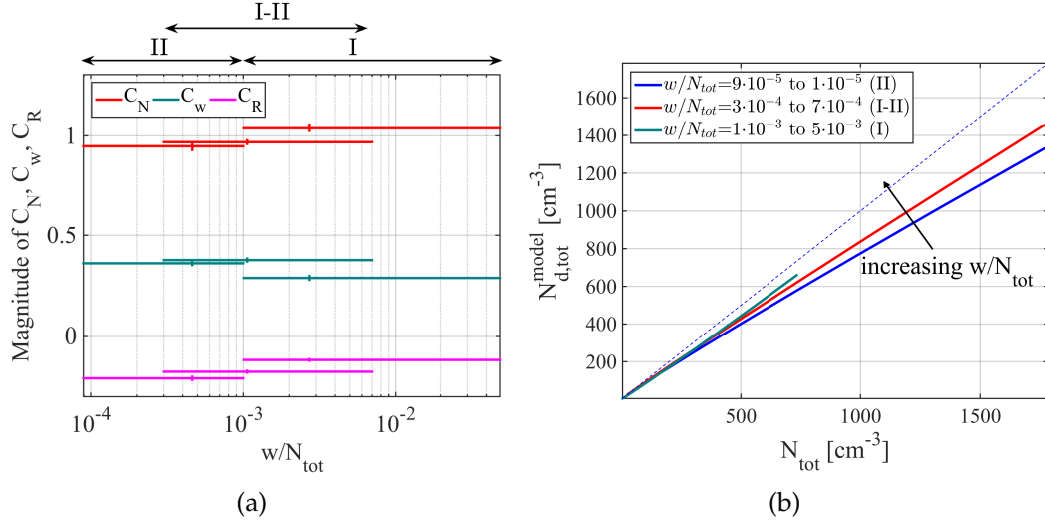
Figure 4.5: (a) w/N_{tot}-ratio dependency of the coefficients of each parameter used in the modeled droplet number concentration $N_{\text{d,tot}}^{model}$. (b) Total number of cloud droplets $N_{\text{d,tot}}$ as function of total number number of particles N_{tot} for different w/N_{tot}-intervals using a constant $R_{0.1\ \mu\text{m}}=300\ \mu\text{m}\ -3$. (**PAPER IV**, [54])

velocity. Thus, the 'roll-off' at different total aerosol levels could be due to the difference in w/N_{tot}-ratio and thus droplet activation regime.

In order to test this hypothesis the data were divided into three overlapping w/N_{tot}-intervals. The relation $N_{\text{d,tot}} \sim N_{\text{tot}}^{C_N}\ w^{C_w}\ R_{0.1\ \mu\text{m}}^{C_R}$ was estimated for each interval using a multiple linear regression model. The resulting exponents are presented in Figure 4.5(a) and Table 4.1. The relative sensitivity of $N_{\text{d,tot}}$ against w and N_{tot} is $\partial N_{\text{d,tot}}/\partial w = C_w$ and $\partial N_{\text{d,tot}}/\partial N_{\text{tot}} = C_N$ respectively. As expected, for increasing w/N_{tot}-ratio the relative sensitivity of $N_{\text{d,tot}}$ against w decreases while the relative sensitivity of $N_{\text{d,tot}}$ against N_{tot} increases. N_{tot} is determined in the dry diameter size range between 0.1 μm and 0.7 μm. Thus, in case droplets would form on particles with a dry diameter smaller than 0.1 μm, $N_{\text{d,tot}}$ could exceed N_{tot}, which would lead to an exponent C_N larger one.

An explanation for the 'roll-off" could be, that with sufficiently high aerosol concentration, aerosol particles compete for water vapor for the benefit of the larger particles, since they have a lower surface curvature and a higher amount of soluble material (water vapor depletion, [57]). This would lead to larger D_{50} [21] and the observed 'roll-off'.

When examining the w/N_{tot}-ratio in relation to droplet number and total aerosol number concentration, the observed 'roll-off'-onset shifts towards higher total number concentration when going towards the aerosol limited regime

	w/N_tot-interval	C_N	C_w	C_R	R^2	D_{50} [μm]	LWC [$\frac{\text{g}}{\text{cm}^3}$]	$R_{0.1\ \text{μm}}$ [m^{-3}]
II	$[9 \cdot 10^{-5}$ to $1 \cdot 10^{-3}]$	0.95	0.36	-0.21	0.85	0.158	0.234	143
I-II	$[3 \cdot 10^{-4}$ to $7 \cdot 10^{-3}]$	0.97	0.38	-0.18	0.93	0.144	0.287	153
I	$[1 \cdot 10^{-3}$ to $5 \cdot 10^{-2}]$	1.04	0.29	-0.12	0.95	0.134	0.325	169

Table 4.1: Exponents of the relation $N_\text{d,tot} \sim N_\text{tot}^{C_N}\ w^{C_w}\ R_{0.1\ \text{μm}}^{C_R}$ estimated for each w/N_tot-interval using a multiple linear regression model. Averages of D_{50}, LWC and $R_{0.1\ \text{μm}}$ for N_tot between 64 cm^{-3} and 561 cm^{-3}. I, I-II, and II according to Figure 4.5(a).

(for increasing w/N_tot-ratio), which supports the idea of w/N_tot-ratio dependent 'roll-off' at different total aerosol level (see Fig. 4.5(b)).

When comparing the model result when using N_tot only or both N_tot and w, including w does not improve the fit in terms of R^2 in the w/N_tot-interval between 1 10^{-3} and 5 10^{-2} (see Table 4.2). Thus, droplet activation is less dependent on updraft velocity when going towards the aerosol limited regime. The updraft velocity creates sufficiently high maximum supersaturation S_{max} to activate a major fraction of the total aerosol into cloud droplets.

For the same N_tot, higher updraft velocities w and maximum supersaturation S_{max} are expected in the aerosol limited regime compared to the transitional regime. Thus, water vapor depletion would occur at higher total aerosol concentrations, which could explain the difference in onset of the 'roll-off' in relation to w/N_tot-ratio.

	n	w/N_tot-interval	$C1_N$	R^2	$C2_N$	$C2_w$	R^2
II	663	$[9 \cdot 10^{-5}$ to $1 \cdot 10^{-3}]$	1.07	0.79	0.93	0.36	0.84
I-II	987	$[3 \cdot 10^{-4}$ to $7 \cdot 10^{-3}]$	1.01	0.91	0.99	0.31	0.93
I	513	$[1 \cdot 10^{-3}$ to $5 \cdot 10^{-2}]$	1.09	0.95	1.05	0.22	0.95

Table 4.2: Exponents of the relation $N_\text{d,tot} \sim N_\text{tot}^{C1_N}$ and $N_\text{d,tot} \sim N_\text{tot}^{C2_N}\ U^{C2_w}$ estimated for each interval using a multiple linear regression model. I, I-II, and II according to Figure 4.5(a), n is the number of data points in the interval.

The influence of the size distribution shape was not examined by Reutter et al. [21]. For the data set presented here, as expected, a shift of the size distribution towards smaller particles would lead to a decrease in cloud droplet number in all of the examined w/N_tot-intervals (see Fig. 4.6(a)). The relative sensitivity of $N_\text{d,tot}$ against $R_{0.1\ \text{μm}}$ is $\partial N_\text{d,tot}/\partial R_{0.1\ \text{μm}} = C_R$. The absolute relative sensitivity of $N_\text{d,tot}$ against $R_{0.1\ \text{μm}}$ increases from the aerosol limited towards the transitional

(a)
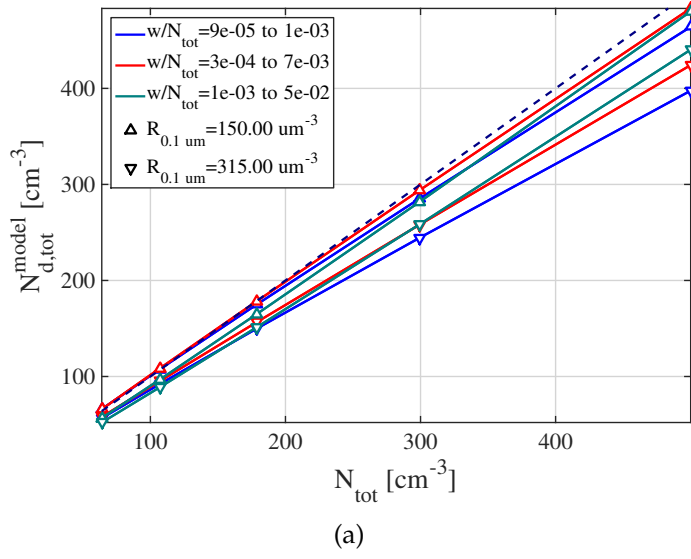
Figure 4.6: Total number of cloud droplets $N_{\mathrm{d,tot}}$ as function of total number number-ber of particles N_{tot} for different w/N_{tot}-intervals and $R_{0.1\ \mu m}=150$ and $315\ \mu m^{-3}$.

regime (decreasing w/N_{tot}-ratio). An explanation could be the lower updraft velocities w and thus lower maximum supersaturation reached in the transitional regime compared with the aerosol limited regime, for the same N_{tot}. Thus the size of the particles gets more important. Assuming similar chemical composition and $R_{0.1\ \mu m}$, for a lower maximum supersaturation the amount of the particles activated would decrease, leading to a lower fraction of activated particles and a lower $N_{\mathrm{d,tot}}$.

Chapter 5

Conclusion and Outlook

5.1 Conclusions

This thesis presents results of aerosol-cloud interaction measurements that have been performed with an improved, more automatic Droplet Aerosol Analyzer (DAA) with higher time resolution (10 min) than the previous version of the instrument. The DAA is unique in providing the number and the direct relationship between cloud droplet and residual particle size. Furthermore, the inversion algorithm was improved, with automatic fitting of the charge distribution in order to evaluate larger amounts of data.

Measurements have been performed between June and October 2010 at the summit of Mt. Brocken ($51.80°$ N, $10.62°$ E, 1142 m a.s.l.) in central Germany. The cloud droplet activation regime regarding the ratio between updraft velocity and particle number concentration (w/N_{tot}) was determined according to Reutter et al. [21].

The relation between cloud droplet number concentration $N_{\mathrm{d,tot}}$ and total number concentration N_{tot}, updraft velocity w_{pred}, and size distribution shape $R_{0.1\ \mu m}$ has been determined for three overlapping w/N_{tot}-intervals. As expected, for increasing w/N_{tot}-ratio (from the transitional regime towards aerosol limited regime) the relative sensitivity of $N_{\mathrm{d,tot}}$ against w decreases, while the relative sensitivity of $N_{\mathrm{d,tot}}$ against N_{tot} increases. The influence of the size distribution shape $R_{0.1\ \mu m}$ was examined and the absolute relative sensitivity of $N_{\mathrm{d,tot}}$ against $R_{0.1\ \mu m}$ was observed to decrease from the transitional towards the aerosol limited regime.

The onset of 'roll-off', where an increase in N_{tot} does not lead to a proportional increase in $N_{\mathrm{d,tot}}$, shifted towards higher total number concentration for increasing w/N_{tot}-ratio.

5.2 Relevance of the Obtained Results

Some previous measurements of the relation between cloud droplet number and total aerosol number show a 'roll-off' at different total aerosol levels [22–24] or not at all [25]. The relation between cloud droplet number and total aerosol depends on cloud dynamics and the size and composition of the aerosol [26]. In this data set the 'roll-off'-onset total number concentration was dependent on the difference in w/N_{tot} and droplet activation regime.

The presented results show that the relation between cloud droplet number and total aerosol number depends on droplet activation regime. Thus care has to be taken when using cloud parameterizations for other regimes than the one they have been determined in.

5.3 Outlook

In order to be able to compare cloud measurement performed at different locations, it is important to determine the range of validity of the measurements and the derived parametrization. It is, for example, difficult to compare the observed 'roll-off' level with previous measurements, since N_{tot} might not be the limiting factor at 'roll-off'. For decreasing w/N_{tot}-ratio the updraft velocity becomes more important for droplet formation. Thus the 'roll-off'-level could be characteristic for a specific w/N_{tot}-ratio.

Thus, most interesting for future measurements could be those conditions, where updraft velocity and/or hygroscopic properties and/or the size distribution shape of the aerosol activated play a significant role for cloud formation.

Another aspect not addressed in this thesis is the aerosol particle composition and hygroscopicity. Chemical effects on cloud droplet activation can be significant under some conditions compared to the effect of increased total aerosol number concentration [58]. A future goal would be to develop further dimensions of the regimes that include aerosol composition. A strong candidate for a parameter is the hygroscopicity parameter κ [59]. It is a single parameter describing the CCN activity and hygroscopic growth of atmospheric particles including solubility [60] and surface activity [61]. The importance of chemical composition, represented by κ with/without including solubility, in relation to updraft velocity and total aerosol number for cloud droplet was tested by Reutter et al. [21]. For continental atmospheric aerosols ($\kappa \sim 0.05$ to 0.6) the cloud droplet number was found to depend weakly on κ. However, hygroscopicity was found to play a significant role for very low hygoscopicity ($\kappa < 0.05$), as represented by submicron Saharan dust particles [62], or for hygroscopic aerosols ($\kappa > 0.3$) in the updraft limited regime, as for example in stratus clouds which might be more limited by updraft then by total aerosol number.

Acknowledgements

dass euch das manches mal an den Rand der Verzweiflung gebracht hat. Ich kann euch beruhigen, ihr seid damit nicht allein. Danke dass ihr mir meine Ausbildung ermöglicht habt, und danke für eure Unterstützung über all die Jahre.

Bibliography

[1] D. L. Hartmann, A. M. G. Klein Tank, M. Rusticucci, L. V. Alexander, S. Brönnimann, Y. Charabi, F. J. Dentener, E. J. Dlugokencky, D. R. Easterling, A. Kaplan, B. J. Soden, P. W. Thorne, M. Wild, and P. M. Zhai. Observations: Atmosphere and surface. In T. F. Stocker, D. Qin, G.-K. Plattner, M. Tignor, S. K. Allen, J. Boschung, A. Nauels, Y. Xia, V. Bex, and P. M. Midgley, editors, *Climate change 2013: The physical science basis. Contribution of working group I to the fifth assessment report of the intergovernmental panel on climate change*, book section 2, page 96. Cambridge University Press, Cambridge, United Kingdom and New York, NY, USA, 2013. ISBN 978-1-107-66182-0.

[2] C. J. Stubenrauch, W. B. Rossow, S. Kinne, S. Ackerman, G. Cesana, H. Chepfer, L. Di Girolamo, B. Getzewich, A. Guignard, A. Heidinger, B. C. Maddux, W. P. Menzel, P. Minnis, C. Pearl, S. Platnick, C. Poulsen, J. Riedi, S. Sun-Mack, A. Walther, D. Winker, S. Zeng, and G. Zhao. Assessment of global cloud datasets from satellites: Project and database initiated by the GEWEX radiation panel. *Bulletin of the American Meteorological Society (BAMS)*, 94(7):1031–1049, 2013.

[3] A. Donohoe and D. S. Battisti. Atmospheric and surface contributions to planetary albedo. *Journal of Climate*, 24(16):4402 – 4418, 2011. ISSN 08948755.

[4] J. Warner and S. Twomey. The production of cloud nuclei by cane fires and the effect on cloud droplet concentration. *Journal of Atmospheric Sciences*, 24:704–706, November 1967.

[5] G. Feingold, L. A. Remer, J. Ramaprasad, and Y. J. Kaufman. Analysis of smoke impact on clouds in brazilian biomass burning regions: An extension of twomey's approach. *Journal of Geophysical Research: Atmospheres*, 106(D19):22907–22922, 2001. ISSN 2156-2202.

[6] IPCC. Summary for policymakers. In T. F. Stocker, D. Qin, G.-K. Plattner, M. Tignor, S. K. Allen, J. Boschung, A. Nauels, Y. Xia, V. Bex, and P. M. Midgley, editors, *Climate change 2013: The physical science basis.*

Contribution of working group I to the fifth assessment report of the intergovernmental panel on climate change, book section SPM, page 28. Cambridge University Press, Cambridge, United Kingdom and New York, NY, USA, 2013. ISBN 978-1-107-66182-0.

[7] A. D. Lopez, C. D. Mathers, M. Ezzati, D. T. Jamison, and C. J. L. Murray. Global and regional burden of disease and risk factors, 2001: systematic analysis of population health data. *The Lancet*, 367(9524):1747 – 1757, 2006. ISSN 0140-6736.

[8] J. Löndahl, E. Swietlicki, E. Lindgren, and S. Loft. Aerosol exposure versus aerosol cooling of climate: what is the optimal emission reduction strategy for human health? *Atmospheric Chemistry and Physics*, 10(19): 9441–9449, 2010.

[9] G. Myhre, D. Shindell, F.-M. Bréon, W. Collins, J. Fuglestvedt, J. Huang, D. Koch, J.-F. Lamarque, D. Lee, B. Mendoza, T. Nakajima, A. Robock, G. Stephens, T. Takemura, and H. Zhang. Anthropogenic and natural radiative forcing. In T. F. Stocker, D. Qin, G.-K. Plattner, M. Tignor, S. K. Allen, J. Boschung, A. Nauels, Y. Xia, V. Bex, and P. M. Midgley, editors, *Climate Change 2013: The Physical Science Basis. Contribution of Working Group I to the Fifth Assessment Report of the Intergovernmental Panel on Climate Change*, book section 8, pages 659–740. Cambridge University Press, Cambridge, United Kingdom and New York, NY, USA, 2013. ISBN 978-1-107-66182-0.

[10] S. Twomey. Pollution and the planetary albedo. *Atmospheric Environment (1967)*, 8(12):1251 – 1256, 1974.

[11] D. Rosenfeld. Suppression of rain and snow by urban and industrial air pollution. *Science*, 287(5459):1793–1796, 2000.

[12] B. A. Albrecht. Aerosols, cloud microphysics, and fractional cloudiness. *Science*, 245:1227–1230, 1989.

[13] J. D. Small, P. Y. Chuang, G. Feingold, and H.i Jiang. Can aerosol decrease cloud lifetime? *Geophysical Research Letters*, 36(16):n/a–n/a, 2009. ISSN 1944-8007. L16806.

[14] I. Koren, Y. J. Kaufman, D. Rosenfeld, L. A. Remer, and Y. Rudich. Aerosol invigoration and restructuring of atlantic convective clouds. *Geophysical Research Letters*, 32(14), 2005.

[15] I. Koren, Y. J. Kaufman, L. A. Remer, and J. V. Martins. Measurement of the effect of amazon smoke on inhibition of cloud formation. *Science*, 303 (5662):1342–1345, 2004.

[16] R. G. Knollenberg. Techniques for probing cloud microstructure. In *Clouds - Their formation, optical properties, and effects; Proceedings of the Symposium, Williamsburg, VA, May 13, 14, 1980. (A82-12426 02-47) New York, Academic Press, 1981, p. 15-89; Discussion, p. 90, 91.*, pages 15–89, 1981.

[17] B. G. Martinsson. Physical basis for a droplet aerosol analysing method. *Journal of Aerosol Science*, 27(7):997 – 1013, 1996.

[18] G. P. Frank, S.-I. Cederfelt, and B. G. Martinsson. A method for studies of the interaction between atmospheric aerosol particles and cloud and fog droplets. *Journal of Aerosol Science*, 29(Supplement 2):S871 – S872, 1998.

[19] B. G. Martinsson, G. Frank, S.-I. Cederfelt, O. H. Berg, B. Mentes, G. Papaspiropoulos, E. Swietlicki, J. Zhou, M. Flynn, K. N. Bower, T. W. Choularton, J. Mäkelä, A. Virkkula, and R. Van Dingenen. Validation of very high cloud droplet number concentrations in air masses transported thousands of kilometres over the ocean. *Tellus B*, 52(2):801–814, 2000.

[20] B. G. Martinsson, G. P. Frank, S.-I. Cederfelt, E. Swietlicki, O. H. Berg, J. Zhou, K. N. Bower, C. Bradbury, W. Birmili, F. Stratmann, M. Wendisch, A. Wiedensohler, and B. A. Yuskiewicz. Droplet nucleation and growth in orographic clouds in relation to the aerosol population. *Atmospheric Research*, 50(3-4):289 – 315, 1999.

[21] P. Reutter, H. Su, J. Trentmann, M. Simmel, D. Rose, S. S. Gunthe, H. Wernli, M. O. Andreae, and U. Pöschl. Aerosol- and updraft-limited regimes of cloud droplet formation: influence of particle number, size and hygroscopicity on the activation of cloud condensation nuclei (ccn). *Atmospheric Chemistry and Physics*, 9(18):7067–7080, 2009.

[22] W. R. Leaitch, G. A. Isaac, J. W. Strapp, C. M. Banic, and H. A. Wiebe. The relationship between cloud droplet number concentrations and anthropogenic pollution: Observations and climatic implications. *Journal of Geophysical Research: Atmospheres*, 97(D2):2463–2474, 1992. ISSN 2156-2202.

[23] P. Glantz and K. J. Noone. A physically-based algorithm for estimating the relationship between aerosol mass and cloud droplet number. *Tellus B*, 52(5):1216–1231, 2000.

[24] K. N. Bower, T. W. Choularton, M. W. Gallagher, K. M. Beswick, M. J. Flynn, A. G. Allen, B. M. Davison, J. D. James, L. Robertson, R. M. Harrison, C. N. Hewitt, J. N. Cape, G. G. McFadyen, C. Milford, M. A Sutton, B. G. Martinsson, G. Frank, E. Swietlicki, J. Zhou, O. H. Berg, B. Mentes, G. Papaspiropoulos, H.-C. Hansson, C. Leck, M. Kulmala, P. Aalto, M. Väkevä, A. Berner, M. Bizjak, S. Fuzzi, P. Laj, M.-C. Facchini, G. Orsi, L. Ricci, M. Nielsen, B. J. Allan, H. Coe, G. McFiggans, J. M. C. Plane, J. L. Collett, K. F. Moore, and D. E. Sherman. Ace-2 hillcloud. an overview of the ace-2 ground-based cloud experiment. *Tellus B*, 52(2): 750–778, 2000. ISSN 1600-0889.

[25] D. A. Hegg, D. S. Covert, H. H. Jonsson, and R. K. Woods. A simple relationship between cloud drop number concentration and precursor aerosol concentration for the regions of earth's large marine stratocumulus decks. *Atmospheric Chemistry and Physics*, 12(3):1229–1238, 2012.

[26] R. L. Modini, A. A. Frossard, L. Ahlm, L. M. Russell, C. E. Corrigan, G. C. Roberts, L. N. Hawkins, J. C. Schroder, A. K. Bertram, R. Zhao, A. K. Y. Lee, J. P. D. Abbatt, J. Lin, A. Nenes, Z. Wang, A. Wonaschütz, A. Sorooshian, K. J. Noone, H. Jonsson, J. H. Seinfeld, D. Toom-Sauntry, A. M. Macdonald, and W. R. Leaitch. Primary marine aerosol-cloud interactions off the coast of california. *Journal of Geophysical Research: Atmospheres*, 120(9):4282–4303, 2015. ISSN 2169-8996.

[27] K. Acker, D. Möller, W. Wieprecht, D. Kalaß, and R. Auel. Investigations of ground-based clouds at the mt. brocken. *Fresenius' Journal of Analytical Chemistry*, 361(1):59–64, 1998.

[28] D. Möller, K. Acker, and W. Wieprecht. A relationship between liquid water content and chemical composition in clouds. *Atmospheric Research*, 41:321 – 335, 1996. ISSN 0169-8095. Cloud-Aerosol Interactions.

[29] K. Acker, D. Möller, W. Wieprecht, R. Auel, D. Kalass, and W. Tscherwenka. Nitrous and nitric acid measurements inside and outside of clouds at mt. brocken. *Water, Air, and Soil Pollution*, 130(1-4): 331–336, 2001. ISSN 0049-6979.

[30] K. Acker, Mertes S., Möller D., W. Wieprecht, and R. Auel. Case study of cloud physical and chemical processes in low clouds at mt. brocken. *Atmospheric Research*, 64(14):41 – 51, 2002. ISSN 0169-8095. 2nd International Conference on Fog and Fog Collection.

[31] G. P. Frank, M. I. A. Berghof, S. Sjogren, and B. G. Martinsson. Development of the droplet aerosol analyser for long-term unattended in-cloud measurements of aerosol-cloud interactions. 2015.

[32] M. I. A. Berghof, G. P. Frank, S. Sjogren, and B. G. Martinsson. Inversion of droplet aerosol analyzer data for long-term aerosol-cloud interaction measurements. *Atmospheric Measurement Techniques*, 7(4):877–886, 2014.

[33] S. Sjogren, G. P. Frank, M. I. A. Berghof, and B. G. Martinsson. Continuous stand-alone controllable aerosol/cloud droplet dryer for atmospheric sampling. *Atmospheric Measurement Techniques*, 6(2):349–357, 2013.

[34] G. P. Frank, S.-I. Cederfelt, and B. G. Martinsson. Characterisation of a unipolar charger for droplet aerosols of 0.1-20 μm in diameter. *Journal of Aerosol Science*, 35(1):117 – 134, 2004.

[35] P. Intra and N. Tippayawong. An overview of differential mobility analyzers for size classification of nanometer-sized aerosol particles. *Songklanakarin J. Sci. Technol*, 30(2):243–256, 2008.

[36] B. G. Martinsson, M. N. A. Karlsson, and G. Frank. Metodology to estimate the transfer function of individual differential mobility analyzers. *Aerosol Science and Technology*, 35:815–823, 2001.

[37] M. N. A. Karlsson and B. G. Martinsson. Methods to measure and predict the transfer function size dependence of individual dmas. *Journal of Aerosol Science*, 34:603–625, 2003.

[38] P. A. Lawless. Particle charging bounds, symmetry rrelation, and an analytic charging rate model for the continuum regime. *Lournal of Aerosol Science*, 27:191–215, 1996.

[39] W. C Hinds. *Aerosol technology: properties, behavior, and measurement of airborne particles*. John Wiley & Sons, 2012.

[40] A. Wiedensohler. An approximation of the bipolar charge distribution for particles in the submicron size range. *Journal of Aerosol Science*, 19(3): 387–389, 6 1988.

[41] W. A. Hoppel and G. M. Frick. The nonequilibrium character of the aerosol charge distributions produced by neutralizes. *Aerosol Science and Technology*, 12(3):471–496, 1990.

[42] H. Tammet. Reduction of air ion mobility to standard conditions. *Journal of Geophysical Research: Atmospheres*, 103(D12):13933–13937, 1998. ISSN 2156-2202.

[43] S.-I. Cederfelt, B. G. Martinsson, B. Svenningsson, A. Wiedensohler, G. Frank, H.-C. Hansson, E. Swietlicki, M. Wendish, K. M. Beswick, K. N. Bower, M. W. Gallagher, S. Pahl, R. Maser, and D. Schell. Field validation of the droplet aerosol analyser. *Atmospheric Environment*, 31(16):2657 – 2670, 1997. ISSN 1352-2310. The Great Dun Fell Cloud Experiment 1993, Eurotrac sub-project Ground-based Cloud Experiment (GCE).

[44] M. R. Stolzenburg. *An ultrafine aerosol size distribution measuring system.* PhD thesis, University of Minnesota, 1988.

[45] S. P. Belyaev and L. M. Levin. Techniques for collection of representative aerosol samples. *Journal of Aerosol Science*, 5(4):325 – 338, 1974. ISSN 0021-8502.

[46] N. Kivekäs, V.-M. Kerminen, T. Anttila, H. Korhonen, H. Lihavainen, M. Komppula, and M. Kulmala. Parameterization of cloud droplet activation using a simplified treatment of the aerosol number size distribution. *Journal of Geophysical Research: Atmospheres*, 113(D15), 2008. ISSN 2156-2202. D15207.

[47] D. Hertel and D. Schöling. Below-ground response of Norway spruce to climate conditions at Mt. Brocken (Germany)–A re-assessment of Central Europe's northernmost treeline. *Flora - Morphology, Distribution, Functional Ecology of Plants*, 206(2):127 – 135, 2011. ISSN 0367-2530.

[48] G. Adrian and F. Fiedler. Simulation of unstationary wind and temperature fields over complex terrain and comparison with observations. *Beitr. Phys. Atmosph.*, 64:27–48, 1991. cited By 96.

[49] F. Beyrich, K. Acker, D. Kalaß, O. Klemm, D. Möller, E. Schaller, J. Werhahn, and U. Weisensee. Boundary layer structure and photochemical pollution in the Harz Mountains – An observational study. *Atmospheric Environment*, 30(8):1271 – 1281, 1996. ISSN 1352-2310.

[50] Vaisala. *Ceilometer CT25 User's Guide.* Vaisala, Helsinki, Finland, ct25k-u059en-2.1 edition, 1999.

[51] S. G. Gopalakrishnan, S. Baidya Roy, and R. Avissar. An evaluation of the scale at which topographical features affect the convective boundary layer

using large eddy simulations. *Journal of Atmospheric Sciences*, 57:334–351, January 2000.

[52] R. R. Draxler and G. D. Rolph. Hysplit (hybrid single-particle lagrangian integrated trajectory) model access via noaa arl ready website (http://ready.arl.noaa.gov/hysplit.php). NOAA Air Resources Laboratory, Silver Spring, MD, 2013.

[53] P. K. Hopke, L. A. Barrie, S.-M. Li, M.-D. Cheng, C. Li, and Y. Xie. Possible sources and preferred pathways for biogenic and non-sea-salt sulfur for the high arctic. *Journal of Geophysical Research: Atmospheres*, 100(D8): 16595–16603, 1995. ISSN 2156-2202.

[54] M. I. A. Berghof, B. Svenningsson, G. P. Frank, S. Sjogren, and B. G. Martinsson. Daa field study on cloud droplet activation related to aerosol updraft regimes. 2015.

[55] J. Crawford, S. Chambers, L. Cohen, D. D. andDyer, T. Wang, and W. Zahorowski. Receptor modelling using positive matrix factorisation, back trajectories and radon-222. *Atmospheric Environment*, 41(32):6823 – 6837, 2007. ISSN 1352-2310.

[56] C. R. Hoyle, C. S. Webster, H. E. Rieder, E. Hammer, M. Gysel, N. Bukowiecki, E. Weingartner, M. Steinbacher, and U. Baltensperger. Chemical and physical influences on aerosol activation in liquid clouds: an empirical study based on observations from the jungfraujoch, switzerland. *Atmospheric Chemistry and Physics Discussions*, 15(11): 15469–15510, 2015.

[57] S. J. Ghan, L. R. Leung, R. C. Easter, and H. Abdul-Razzak. Prediction of cloud droplet number in a general circulation model. *Journal of Geophysical Research: Atmospheres*, 102(D18):21777–21794, 1997. ISSN 2156-2202.

[58] A. Nenes, R. J. Charlson, M. C. Facchini, M. Kulmala, A. Laaksonen, and J. H. Seinfeld. Can chemical effects on cloud droplet number rival the first indirect effect? *Geophysical Research Letters*, 29(17):29–1, 2002.

[59] M. D. Petters and S. M. Kreidenweis. A single parameter representation of hygroscopic growth and cloud condensation nucleus activity. *Atmospheric Chemistry and Physics*, 7(8):1961–1971, 2007.

[60] M. D. Petters and S. M. Kreidenweis. A single parameter representation of hygroscopic growth and cloud condensation nucleus activity–part 2:

Including solubility. *Atmospheric Chemistry and Physics*, 8(20):6273–6279, 2008.

[61] M. D. Petters and S. M. Kreidenweis. A single parameter representation of hygroscopic growth and cloud condensation nucleus activity–part 3: Including surfactant partitioning. *Atmospheric Chemistry and Physics*, 13(2): 1081–1091, 2013.

[62] K. A. Koehler. *The impact of natural dust aerosol on warm and cold cloud formation.* PhD thesis, Colo. State Univ., Fort Collins., 2008.

Paper I: Continuous stand-alone controllable aerosol/cloud droplet dryer for atmospheric sampling

Paper I

Atmospheric
Measurement
Techniques

Open Access

Continuous stand-alone controllable aerosol/cloud droplet dryer for atmospheric sampling

S. Sjogren, G. P. Frank, M. I. A. Berghof, and B. G. Martinsson

Division of Nuclear Physics, Lund University, Lund, Sweden

Correspondence to: S. Sjogren (staffan.sjogren@yahoo.com)

Abstract. We describe a general-purpose dryer designed for continuous sampling of atmospheric aerosol, where a specified relative humidity (RH) of the sample flow (lower than the atmospheric humidity) is required. It is often prescribed to measure the properties of dried aerosol, for instance for monitoring networks. The specific purpose of our dryer is to dry cloud droplets (maximum diameter approximately $25 \, \mu m$, highly charged, up to 5×10^2 charges). One criterion is to minimise losses from the droplet size distribution entering the dryer as well as on the residual dry particle size distribution exiting the dryer. This is achieved by using a straight vertical downwards path from the aerosol inlet mounted above the dryer, and removing humidity to a dry, closed loop airflow on the other side of a semi-permeable GORE-TEX membrane (total area $0.134 \, m^2$).

The water vapour transfer coefficient, k, was measured to be $4.6 \times 10^{-7} \, kg \, m^{-2} \, s^{-1} \, \% \, RH^{-1}$ in the laboratory (temperature 294 K) and is used for design purposes. A net water vapour transfer rate of up to $1.2 \times 10^{-6} \, kg \, s^{-1}$ was achieved in the field. This corresponds to drying a $5.7 \, L \, min^{-1}$ ($0.35 \, m^3 \, h^{-1}$) aerosol sample flow from 100 % RH to 27 % RH at 293 K (with a drying air total flow of $8.7 \, L \, min^{-1}$). The system was used outdoors from 9 May until 20 October 2010, on the mountain Brocken (51.80° N, 10.67° E, 1142 m a.s.l.) in the Harz region in central Germany. Sample air relative humidity of less than 30 % was obtained 72 % of the time period. The total availability of the measurement system was > 94 % during these five months.

1 Introduction

Atmospheric aerosol is important for climate. Large efforts are done to systematically investigate and monitor its properties. Many aerosol properties vary with relative humidity (RH). For measurements, and especially for data quality concerns for comparisons between stations/networks, a dry aerosol is important. Aerosol dryers and the drying process have been described previously (e.g. Martinsson et al., 1992). An automatically regenerating dryer has recently been presented by Tuch et al. (2009); see references therein for additional drying methods. That dryer used a three-way valve alternating between two silica gel dryers. Transmission for that system was well characterized in the diameter size range from 3 to 800 nm. The 50 % transmission for larger particles was calculated at 6 μm diameter. In our application we want to extend the aerosol measurement size range to drying of larger particles and cloud/fog droplets up to 25 μm diameter, which require a straight vertical path, in order to reduce impaction and sedimentation losses. This excludes the use of a standard valve or tee. The dryer should also work continuously. Therefore the design presented in this paper was used. In addition, the drying airflow rate can be varied to maintain a set RH (lower than ambient) in the sample flow, should that be required (in the future an additional humidifying setup can also be envisaged to maintain constant say 25 % RH). A closed loop for the drying air was designed for minimum variability due to flow changes and gas transfer into the aerosol sample flow.
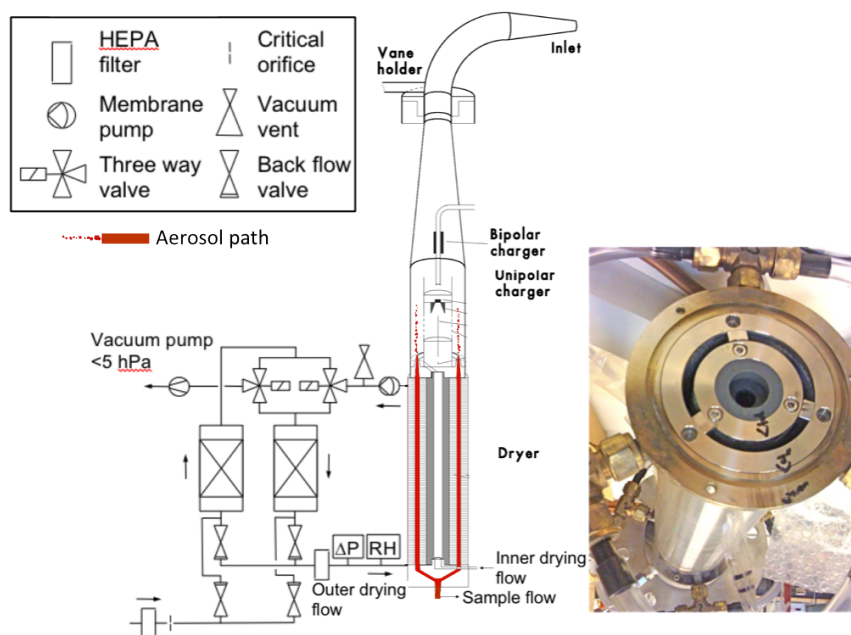
Fig. 1. Schematic drawing of the inlet part of the DAA with dryer and dry air regeneration system of the outer drying air (left panel) and photo of the entry to the dryer only (right panel). The aerosol sample flows downwards into the three slots; the metal nets are visible on the inside of the slots. The central circular hole is for the exit flow of the inner drying airflow. Further details of the inlet, situated above the dryer, are found in Frank et al. (2004).

2 Materials and methods

Below the criteria for designing a dryer are detailed, as well as the method to measure the particle transmission and the water vapour removal of the dryer.

2.1 Design criteria

The main principle of the dryer is to dry sample air flowing vertically downwards in counterflow with dry airflows, these flows being separated by membranes. Two concentric, cylindrical membranes were used, with the sample flow in the middle, annularly, between the dry airflows (see Fig. 1). The membrane is needed due to different flow velocities and flow directions of sample flow and drying flow, which would otherwise result in mixing between the two. The membrane allows water vapour exchange by diffusion, but no particle transfer. The two dry airflows used are arranged in closed loops, in order to prevent leakage of air between sample flow and either closed loop flow through the membrane. The closed loops should be tight and of good quality, to avoid leaks developing over time.

The actual dryer described here is used for an instrument measuring cloud droplet size distributions, the droplet aerosol analyser (DAA) (Martinsson, 1996). The DAA requires typical cloud droplets to be transported by a flow vertically into and inside the dryer, at least until dried to submicrometer-sized droplets or particles, in order to mini-

mize droplet losses due to impaction. Such losses prevent us from using any ordinary type of valve before the drying process, and we have thus chosen a straight vertical path from the inlet through the dryer. Further details of the inlet situated above the dryer are found in Frank et al. (2004). The dryer considered consists of two concentric, cylindrical stainless steel mesh metal nets (wire diameter 0.35 mm, open area 2.25 mm^2) (see Fig. 1), with the sample flow in the middle between these. On the other sides of the metal nets are two cylindrical membranes (inner and outer membrane tube). The plastic fiber mats (see below) supporting these membranes face towards the metal nets and the aerosol flow. Two separate closed loop dry airflows circulate on each of the other sides of the membrane tubes, achieving the transfer of humidity from the sample flow due to the humidity gradient (pumps used are model 6025se/12vdc, Thomas, USA). The metal nets reduce electrostatic charging of the membranes and are fixed and grounded to the stainless steel main housing of the dryer, and also act to stabilise the membranes mechanically (Ogren et al., 1985).

As a design criterion a sufficient transfer rate of water vapour is required to maintain the dried sample flow below a user-specified maximum RH. This specified RH and the minimum expected temperature of the dried sample flow define the maximum allowed specific humidity tolerated, after drying. The ambient corresponding parameters to consider for this criterion are the estimated maximum ambient RH and

Table 1. Characteristics of the two tubes used in the DAA dryer, and resulting characteristics for the aerosol flow space in between, at sample flow 5.5 L min^{-1} (0.33 m^3 h^{-1}). For that sample flow a dry airflow of at least 5 and 6.5 L min^{-1} for the inner and outer side is recommended.

Parameters	Inner tube, inner flow	Outer tube, outer flow	Sample flow/air space
GORE-TEX order number	Industrial dry filtration bag	Industrial dry filtration bag	–
(tubes, welded at seam)	4327 4327c53-0415	4327 4327T67-0415	–
Diameter [mm]	D_{Outer}: 53.2	D_{Inner}: 67.2	–
Length [mm]	415 ($\pm$3)	415 ($\pm$3)	405
Area, effective [m^2]	0.058	0.076	0.134
Airflow [L min^{-1}]	5	6.5	5.5
Width [mm]	–	–	12
Top cross-section [m^2]	–	–	0.0011
Airflow velocity [m s^{-1}]	0.13	0.12	0.084
Residence time [s]	3	3.3	5.5
Reynolds number [−]	71	64	78 (laminar)

the maximum ambient temperature (i.e. the maximum ambient specific humidity), at times when drying is required. The difference between these two values of specific humidities determines the transfer rate of water vapour required, for a given sample flow. This transfer rate, in turn, determines the area of the membrane (A_{mem}) needed, and as well defines the drying airflow rate required, which takes up the humidity. We used GORE-TEX membrane due to performance, flexibility in fabrication options and dimensions, as well as having former experience with this type (Weingartner et al., 2002). The GORE-TEX membrane itself is thin and fragile and must be fixed on a holding surface, such as textile or plastic fiber mat (we chose plastic). For our setup, tests we made (at 294 K) resulted in a practical water vapour transfer coefficient, k, of 4.6×10^{-7} kg m^{-2} s^{-1} % RH^{-1} from the humid to the dry side, defined as the amount of water vapour passing 1 m^2 membrane per s per % RH difference between the two sides of the membrane. % RH is chosen as the unit here as that is most readily available during measurements. The transfer rate for a membrane can vary substantially with temperature, due to physical changes in the microstructure of the membrane material, influencing its porosity. The dryer has a total effective area of 0.134 m^2 (see Table 1).

Once the area of the membrane has been chosen, several design geometries can be proposed. One can envisage for instance a maximum distance from a sample air streamline to the dry airflow in order to avoid too large inhomogeneities in humidity in the sample flow, as well as a simpler geometry than ours, with only one layer of membrane used (one tube, with aerosol in the middle and dry air on the outside; however, then practical limitations on length might occur for a given drying capacity). Further design geometry considerations are outside the scope of this paper. However, there are three further design criteria to be considered once the area is determined: limitations of *diffusion and impaction losses* (e.g. von der Weiden et al., 2009), *electrostatic losses* (Fuchs, 1989) and *residence time needed for drying*. These will be briefly described in the following three sections. The criteria could be less stringent if only submicrometer aerosol were dried, or one criterion might require more attention, such as diffusion losses if nanoparticles should be studied, for instance.

2.1.1 Diffusion/impaction losses

The purpose of the DAA is to measure submicrometer aerosol down to a minimum dry size, D_p, of about 50 nm. For D_p 50 nm particles, the fraction penetrating the dryer due solely to diffusion losses (from top to bottom, tubing afterwards not included) is larger than 99.7 % according to theoretical calculations, which is acceptable. We used the equation describing diffusional losses under laminar conditions, i.e. the transport efficiency (Willeke and Baron, 2005):

$$\eta_{diff} = e^{(-\xi Sh)}, \tag{1}$$

where Sh is the Sherwood number; the dimensionless diffusion parameter, $\xi = \pi D L/Q$, where D is the particle diffusion coefficient, L is the tube length and Q is the flow rate. On the other hand for 3-nm-diameter particles, if that were the aim of a study, the fraction penetrating is theoretically only about 87 %, where an improvement would require optimal flow rate (towards limit of turbulence) and shortest possible dryer length, for a specified required drying capacity. For particles larger than D_p 50 nm, diffusion losses are negligible for many applications, but for supermicron particles impaction and sedimentation losses become important. When the dryer is used in the DAA, the flow field arrangement allows cloud droplets to be transported vertically into the cross-section between the two membranes, where they dry out (see below) and become residual particles. The residual particle size distribution is measured and is typically in submicrometer-size (depending on measurement site), with low losses as mentioned above. If supermicrometer-sized dry aerosol particles were a topic of a study, the exit of a dryer and the following tubing used in relevant instrumentation would require careful design (design tactics: straight, vertical
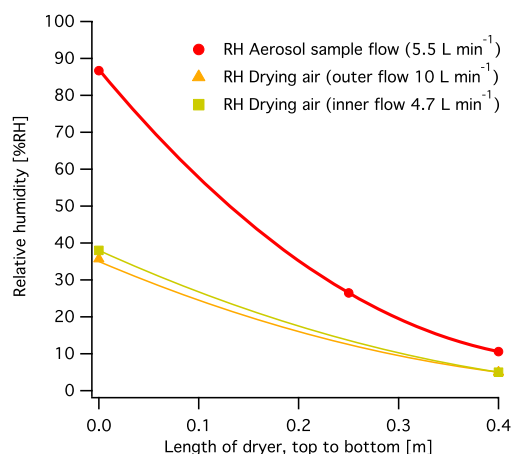
Fig. 2. RH profiles inside the dryer. Points are measurements, lines a guide to the eye, assuming a logarithmic function describing the water vapour removal.

and few diameter contractions); see von der Weiden et al. (2009).

2.1.2 Electrostatic losses

The GORE-TEX membrane is made of highly resistive PTFE (teflon) and as such can acquire electrostatic charging locally inside the dryer. Static charging would result in an electric field, which would influence charged aerosol particles with a force, causing them to move. Assuming the charge is situated at a point on the membrane wall, the particle trajectory would be affected, and if arriving at the dryer wall would mostly be deposited there; i.e. this process would result in a lower fraction of aerosol particles penetrating. Collisions with other (neutral, or larger, with lower mobility) aerosol particles would during this transport be negligible, due to the often low total concentrations in the DAA. In order to reduce electrostatic charging and thus to reduce the resulting electric field in the dryer, grounded metal nets are fitted on both sides facing the sample flow (see above). Furthermore, if the particles are charged, they might themselves create an electric field (Fuchs, 1989) resulting in particle movements, called electrostatic scattering. Measurements done in laboratory confirmed that no significant ($< 5\%$) losses of accumulation mode sized particles occur for up to 1000 charges on each single particle and relevant concentrations in the dryer, which was also noted by Martinsson (1996).

2.1.3 Residence time

Residence time needed to dry the largest ambient droplets that contain relevant aerosol for the study in question must be guaranteed. Otherwise the losses, especially for the larger aerosol particles, will increase by impaction and sedimentation. For instance for the DAA system, the inlet can sample

Table 2. Example calculation of droplet evaporation time for pure water at lab conditions and 50 % RH (from www.aerosols.wustl.edu/AAARworkshop08/software/AEROCALC-11-3-03.xls, the AeroCalc by Paul Baron).

Parameters	
Temperature [K]	293.15
Vapour diffusion coefficient [$m^2 s^{-1}$]	0.000024
Vapour molecular weight [$kg\,mol^{-1}$]	0.018
Saturation ratio [$-$]	0.5
Initial particle diameter [μm]	25
Particle density [$kg\,m^{-3}$]	1000
Saturation vapour pressure [hPa]	23.4
Temperature at drop surface [K]	286.5
Vapour pressure at drop surface [hPa]	15.4
Time to droplet evaporation [s]	1.09

up to approximately 25 μm diameter droplets. These droplets should have enough residence time to be dried before entering various tubing and instrumentation after the dryer in order to reduce transport losses. Droplet residuals can however be supermicron, and such large particles are difficult to sample, increasingly with increasing size. Assuming a 25 μm water droplet, the total droplet evaporation time needed can be calculated to 1.09 s at 293 K (see Table 2). The average residence time in the dryer is 5.5 s, and the RH is below 50 % more than half that time (see Fig. 2). The drying time necessary increases significantly if the RH surrounding the aerosol particle is higher. Further, at lower temperature, for instance at 273 K the corresponding total drying time required is 3.0 s, approaching the limit of the system.

Further, surfactants (creating a surface layer – during the drying process) or sparingly soluble organics (that precipitate during the drying process) might reduce the vapour pressure of water from the diluted droplet (e.g. Shulman et al., 1996; Shantz et al., 2003). These effects are reduced as the supermicron size increases; thus the beginning of drying of a 25 μm droplet should be unhindered by such processes. It is important to reach accumulation mode size inside the dryer to avoid losses during onwards transport of the aerosol particles/drops. The last equilibration to dry particles at instrumentation RH (often $< 30\%$ RH) can generally be done in tubing and additional volumes, if required, after the dryer, simply by the added residence time. Furthermore the sample flow is laminar; thus the center streamline flow velocity is approximately twice the average. Consequently, the center streamline has half the average residence time. If more drying time is required, the dryer must be larger, or the flow smaller. We use an additional modular section with the same flange for increased residence time in this case. The two abovementioned requirements of minimum diffusion losses (increases with time) vs. residence time for drying (increasing time is advantageous) need to be balanced. The two can

in many situations be characterised and corrected for, to some extent.

2.2 Design – generation of dry air

The dry air came from circulation through aluminium oxide (Al_2O_3) pellets (spherical diameter 2–4 mm) (Martinsson et al., 1992). Each container had 1 kg Al_2O_3. The Al_2O_3 pellets were dried, regenerated, with low-pressure (about 4 hPa) evaporation drying, alternating between two containers (see left side of Fig. 1). A membrane vacuum pump was in constant use to generate the low pressure (Vacuubrand model MV 2NT, Germany). Two 0.002 m^3 stainless steel containers were used for each drying flow used (i.e. 4 in total, in two pairs), each pair alternating in either regenerating mode or supplying dry air after the airflow had passed the Al_2O_3 pellets (at ambient pressure). The switching was done with three-way impulse solenoid valves. At the moment the valves switch, initially the low pressure from the container just having been dried is connected to the inlet volume. To avoid a large pressure change, two vacuum vent valves, which open if pressure is less than ca. 500 hPa, were fitted, one on each of the drying airflow circuits (see Fig. 1). The switching of the main dryer valves can be set when different conditions are met, such as if the aerosol RH is too high, or if the RH in the drying branches is too high. We used as a condition that the dryer (both branches simultaneously) should switch if the RH of the outer drying airstream was larger than 17 %, measured at its approximately ambient temperature (in an outdoor metal box) before entering the drier at the lower port. Further we used a minimum time between switching, which was set to 20 000 s (about 5.5 h), and in addition the switch was done only at end of a measurement cycle. During ambient conditions close to 100 % RH, the system switched constantly at the minimum time interval. Following a switch the system waited 30 s before next measurement started again, in order to minimise any disturbances.

2.3 Aerosol particle transmission and vapour transfer characterisation

In order to characterise the aerosol transmission through the dryer, measurements were done comparing the aerosol concentration at the exit of the dryer, C_{exit}, with that at the entry, C_{in}. Concentrations were measured with condensation particle counters (CPCs, Model 7610, TSI, USA). The CPCs had a lower detection limit of 15 nm (Hermann and Wiedensohler, 2001). The upper limit is > 3 µm according to the manual. For the largest sizes studied, it would have been advantageous to use an optical particle sizer. Nevertheless, we included all measured data below. The transmission was defined as C_{exit}/C_{in}. Particles in the range D_p 0.03–4.9 µm were evaluated. The setup can be seen in Fig. 3. Firstly a vibrating orifice aerosol generator (VOAG, model 3450, TSI, USA) was used to produce dry (RH 30 %) ammonium sul-
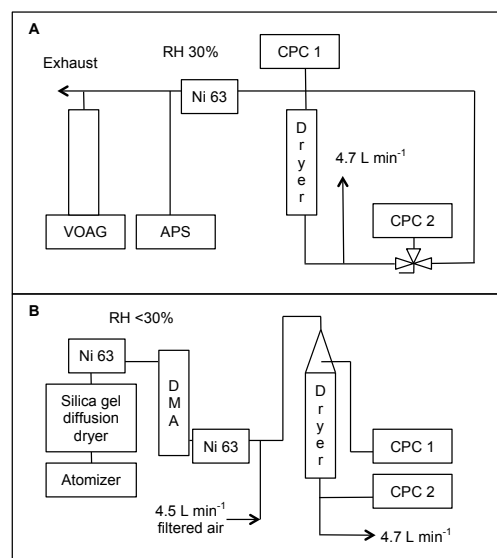
Fig. 3. Experimental setups for transmission measurements. In **(A)** the vibrating orifice aerosol generator (VOAG) is shown, aerosol particle sizer (APS), neutralizer (Ni 63). 2 CPCs were used, each with a flow of 1 L min^{-1}, similar in **(B)**, showing the setup with an atomizer, for submicron-sized particles. A larger cone was used on top of the dryer, from where the sample flow to CPC 1 was drawn. The flow through the dryer was 5.7 L min^{-1} for both setups.

phate (AS, p.a.) particles, from a solution in Milli-Q water, ranging from geometric diameter (D_{geo}) 0.84 to 4.9 µm. The aerodynamic diameter, D_{aero}, was measured with an aerosol particle sizer (APS, TSI model 3321) and was converted to D_{geo} under assumption of spherical particles according to $D_{geo} = D_{aero}/\sqrt{\rho}$, where ρ is particle density (1770 kg m^{-3} for AS). The aerosol was neutralised with a ^{63}Ni source (case design at Lund University, serial number KF11, source model NB14, 555 MBq, 2008, QSA Global, USA). This was in order to reduce the electrostatic losses and to only test sedimentation and impaction losses in this experiment. The particles were fed directly into the dryer, with a four-way connector, connected to a first CPC, and a second CPC measured the concentration after the dryer. The second CPC thus had two additional 90° bends in the experimental setup, which resulted in supermicron particle losses from the setup for these VOAG tests (see below).

Secondly, smaller sized AS particles were produced with a TSI atomizer (TSI 3076 model), ranging from dry mobility diameter 0.03 to 0.4 µm. The aerosol was neutralised, in order to achieve a known charge distribution (Wiedensohler, 1988), and a monomodal size was selected with a Vienna type DMA (differential mobility analyzer, sheath and aerosol flow rates of 9.8 and 2.2 L min^{-1}) and then neutralised again. The second source reduced the double charged particles passing the DMA, in order to reduce electrostatic losses as mentioned above. However, the second source was redundant

for these experiments (within measurement uncertainty). The aerosol flow was diluted via a filter with a low-pressure drop for a total sample flow rate of $6.7\,\mathrm{L\,min^{-1}}$. During these experiments, a metal cone was used upstream the dryer, with a port where the first CPC sampled $1\,\mathrm{L\,min^{-1}}$, and the second CPC measured the concentration after the dryer ($1\,\mathrm{L\,min^{-1}}$). The remaining $4.7\,\mathrm{L\,min^{-1}}$ were exhausted, with a valve as critical orifice, to the vacuum system in the laboratory, for a total flow of $5.7\,\mathrm{L\,min^{-1}}$ passing through the dryer.

Further experiments in order to estimate the vapour transfer property of the membrane were performed. Humidity was produced by bubbling air through Milli-Q water in an impinger, heated to lab temperature, which was 294 K (as the water otherwise cools due to evaporation). The sample air entered with 87 % RH, measured with a capacity RH sensor (HygroClip S, Rotronic). The Rotronic sensor had an accuracy of 1.5 % RH and 0.3 K. The RH inside the dryer was investigated by inserting a small tube, extracting a small airflow (corresponding to the area of the tube compared to total cross-sectional area of dryer) and measuring the RH of this small flow at lab temperature.

The water vapour transfer coefficient k was used to describe membrane performance (Bierwerth, 2001):

$$k = \left(\dot{m}_{\mathrm{H_2O}}\right) / \left(A_{\mathrm{mem}}\,\Delta\mathrm{RH_{log}}\right) \tag{2}$$

where $\dot{m}_{\mathrm{H_2O}}$ is the transfer rate of water vapour ($\mathrm{kg\,s^{-1}}$, using $0.015\,\mathrm{kg\,kg^{-1}}$ $\mathrm{H_2O}$ in the dry air at $10^5\,\mathrm{Pa}$), A_{mem} is the membrane surface and $\Delta\mathrm{RH_{log}}$ is the logarithmic mean difference in RH, defined as

$$\Delta\mathrm{RH_{log}} = \frac{(\Delta\mathrm{RH_{Max}} - \Delta\mathrm{RH_{Min}})}{\ln\left(\frac{\Delta\mathrm{RH_{Max}}}{\Delta\mathrm{RH_{Min}}}\right)}, \tag{3}$$

where $\Delta\mathrm{RH_{Max}}$ and $\Delta\mathrm{RH_{Min}}$ are the differences of RH at each side of the dryer, maximum and minimum of these, respectively.

2.4 Ambient measurements

The dryer was used for continuous long-term measurements at the summit of the mountain Brocken (51.80° N, 10.67° E, 1142 m a.s.l.) in the Harz region in central Germany. The RH at ambient temperature (T_{amb}) directly after the exit of the dryer ($\mathrm{RH_{dried}}$) was evaluated by using a Rotronic capacity RH sensor. However, this sensor measured the sample aerosol RH ($\mathrm{RH_{station}}$), inside the measurement station (at its temperature, T_{station} and in a small side-flow from a tee in the main sample flow). This reading was converted to $\mathrm{RH_{dried}}$ as follows. The vapour pressure ($p_{\mathrm{H_2O}}^{\mathrm{station}}$, Pa) in the sample flow is defined as

$$p_{\mathrm{H_2O}} = \frac{\mathrm{RH}_i}{100}\,p_{\mathrm{sat}} \tag{4}$$

where p_{sat} is the saturation vapour pressure of water, calculated from the following empirical formula (Weingartner et

al., 1997):

$$p_{\mathrm{sat}} = 610.8\,e^{\left(5350\left(\frac{1}{273.15} - \frac{1}{T_i}\right)\right)}, \tag{5}$$

with T_i in K and i = station. The above vapour pressure equation was confirmed with the Magnus equation (e.g. Murray, 1967), with a deviation of ≤ 0.1 % in the range 273–293 K. That same vapour pressure is then used in the above equations, rearranged, to calculate the $\mathrm{RH_{dried}}$, at T_{amb} (assuming isobaric cooling without condensation).

Furthermore the ambient RH ($\mathrm{RH_{amb}}$) was measured (sensor model *GHTU.SGT010*, Greisinger, Germany). The difference between the ambient water vapour flow into the system and the water vapour flow after the dryer is the water vapour removed from the sample flow (denoted $\dot{m}_{\mathrm{dried}}$, $\mathrm{kg\,s^{-1}}$). This was calculated according to

$$\dot{m}_{\mathrm{dried}} = x_{\mathrm{ambient}}\,\dot{m}_{\mathrm{ambient}} - x_{\mathrm{station}}\,\dot{m}_{\mathrm{station}}, \tag{6}$$

where $\dot{m}_i$ and x_i are the mass flow of dry air ($\mathrm{kg\,s^{-1}}$) and specific humidity ($\mathrm{kg\,kg^{-1}}$) for the ambient sample flow and the sample flow conditioned inside the station, respectively. $\dot{m}_{\mathrm{ambient}}$ and $\dot{m}_{\mathrm{station}}$ are identical and represent the dry airflow through the system. The density changes up to 10 % at occasions between these conditions.

3 Results

Here we present tests from the laboratory, aiming to describe the dryer under controlled conditions, as well as long-term results from the field, showing the overall performance of the dryer.

3.1 Laboratory measurements

The transmission through the dryer from entry to exit is shown in Fig. 4. An average transmission for accumulation mode particles (D_{p} 0.1–1 µm) of 99.9 % was observed. The transmission decreases with decreasing particle size below 0.1 µm. The Particle Loss Calculator (von der Weiden et al., 2009) was used to model losses in the dryer (thick line in figure). This software is described in the open access publication, and "employs relevant empirical and theoretical relationships found in established literature". For supermicronsized particles from the VOAG, the transmission decreases due to two additional 90° bends situated after the dryer in the experimental setup. These bends do not need to be used during actual measurements in the field. The two bends can be accounted for (modelled with the thin grey line in Fig. 4) and indicate the importance of designing a proper exit from the dryer, should large particles be studied.

The uncertainty in transmission as shown in Fig. 4 is composed of counting statistics (Poisson error), flow settings (pressure changes) and dilution (leaks). The Poisson error was ≤ 1 % for the accumulation mode sizes measured; the
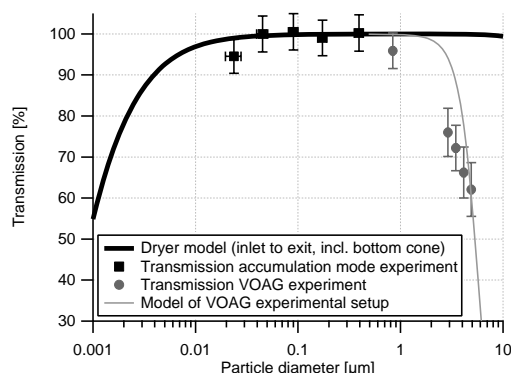
Fig. 4. Transmission through dryer at $5.7 \, \text{L min}^{-1}$ sample flow. Particles were neutralised (i.e. negligible electrostatic scattering). Concentrations tested varied between $1–3500 \, \text{cm}^{-3}$. Thick line is model of transmission through dryer. The measurements showing low transmission above 1 μm are due to two 90° bends in the experimental setup. The experiments were performed with dry conditions, 30 % RH.

error in flows was estimated to $\leq 3 \, \%$ and dilution $\leq 3 \, \%$, giving a total error of 4.4 %. The uncertainty in transmission increases with increasing particle size, due to mainly lower particle concentrations generated. The uncertainty in size is 3 % for the VOAG setup (standard deviation between size deduced from VOAG settings and measured size from APS) and estimated to be $\leq 10 \, \%$ for the atomizer DMA setup (from uncertainty in dimensions, flows and high voltage supply for the DMA).

The water vapour transfer of the dryer was tested in the laboratory, geometry of dryer as described above. Humidity was produced by bubbling air through Milli-Q water in an impinger, heated to lab temperature. RH of 10.6 % at the dryer exit was achieved in the air sample flow with $5.5 \, \text{L min}^{-1}$ ($0.33 \, \text{m}^3 \, \text{h}^{-1}$). In Fig. 2 measured RHs are shown. The lines to guide the eye are based on the assumption of a logarithmic dependence of RH along the dryer (Bierwerth, 2001). The sample flow between the two concentric membranes is surrounded by two closed loop drying flows (the outside flow rate being $10 \, \text{L min}^{-1}$ and the inside (inner dry flow) being $4.7 \, \text{L min}^{-1}$). The total drying airflow is approximately three times as large as the sample flow. During these laboratory tests the flow ratio of the drying air (outside/inside) was 2.1, which was set too high. The a priori most favourable flow ratio, for a symmetrical drying effect, should be the ratio of the areas of the membranes, which is 1.3. During the operation in the field, the flows where 5.0 and $3.7 \, \text{L min}^{-1}$, outer and inner respectively, and the ratio was 1.4.

$\Delta \text{RH}_{\text{log}}$ was 20.6 and 19.9 % RH for the outer and inner dry airflow, respectively. The water vapour transfer coefficient k was calculated from Eq. (2) to be $4.6 \times 10^{-7} \, \text{kg m}^{-2} \, \text{s}^{-1} \, \% \, \text{RH}^{-1}$. k can be compared to the

manufacturer's specification and literature values of approximately $8–13 \times 10^{-7} \, \text{kg m}^{-2} \, \text{s}^{-1} \, \% \, \text{RH}^{-1}$ (Huang and Qian, 2007), for the membrane, and it is probable that we obtain a significantly lower value due to membrane support structure and metal nets fitted, which reduce the water vapour transfer.

3.2 Long-term ambient measurements

The dryer was used for continuous long-term measurements at the summit of the mountain Brocken (51.80° N, 10.67° E, 1142 m a.s.l.) in the Harz region in central Germany from May to October 2010. The project is in collaboration with the Air Chemistry Group of the Technical University of Brandenburg (BTU Cottbus), who has had a cloud measurement site at mount Brocken for many years.

The average RH_{dried} during this time period (the measurements at Brocken) was $26.6 \pm 7.3 \, \% \, \text{RH}$ (one standard deviation). Average T_{ambient} was 282.4 K and average T_{station} was 296 K. The RH_{dried} is the quality criterion to ensure a sufficient dry sample flow for the drying of droplets. Furthermore, a second criterion for the highest allowable RH inside instrumentation in the station can be defined, primarily in order to deal with situations when the outdoor part of the instrument is warmer than the indoor part. In our case we considered data with $\text{RH}_{\text{dried}} < 30 \, \% \, \text{RH}$ to be used as is.

The specific humidity can be calculated as

$$x_i = \frac{M_{\text{H}_2\text{O}}}{M_{\text{Air}}} \left(\frac{p_{\text{H}_2\text{O}}}{P_{\text{amb}} - p_{\text{H}_2\text{O}}} \right), \tag{7}$$

where $M_{\text{H}_2\text{O}}$ and M_{Air} are the molecular masses of water and air, respectively. P_{amb} is the ambient pressure and $p_{\text{H}_2\text{O}}$ is calculated from the measured RH and temperature (station) with Eqs. (4) and (5). The sample mass flow of dry air relates to the volume flow (continuously monitored in the instrument) as follows:

$$\dot{m}_{\text{station}} = \rho_{\text{air}} \, Q_{\text{samplestation}}, \tag{8}$$

where ρ_{air} is the density of air (at P_{amb} and at T_{station}) and $Q_{\text{samplestation}}$ is the dry aerosol sample flow. The above assumes the dried volume sample flow to be similar to the dry airflow, which are within 0.5 % up to 293 K and 30 % RH. The maximum $\dot{m}_{\text{dried}}$ achieved was $1.2 \times 10^{-6} \, \text{kg s}^{-1}$. Furthermore the fog/cloud droplet water is also removed, which is of lesser quantity, and if included would slightly increase the calculated water vapour removed from the system. The fog/cloud droplet entering the dryer can be estimated to rarely exceed $0.002 \, \text{kg m}^{-3}$ (with an example cloud of 500 cloud droplets cm^{-3}, with diameter 20 μm). Generally the specific humidity at the site was in the range $0.005–0.02 \, \text{kg m}^{-3}$.

During these measurements the RHs of the dry airflows were not measured. Thus the logarithmic mean RH was not known, so we could not relate the water vapour transfer to the performance of the membrane measured in the laboratory. The drying capacity, $\dot{m}_{\text{dried}}$, represents what was
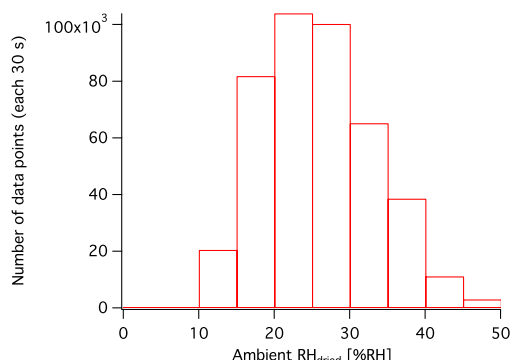
Fig. 5. Histogram of RH_{dried}, i.e. air sample RH after drying. 72 % of the time the RH was below 30 %. The $T_{station}$ range was 285–307 K, the $T_{ambient}$ range 270.6–301 K and $RH_{ambient}$ range 9.5–100 % during the measurements. Approximately 140 days of data.

achieved in the field and corresponds to drying a $5.7 \, L \, min^{-1}$ ($0.35 \, m^3 \, h^{-1}$) aerosol sample flow from 100 to 27 % RH at 293 K (with a drying air total flow of $8.7 \, L \, min^{-1}$).

The percentage of the time the system operated was 94.2 %. Some of the downtime was due to planned maintenance of the system; thus the reliability of the dryer was higher than this. During October the inlet and dryer also automatically shut down a few occasions due to freezing and icing conditions. The time fraction that the dryer resulted in a sample RH below 30 % was 72.2 %, from 9 May until 20 October 2010, when data were available (see Fig. 5). We investigated possible reasons for the spread of RH_{dried}, such as variations in ambient vapour pressure, T_{amb}, diurnal variations and longer time series; however, no single factor influenced the results. Specifically, the RH after the dryer virtually depends on neither ambient nor laboratory temperature. The ambient RH is not a good indicator for performance, because the water removed reduces at colder temperatures. However, the water vapour removed from the sample flow increases linearly with the ambient water vapour pressure, indicating that the system can dry air up to at least the humidities measured during these field tests.

4 Discussion

Although the dryer worked without failures during the field measurement period, on occasions the RH_{dried} was above 30 %, which should be improved. No single environmental factor has been found to limit the system, but rather a combination of factors contributes to time periods with RH_{dried} above 30 %. Thus a general improvement is required. There are two major refinements to do with the drying system presented. The first is to supply a higher dry airflow on the outside of the GORE-TEX membranes. We were presently limited to pumps that were slightly too close to design criteria (regarding flow, durability and ambient cold conditions).

That improvement should reduce the sample RH. Secondly the drying circuits (the Al_2O_3 containers specifically) were also situated outdoors at cold conditions, and as these are regenerated, they cool further. If these circuits were to be situated indoors, or heated, the regeneration process would be more efficient. Indoor placement of the pumps would also be beneficial for durability. However, this would require adjustments depending on ambient and indoor temperature differences, in order to achieve a constant flow. The dry airflow can vary to some extent, without hampering the drying process.

Currently, the regulation of the switching of dryers was when the RH in the drying airflow increased above a threshold value, as mentioned above. This would be improved by using RH_{dried} of the sample at T_{amb}. The threshold for switching could then be set directly at a defined sample RH, for instance 25 %. In addition a criterion for the indoor RH in the instrument should be used, which when exceeded should also switch dryers.

5 Conclusions

A dryer designed for continuous sampling of atmospheric aerosol, where a specified relative humidity of the sample flow (lower than the atmospheric humidity) is required, has been designed and tested. The specific purpose of the dryer presented here is to dry fog/cloud droplets (maximum diameter approximately 25 μm, highly charged, up to 5×10^2 charges) with minimum losses of droplets and particles from entrance to exit of the dryer. The accumulation mode particle transmission was measured to be independent of particle size and 99.9 %, corresponding well with theory.

The water vapour transfer coefficient k was measured to be $4.6 \times 10^{-7} \, kg \, m^{-2} \, s^{-1} \, \% \, RH^{-1}$ in the laboratory (temperature 294 K) and is used for design purposes.

The system was tested from 9 May until 20 October 2010, on the mountain Brocken (51.80° N, 10.67° E, 1142 m a.s.l.) in the Harz region in central Germany. A maximum water vapour transfer rate of $1.2 \times 10^{-6} \, kg \, s^{-1}$ was achieved, corresponding to drying from 100 to 27 % RH at 293 K for a $5.7 \, L \, min^{-1}$ ($0.35 \, m^3 \, h^{-1}$) aerosol sample flow. This can be improved with a closed loop higher dry airflow and warming of the dry air generation system, in order to achieve a more effective dry air regeneration, in our case. The sample flow was below 30 % relative humidity 72 % of that time period. Measurements were done > 94 % during the deployment in the field, and the dryer functioned all that time.

References

Bierwerth, W.: Tabellenbuch Chemietechnik, 2nd Edn., Europa-Lehrmittel, Haan-Gruiten, 2001.

Frank, G. P., Cederfelt, S.-I., and Martinsson, B. G.: Characterisation of a unipolar charger for droplet aerosols of 0.1–20 μm in diameter, J. Aerosol Sci., 35, 117–134, 2004.

Fuchs, N. A.: The Mechanics of Aerosols, republication edition, edited by: Davies, C. N., Dover Publications, New York, 1989.

Hermann, M. and Wiedensohler, A.: Counting efficiency of condensation particle counters at low-pressures with illustrative data from the upper troposphere, J. Aerosol Sci., 32, 975–991, 2001.

Huang, J. and Qian, X.: A new test method for measuring the water vapour permeability of fabrics, Meas. Sci. Technol., 18, 3043–3047, 2007.

Martinsson, B. G.: Physical basis for a droplet aerosol analysing method, J. Aerosol Sci., 27, 997–1013, 1996.

Martinsson, B. G., Hansson, H.-C., Asking, L., and Cederfelt, S.-I.: A relative humidity processing method for the sampling of aerosol particles with low growth-ability, Tellus B, 44, 632–644, 1992.

Murray, F. W.: On the computation of saturation vapor pressure, J. Appl. Meteorol., 6, 203–204, 1967.

Ogren, J. A., Heintzenberg, J., and Charlson, R. J.: In-situ sampling of clouds with a droplet to aerosol converter, Geophys. Res. Lett., 12, 121–124, 1985.

Shantz, N. C., Leaitch, W. R., and Caffrey, P. F.: Effect of organics of low solubility on the growth rate of cloud droplets, J. Geophys. Res., 108, 4168–4177, 2003.

Shulman, M. L., Jacobson, M. C., Carlson, R. J., Synovec, R. E., and Young, T. E.: Dissolution behavior and surface tension effects of organic compounds in nucleating cloud droplets, Geophys. Res. Lett., 23, 277–280, 1996.

Tuch, T. M., Haudek, A., Müller, T., Nowak, A., Wex, H., and Wiedensohler, A.: Design and performance of an automatic regenerating adsorption aerosol dryer for continuous operation at monitoring sites, Atmos. Meas. Tech., 2, 417–422, doi:10.5194/amt-2-417-2009, 2009.

von der Weiden, S.-L., Drewnick, F., and Borrmann, S.: Particle Loss Calculator – a new software tool for the assessment of the performance of aerosol inlet systems, Atmos. Meas. Tech., 2, 479–494, doi:10.5194/amt-2-479-2009, 2009.

Weingartner, E., Burtscher, H., and Baltensperger, U.: Hygroscopic properties of carbon and diesel soot particles, Atmos. Environ., 31, 2311–2327, 1997.

Weingartner, E., Gysel, M., and Baltensperger, U.: Hygroscopicity of aerosol particles at low temperatures, 1. New low-temperature H-TDMA instrument: Setup and first applications, Environ. Sci. Technol., 36, 55–62, 2002.

Wiedensohler, A.: An approximation of the bipolar charge distribution for particles in the submicron size range, J. Aerosol Sci., 19, 387–389, 1988.

Willeke, K. and Baron, P.: Aerosol Measurement: Principles, Techniques, and Applications, Van Nostrand Reinhold, New York, 2005.

Paper II: Inversion of droplet aerosol analyzer data for long-term aerosol-cloud interaction measurements

Paper II

Atmospheric
Measurement
Techniques

Open Access

Inversion of droplet aerosol analyzer data for long-term aerosol–cloud interaction measurements

M. I. A. Berghof[1], **G. P. Frank**[1], **S. Sjogren**[1,*], **and B. G. Martinsson**[1]

[1]Department of Physics, Lund University, Lund, Sweden
[*]now at: University of Applied Sciences Northwestern Switzerland, Brugg-Windisch, Switzerland

Correspondence to: M. Berghof (maria.berghof@pixe.lth.se)

Abstract. The droplet aerosol analyzer (DAA) was developed to study the influence of aerosol properties on clouds. It measures the ambient particle size of individual droplets and interstitial particles, the size of the dry (residual) particles after the evaporation of water vapor and the number concentration of the dry (residual) particles. A method was developed for the evaluation of DAA data to obtain the three-parameter data set: ambient particle diameter, dry (residual) particle diameter and number concentration. First results from in-cloud measurements performed on the summit of Mt. Brocken in Germany are presented. Various aspects of the cloud–aerosol data set are presented, such as the number concentration of interstitial particles and cloud droplets, the dry residue particle size distribution, droplet size distributions, scavenging ratios due to cloud droplet formation and size-dependent solute concentrations. This data set makes it possible to study clouds and the influence of the aerosol population on clouds.

1 Introduction

Clouds affect the Earth's climate in a number of ways: for example, they regulate the hydrological cycle and redistribute energy via the transport of water vapor and latent heat in the atmosphere. Many factors influence the macrophysics and microphysics of clouds. The macrophysics of clouds are affected by large-scale meteorological conditions such as updraft velocity, turbulent mixing or atmospheric layering. Cloud droplets form by the condensation of water vapor on aerosol particles. As a consequence, the microphysical conditions are influenced by the macrophysics, the particle number concentration and size distribution, the chemical composition, and the mixing state of the atmospheric aerosol. The first (Twomey) indirect aerosol effect describes changes in cloud properties induced by changes in the properties of aerosol particles (Warner, 1968; Twomey, 1974; Albrecht, 1989; Liou and Ou, 1989; Lohmann and Feichter, 2005). It is still being debated as to whether changes in the microphysical properties of clouds also influence the amount of clouds and liquid water content. These changes are also associated with changes in precipitation efficiency and thus cloud lifetime (second indirect aerosol effect; Albrecht, 1989; Stevens and Feingold, 2009).

This work deals with an instrument, the droplet aerosol analyzer (DAA; Martinsson, 1996), developed for experimental studies of the interaction between aerosol and clouds. This instrument was especially developed to study the interaction between aerosol particles and cloud/fog droplets. The DAA measures the ambient size of individual droplets and interstitial particles, the size of the dry (residual) particles after the evaporation of water vapor and the number concentration. This gives a unique three-parameter data set (ambient particle diameter, dry (residual) particle diameter, and number concentration) for both cloud droplets and interstitial particles. The DAA can provide a direct relationship between cloud droplet size and the size of its dry residue. Other instrumentation for studying clouds, such as differential mobility particle spectrometers (DMPS), optical particle counters (OPC; Sorensen et al., 2011), the ground-based fog monitor (Spiegel et al., 2012) or the counterflow virtual impactor (CVI) that has a variable cut-off diameter for cloud droplets between 1 and 30 µm (Anderson et al., 1993; Noone et al., 1988; Ogren et al., 1985; Schwarzenboeck and Heintzenberg,

2000), cannot provide such a relationship, even when used in parallel.

Previous studies with the DAA include thorough intercomparisons (Cederfelt et al., 1997; Frank et al., 1998; Martinsson et al., 1999, 2000) with other cloud/aerosol instrumentation. Results from previous studies include relationships between particle and cloud number concentrations and cloud dynamics (Martinsson et al., 1997, 1999) as well as observations of validated cloud droplet number concentrations reaching up to 3000 cm^{-3} (Martinsson et al., 2000). Findings from previous DAA studies also include that fogs in polluted regions consisted of droplets that were not activated (Frank et al., 1998).

In order to improve the statistical description of the aerosol impact on cloud microstructure for different dynamical situations, long-term measurements are needed. The previous version of the DAA required daily service to ensure high-quality data. As a result, the instrument was only used in experiments spanning a month or less. Here we present parts of new developments of the DAA. The overall aims of the developments are twofold: to improve the time resolution in the measurements and to prepare the instrument for unattended long-term operation. The time resolution was improved by a factor of 2 by changing method of voltage change in the differential mobility analyzers (DMA) used in the DAA, increasing the number of DMAs from seven to eight where the new DMA provides more efficient coverage in terms of electrical mobility, and by changing the DMA aerosol to sheath air flow ratio. Methodology for long-term operation includes closed-loop sheath air circulation in all DMAs, automated dryers for cloud droplets (Sjogren et al., 2013), automatic fill of liquid consumed by the particle detectors (condensation particle counter (CPC)), regular, remote access to operational parameters, and logging of a large number of parameters. These developments will be presented elsewhere. First results from measurements at Mt. Brocken (Germany) between June and October 2010 will be shown here. These improvements mean that large amounts of data can be produced to study the interaction between aerosols and clouds for different aerosols and for differences in cloud dynamics. The data produced need to be evaluated. The previous method was based on manual fit of the DAA spectra. Here we present an automated methodology to evaluate DAA data. The routine builds on the previous, manual, unpublished method.

2 The DAA instrument

A schematic of the DAA is shown in Fig. 1, and the instrument is described in more detail by Frank et al. (2014). It consists of an outdoor and an indoor part. Cloud droplets and interstitial particles are collected in the outdoor part through an inlet directed towards the wind. To achieve a well-defined charge state, the aerosol is first passed through a bipolar charger (BiCh) and then a unipolar charger (UniCh), where
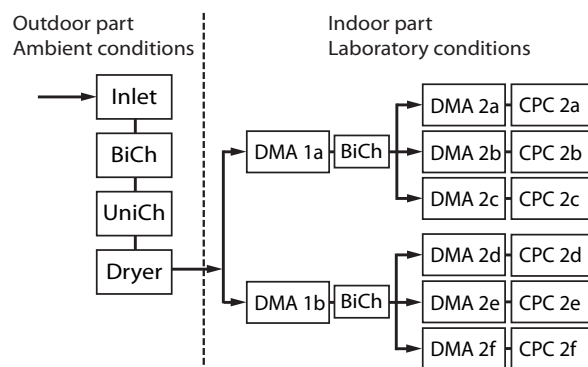
Fig. 1. The principle of the DAA. Droplets and particles are processed in several steps by aerosol charging mechanisms in bipolar (BiCh) and unipolar chargers (UniCh), diffusion drying (Dryer), electrostatic aerosol spectrometry (DMA), and counting in condensation particle counters (CPC) in order to obtain the desired relationships.

the droplets acquire a charge level dependent on their size while still at ambient conditions (Frank et al., 2004)). Water is removed in the dryer, described in Sjogren et al. (2013), and the dry aerosol then enters the indoor part.

At this stage the charge level of the particles is related to their ambient size. The particles are selected according to their electrical mobility in the first differential mobility analyzers (DMA 1a and 1b). The following combination of BiCh, DMA and CPC gives the electrical mobility of the singly charged droplet residuals for a given dry diameter. Once the dry particle diameter and the electric mobility of the residual particles are known, their charge state can be calculated, which is then related to the ambient particle diameter via the calibration of the unipolar charger.

During operation of the DAA, the voltage of the DMAs 2a–f is fixed, while the voltage of DMA 1a and 1b is varied over different charge levels from the unipolar charger. The mobility step between each of the DMAs 2a–f is set to 2. The mobility step in DMA 1a and 1b is set to $\sqrt{2}$ so as to coincide with the DMA 2 mobility of singly, doubly, quadruply, etc. charged particles from the unipolar charger. This allows for efficient detection of small particles carrying few elementary charges. From each DMA 1a and 1b voltage a set of six measurements from DMA 2a to f are obtained.

3 DAA data evaluation

An inversion technique was applied to the DAA raw data to obtain the three-parameter data set consisting of ambient particle diameter, dry (residual) particle diameter and number concentration. The basic variables were first calculated from the corrected raw data, resulting in the charge distribution caused by the unipolar charger (Fig. 1) for every dry particle

diameter measured. Based on the calibration of the unipolar charger, a function can be derived to describe the relation between charge distribution and ambient particle size. In the second step of the data evaluation this function is used to extract the ambient particle diameter, D_d, and concentration, N_{UCh}, of particles and droplets entering the DAA corresponding to each charge distribution and thus to each dry (residual) particle diameter, D_p. The DAA three-parameter data set thus consists of the ambient particle diameter, D_d, the dry (residual) particle diameter, D_p, and the number concentration, N_{UCh}, in each dry particle interval measured.

3.1 Raw data

During one measurement run the voltage of DMA 1a and 1b is stepped over different charge levels, while the voltage of DMA 2a–f is fixed. As the transport times in the instrument is known, it is possible to select steady-state data and to achieve a time resolution of 10 min for one complete measurement.

Two measurement runs are performed at two different voltages of DMA 2a–f. The first run is performed at voltages representing small diameters (59 to 545 nm) and the second run is decreased by a factor of $\sqrt{2}$ in terms of electrical mobility, Z_p, to increase the resolution in dry particle diameter (75 to 776 nm). Both runs can be used independently, giving a time resolution of 10 min and a time resolution of 20 min with full size resolution.

The DAA raw data from each run consist of CPC raw counts, N_{counts}; the CPC counting time, t_{count}; the high voltage of DMA 1a and 1b and DMA 2a–f, U; the sheath air flow, Q_{sh}; and the aerosol flow, Q_{ae}, for each DMA; as well as atmospheric pressure, p, and aerosol temperature T_{ae}. The dry particle diameter, D_p; electrical mobility, Z_p; electrical charge level, q_{DAA}; and the raw number concentration, N_{raw}, can be calculated from this data set.

3.2 Data correction

The DAA raw concentration is corrected for losses that occur after the second bipolar charger (losses in DMA 2a–f). Corrections are also made for particle losses in DMA 1a and 1b that occur upstream of the bipolar charger. The loss-corrected concentration data are then corrected for multiple charging in the second bipolar charger. The results are further corrected after the inversion for minor losses in the dryer (Sjogren et al., 2013) and for deviations from isokinetic sampling of the inlet (Sect. 3.3).

3.2.1 DMA correction

A perfect DMA can be described by an ideal, symmetric transfer function, which is triangular. Imperfections in the DMA may result in broadening of the transfer function and losses of particles (Martinsson et al., 2001). Further losses and broadening due to Brownian diffusion can cause the transfer function to be dependent on particle size

(Stolzenburg, 1988). Two parameters are used to characterize the imperfections of the DMAs. A broadening factor, $\mu (\leq 1)$, describes the width of the transfer function leading to a broader individual transfer function while conserving its area. Particle loss is described by a loss factor, $\lambda (\leq 1)$, leading to a decrease in area while conserving its width. Both parameters are specific to each DMA and were determined experimentally for 230 nm particles, as described in Martinsson et al. (2001). The size dependence of both parameters was estimated as described in Karlsson and Martinsson (2003). The resulting parameters were averaged for each DMA over both DAA runs, leading to an error of less than 0.5 % due to the size dependence of Brownian diffusion. The estimates for the eight DMAs are in the range $\mu = 0.87$ to 1.00 and $\lambda = 0.81$ to 1.00. Both DMA loss and broadening are accounted for in each charge distribution before the bipolar charge correction.

Another feature of the instrument is the size range covered by each of the DMA 2a–f. During a run the voltage of DMA 2a–f is kept constant and the mobility step between each of the DMAs 2a–f is set to 2. In order to quantify the mobility distribution, each DMA measurement must be converted to represent the DMA stepping factor used as described by Cederfelt et al. (1997).

3.2.2 Bipolar charger correction

The ambient particles and droplets entering the DAA are charged, then dried and selected according to charge level in DMA 1a and 1b. Before entering the second series of DMAs, the particles selected by DMA 1a and 1b are multiply charged in a bipolar charger.

In order to correct for multiple charging, it was assumed that the influence of multiply charged particles larger than the largest particle size measured in each run could be neglected. This is approximately valid for size distributions showing a rapid decrease in number concentration with increasing size, which is usually the case for atmospheric aerosol at the maximum sizes in the two different DMA runs (593 and 751 nm). For gradients of a factor of 10 between the largest size and the size corresponding to a factor of 2 increase in electrical mobility, the error for the latter size will be less than 1 %. Due to the strong gradient, this error will not propagate to smaller sizes. Doubly and quadruply charged particles with a dry particle diameter measured by a certain DMA 2a–f will have a higher mobility. These will be detected by the DMA 2a–f measuring the closest and second-closest smaller dry particle diameter. Their fractions were calculated based on the charge distribution described in Wiedensohler (1988).

To be able to correct for triply charged particles, a linear relation was assumed between the concentration of triply charged particles and the concentration of doubly and quadruply charged particles. The fraction of triply charged particles, $f(D_P, -3)$, can thus be included in the fraction of doubly, $f(D_P, -2)$, and quadruply, $f(D_P, -4)$, charged particles:

$$f_{D_{P},-2}^{*} = f_{D_{P},-2} + \frac{1}{2}f_{D_{P},-3}, \qquad (1)$$

$$f_{D_{P},-4}^{*} = f_{D_{P},-4} + \frac{1}{2}f_{D_{P},-3}. \qquad (2)$$

The uncertainty of this approximation is dependent on particle size and the width of size modes. The strongest effects can be expected when the triply charged particle is at the peak of a mode. An aerosol with narrow aerosol modes was found in Hoppel et al. (1996). The number concentration of triply charged particles close to the peak at 180 nm diameter will be underestimated by 15 %. The effect on the only important result, i.e., the number of singly charged particles, would be an overestimation by 1.4 %. Due to the dominance of single charge for still smaller particles, the error will not propagate. For distributions with modes more narrow than in Hoppel et al. (1996) (Fig. 1), the error due to the approximation will be larger. The charge distribution measured in each of the DMA 2a–f is thus corrected by subtracting the determined amount of doubly and quadruply charged particles from the other DMA 2a–f channels.

Finally, the concentration is corrected to standard laboratory pressure (1013.25 hPa) and temperature (293.15 K) giving the charge distribution measured by the DAA, $N^{\mathrm{DAA}}(q_{\mathrm{DAA}})$.

3.3 DAA inversion algorithm

After applying the above-described corrections, we obtained the corrected charge distribution of the ambient aerosol as measured by the DAA. Figure 2 shows the DAA data obtained during one run for each of the DMA 2a–f with its corresponding dry particle diameter, D_{P}. For small charge levels (i.e., small ambient particles), singly and doubly charged particles can be observed, whereas particles with two consecutive charge levels cannot be resolved higher up in the spectrum. In the next step, a function is fitted to the data, as shown in Fig. 2. The function fitted is the resulting charge distribution of droplets of a certain ambient particle diameter D_{d} passing through the DAA system, using the ambient particle diameter, D_{d}, and the number concentration of particles entering the unipolar charger, N_{UCh}, as fitting variables. The following section describes how this function is obtained by first calculating the charge distribution downstream of the unipolar charger, and then the charge distribution downstream of DMA 1a and 1b and DMA 2a–f.

3.3.1 Unipolar charger

When the aerosol enters the DAA it first passes through a bipolar charger to achieve a well-defined charge state. By passing the unipolar charging unit the aerosol acquires positive charges depending on their particle diameter. The resulting charge distribution thus depends on the ambient size of the particles entering the DAA. The relation between the
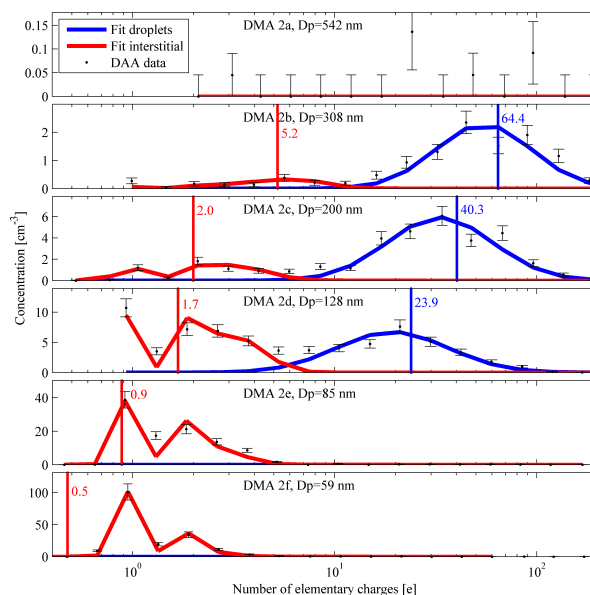
Fig. 2. Example of results obtained from data collected at Mt. Brocken, one run from 31 August 2010, 00:53–01:03 UTC. The panels show charge distribution data from the DMA 2a–f, including the standard error for Poisson counting of the raw counts. In this example, one or two fits were performed for each DMA 2a–f, which can be classified as interstitial particles and droplets. In the top panel, showing the results from DMA 2a for the largest dry particle diameter measured in this run, and in the two lowest panels, showing the results for the two smallest dry particle diameters measures (DMA 2e and 2f), there were insufficient particles and droplets to allow for a fit. Note the varying scale on the y axes.

arithmetic mean charge level and the mean ambient particle diameter in micrometers was calibrated in the size range 0.12 to 17 μm by Frank et al. (2004), and has been used here:

$$D_{\mathrm{d}}(q_{\mathrm{a}}) = -2.394 + (3.103 + 0.377 \times q_{\mathrm{a}})^{0.771}. \qquad (3)$$

Only particles becoming positively charged by the unipolar charger will be detected in the system. To determine the ambient particle size and concentration, the fraction of singly and doubly charged particles must be detectable. This may not be the case for ambient particles with small diameters at low concentrations, since the fraction of detected doubly charged particles may be too small. This leads to an error when determining the ambient particle size. For ambient particles with a size of $D_{P} = 50$ nm, the error in ambient size is 10 % for a concentration of $\mathrm{d}N/\mathrm{d}\log D_{\mathrm{p}} = 12.5$ cm^{-3}.

Large particles can be lost in the DAA inlet; thus the upper limit was set to 25 μm. The calibration range is therefore somewhat smaller than the measurement range. The calibration range was extrapolated by Frank et al. (2004) based on the charging model presented by Lawless (1996).

An α source, Cm-244, used to charge particles passing through the unipolar charger. Since the half-life of this source is 18.1 years, the calibration performed by Frank et al. (2004) may have changed, since radioactive decay would have resulted in a decrease in the number of charges for a certain droplet size. Therefore, the ambient particle diameter used here may be slightly underestimated. However, this will not affect the main subject of this paper.

3.3.2 Charge distribution downstream of the unipolar charger

The shape of the charge distribution downstream of the unipolar charger depends on the ambient particle size, D_d, of the entering particles. Calibrations show that the charge distribution downstream of the unipolar charger for particles smaller than 0.61 μm follows a normal distribution, whereas for particles larger than 3.15 μm it follows a log-normal distribution. Between these limits a linear combination of both distributions was used.

Ambient particles and droplets smaller than 0.61 μm acquire an arithmetic mean charge below $q_a = 2.82$. Their resulting charge distribution downstream of the unipolar charger follows a normal distribution,

$$\frac{dN_{[<0.61\,\mu m]}^{\text{Charger}}(q_i)}{dq_i} =$$
$$\frac{N_{\text{UCh}}}{\sqrt{2\pi}\sigma_a} \exp\left(-\frac{1}{2}\left(\frac{q_i - q_a}{\sigma_a}\right)^2\right), \tag{4}$$

for integer charge bins q_i and an arithmetic mean charge of q_a and standard deviation σ_a

$$q_a = \frac{(D_d[\mu m] + 2.394)^{\frac{1}{0.771}} - 3.103}{0.377} \tag{5}$$
$$\sigma_a = \sqrt{0.28 + 1.51 q_a}. \tag{6}$$

Ambient particles and droplets larger than 3.15 μm acquire an arithmetic mean charge greater than $q_a = 16.23$. Their resulting charge distribution downstream of the unipolar charger follows a log-normal distribution (Frank et al., 2004),

$$\frac{dN_{[>3.15\,\mu m]}^{\text{Charger}}(q_i)}{d\log q_i} = \frac{N_{\text{UCh}}}{\sqrt{2\pi}\log(\sigma_g)} \exp\left(-\frac{\log^2(\frac{q_i}{q_g})}{2\log^2(\sigma_g)}\right), \tag{7}$$

for integer charge bins q_i and a geometric mean charge of q_g and standard deviation σ_g:

$$q_g = \frac{q_a}{\exp\left(\frac{\log^2(\sigma_g)}{2}\right)} \tag{8}$$
$$\sigma_g = 1.99 - 0.027 D_d, \tag{9}$$

with D_d in μm.

In the size range 0.61–3.15 μm, ambient particles and droplets acquire an arithmetic mean charge of $q_a = 2.82$ to 16.23. Here, a combination of normal and log-normal distributions was used,

$$N_{[0.61-3.15\,\mu m]}^{\text{Charger}}(q_i) = \tag{10}$$
$$(1 - \xi(q_i)) \times dq_i \times \left(\frac{N_{\text{UCh}}}{\sqrt{2\pi}\sigma_a} \exp\left(-\frac{1}{2}\left(\frac{q_i - q_a}{\sigma_a}\right)^2\right)\right)$$
$$+ \xi(q_i) \times d\log q_i \times \left(\frac{N_{\text{UCh}}}{\sqrt{2\pi}\log(\sigma_g)} \exp\left(-\frac{\log^2(\frac{q_i}{q_g})}{2\log^2(\sigma_g)}\right)\right),$$

for integer charge bins q_i and the linearly increasing factor $\xi(q_i)$:

$$\xi(q_i) = \tag{11}$$
$$\begin{cases} 0, & q_i \leq 2.82 \\ (q_i - 2.82)/(16.23 - 2.82), & 2.82 < q_i < 16.23 \\ 1, & q_i \geq 16.23 \end{cases}.$$

The resulting charge distribution downstream of the unipolar charger is used to calculate the charge distribution downstream of both series of DMAs, as described below.

3.3.3 Charge distribution downstream of the DMAs

The charged droplets downstream of the unipolar charger are dried and passed through DMA 1a and 1b and one of the second series of DMAs (2a–f). The calculated charge distribution downstream of the DMAs, f_{fit}, is then compared with the measured DAA charge distribution.

It is important to know the individual transfer functions of each of the DMAs in order to estimate the charge distribution downstream of the DMAs. Due to the width of the DMA transfer function when measuring a certain charge, q_{set}, particles within a certain charge range $[q_{\text{min}}, q_{\text{max}}]$ will be selected. The fraction of particles with charges $q_i = 1, 2, \ldots, n$ measured in a certain charge bin, q_{DAA}, of the DAA can be calculated by convolution of the transfer function of DMA 1a or 1b and the corresponding of the DMA 2a–f. These fractions can be expressed in the transmission matrix, **T**. For an ideal DMA with a flow ratio of $\frac{Q_{\text{ae}}}{Q_{\text{sh}}} = \frac{1}{4}$ it can be derived as (here, only part of the matrix is given):

$$q_{\text{DAA}} = \left(\sqrt{2}, 2, 2\sqrt{2}, 4\right), \tag{12}$$
$$q_i = \left(1, 2, 3, 4, 5, 6, 7\right), \tag{13}$$

$$\mathbf{T}(q_{\text{DAA}}, q_i) = \begin{pmatrix} (\sqrt{2}, 1) \xrightarrow{q_i} (\sqrt{2}, 7) \\ \vdots \quad q_{\text{DAA}} \\ (4, 1) \qquad (4, 7) \end{pmatrix}$$

$$= \begin{pmatrix} 0.036 & 0.051 & 0 & 0 & 0 & 0 & 0 \\ 0 & 0.667 & 0.014 & 0 & 0 & 0 & 0 \\ 0 & 0.036 & 0.636 & 0.051 & 0 & 0 & 0 \\ 0 & 0 & 0.094 & 0.667 & 0.256 & 0.014 & 0 \end{pmatrix}. \tag{14}$$

This example shows that around 66.7 % of the particles with a charge of $q_i = 2$ will appear in the DMA channel corresponding to charge $q_{DAA} = 2$, 5.1 % will appear in the DMA channel corresponding to charge $q_{DAA} = \sqrt{2}$, and 3.6 % in the DMA channel corresponding to charge $q_{DAA} = 2\sqrt{2}$.

The charge distribution downstream of the DMAs is the sum of the product of each row of the transmission matrix $\mathbf{T}$ and the charge distribution downstream of the unipolar charger $N^{Charger}(q_i)$,

$$f_{fit}(q_{DAA})$$
$$= \sum_i \Big(\mathbf{T}(\boldsymbol{q}_{DAA}, \mathbf{q}_i) \times N^{Charger}(\boldsymbol{q}_i) \Big). \qquad (15)$$

The function f_{fit} is the calculated charge distribution, assuming that N_{UCh} particles and droplets of ambient particle size D_d enter the unipolar charger. Values of the coefficients N_{UCh} and D_d can be found by nonlinear least-squares curve fitting of the fit function f_{fit} to the measured DAA data $N^{DAA}(q_{DAA})$. It is possible to use more than one size for the ambient particles and droplets.

Having determined the values for the variables N_{UCh} and D_d from the fit, it is possible to directly relate ambient particle diameter, dry (residual) particle diameter and number concentration.

3.3.4 Inlet correction

N_{UCh} is the concentration of particles entering the unipolar charger. In the last step of the data evaluation, losses in the DAA inlet must be accounted for. A wind vane, which consists of an exchangeable cone followed by a 90° bend connected to the unipolar charger unit, directs the DAA inlet towards the wind. Three inlet cones are available, designed for isokinetic sampling at wind speeds of 2, 5 and 10 m s^{-1}. Depending on the actual wind speed, certain ambient particle diameters may be over- or underrepresented in the sampled aerosol. To obtain the concentration, N, of particles entering the DAA inlet, the calculated concentration of particles entering the unipolar charger obtained from the fit, N_{UCh}, must be corrected. The correction depends on the isokinetic sampling speed of the inlet, the actual wind speed and the ambient particle diameter of the aerosol particles, D_d, and was performed as described by Belyaev and Levin (1974).

3.4 Uncertainties

The uncertainties given here are based on laboratory tests. Intercomparisons with other aerosol/cloud sizing instrumentation, which were undertaken with the previous DAA version (Cederfelt et al., 1997; Frank et al., 1998; Martinsson et al., 1999, 2000), have not yet been undertaken with the new version. The DAA measures the number concentration, dry particle diameter and ambient particle diameter. The uncertainty in dry particle diameter is estimated to be 6 %, and is due to

the uncertainties in the DMA high voltage (estimated to be 2 %), the sheath air flow (estimated to be 2 %) and the geometrical dimensions of the DMAs (inner and outer radius and electrode length) (estimated to be 5 %). The uncertainty in ambient particle diameter is estimated to be 12 %, due to uncertainties in the DMA high voltage (estimated to be 2 %), the sheath air flow (estimated to be 2 %), the geometrical dimensions of the DMAs (estimated to be 5 %) and the calibration curve used for the unipolar charger (estimated to be 10 %). Additional uncertainty, at present not quantified, will arise from the decay of the radioactive source in the unipolar charger. The estimated uncertainty in the number concentration $dN/d\log D_p$ for each dry particle diameter obtained from the fitted function is below 13 % for ambient concentrations above $dN/d\log D_p = 50\,cm^{-3}$. This is due to the uncertainties in the standard error for Poisson counting of the raw counts, the uncertainty in aerosol flow (regulated by a proportional–integral–derivative controller (PID), estimated to be 5 %), the correction for the mobility range covered (estimated to be 10 %), and the bipolar charge correction (estimated to be 5 %).

4 Results

After fitting the ambient size distribution for each of the six dry particle diameters measured, it is possible to calculate the ambient particle and dry particle size distributions and several other parameters, as described in this section.

4.1 The capability of the DAA

In 2010, the DAA was placed at the summit of Mt. Brocken in the Harz region of central Germany to perform in-cloud measurements. An event with stable cloud conditions (31 August 2010, 23:30 UTC, to 1 September, 01:30 UTC) was selected to demonstrate the capability of the DAA. The DAA directly relates ambient particle diameter, dry (residual) particle diameter and the number concentration, as, for example, shown in Fig. 3a. Interstitial particles (red) and droplets (blue) can be identified. The cloud droplets were between 6 and 13 μm in diameter, and formed on particles in the size range 86 to 546 nm. The interstitial aerosol formed on dry (residual) particles in the size range from 50 to 300 nm, and had ambient particle diameters from 0.13 to 1.1 μm. The three black lines in the x–y plane indicate the critical diameter of activation according to Köhler's theory for different volume fractions of ammonium sulfate in the particles, $D^*_{V(AS)}$. For large dry particle size, those lines can intersect the drop mode; this indicates that some of the cloud droplets might not have been activated according to Köhler's theory. Although the droplets formed on large dry particles might not be activated according to Köhler's theory, they would be larger than the activated droplets formed on smaller nuclei, and should be regarded as cloud droplets. Both ambient and
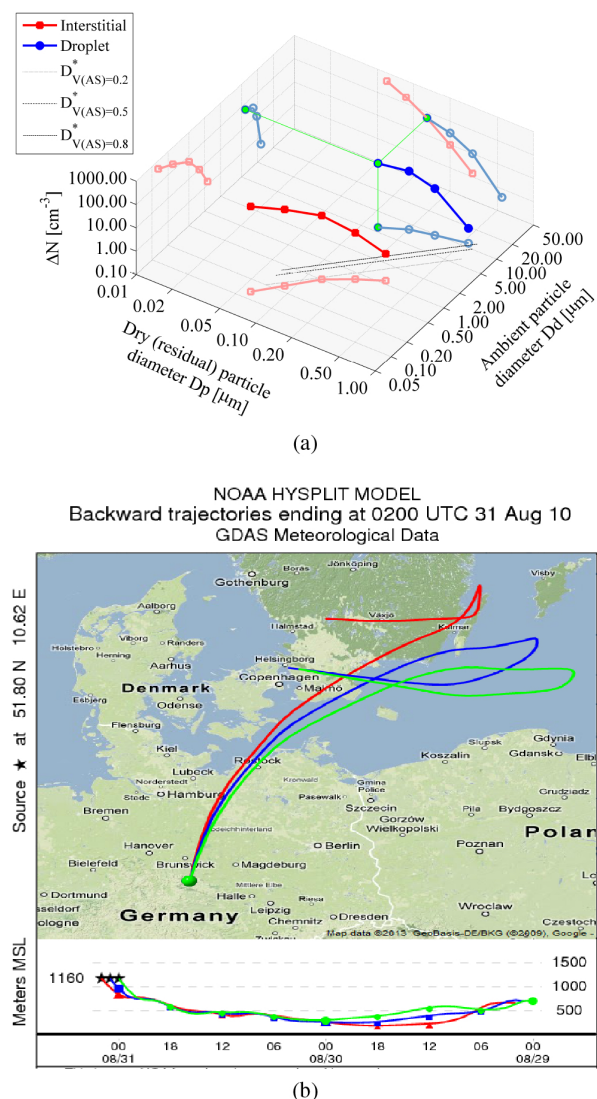
(a)

(b)

Fig. 3. (a) Concentration in each measured size interval ΔN of droplets and residual particles as a function of ambient particle and dry particle diameter on 31 August 2010, 23:51 UTC. The three black lines in the D_P–D_d plane indicate the critical diameter of activation according to Köhler's theory for different volume fractions of ammonium sulfate in the particles, $D_{V(AS)}^*$. The projections in paler colors show the distribution of ambient particles (left, D_d–ΔN plane), the distribution of dry (residual) particles (right, D_P–ΔN plane) and ambient particle diameter D_d as a function of dry (residual) particle diameter D_P (bottom, D_P–D_d plane). **(b)** The 48 h back trajectories arriving at Mt. Brocken at 23:00 UTC, 30 August 2010 (green) and 01:00 UTC (blue) and 02:00 UTC (red), 31 August 2010, derived with the HYSPLIT model are shown. The HYSPLIT trajectories arrive at 1161 m a.s.l., representing 20 m above the station at the summit of Mt. Brocken (Draxler and Rolph, 2013)

dry (residual) size distributions can be derived by projecting the concentration onto the corresponding axis and dividing by $d\log D_P$ or $d\log D_d$ as explained below.

For the selected event, 48 h back trajectories from Mt. Brocken were derived with the HYSPLIT model (Draxler and Rolph, 2013), as shown in Fig. 3. They show that the air arrived via southern Sweden and the Baltic Sea northeast of Mt. Brocken, a region with an annual fine-matter average (PM$_{2.5}$) of less than $10\,\mu\mathrm{g\,m^{-3}}$ according to the European Environment Agency (2012). The air approached Mt. Brocken via northeastern Germany from the north (PM$_{2.5}$ of 10 to $20\,\mu\mathrm{g\,m^{-3}}$) with an average wind speed of $10\,\mathrm{m\,s^{-1}}$ and ambient temperature of $5\,^\circ\mathrm{C}$, measured at the measurement station on summit of Mt. Brocken.

The total number concentration of dry (residual) particles from cloud droplets and interstitial particles in the dry particle size range 49 to 563 nm during the event was stable at $515 \pm 50\,\mathrm{cm^{-3}}$ with $416 \pm 47\,\mathrm{cm^{-3}}$ interstitial particles and $100 \pm 9\,\mathrm{cm^{-3}}$ droplets, as can be seen in Fig. 4a.

During the event, droplets formed on particles that were 85 nm and larger, i.e., mainly on accumulation mode particles, the highest drop concentration being observed for 168 nm particles (denoted by the blue circles in Fig. 4). Since accumulation mode particles have a long lifetime if not removed by rainout or washout, their source region may be southern Sweden as well as the Baltic Sea and northern Germany.

The scavenging ratio (number of cloud droplets divided by the total number concentration) can be obtained either from pre-cloud size distribution combined with cloud interstitial measurements or from size distributions of cloud droplet and interstitial particles dry residuals. The former method suffers from low precision due to problems of sampling the same air mass, whereas the latter does not exactly describe the size distribution of the aerosol entering the cloud due to the possible effect of chemical processing in clouds. Figure 4 shows the scavenging ratio of the latter kind. A steep rise for particles up to 150 nm can be seen, while for larger particles the increase is slower. A double sigmoid was fitted to the data (black line) and the diameter of 50 % activation of 130 nm is indicated (green vertical line). The scavenging ratio is similar to that in previous studies by Svenningsson et al. (1997), Martinsson et al. (1999) and Mertes et al. (2005), the steep rise indicating a higher degree of internally mixed particles and more hygroscopic particles. The slower increase for particles larger than 150 nm may be due to more externally mixed particles with a fraction of less hygroscopic particles that gradually become activated, although the larger size would, on the other hand, favor droplet formation for particles of similar composition.

The size of the ambient cloud interstitial aerosol particles in the cloud in relation to their dry particle size shows a steady increase for the smallest residue sizes, as shown in Fig. 5. This increase would continue throughout the measured dry particle size range for particles of similar
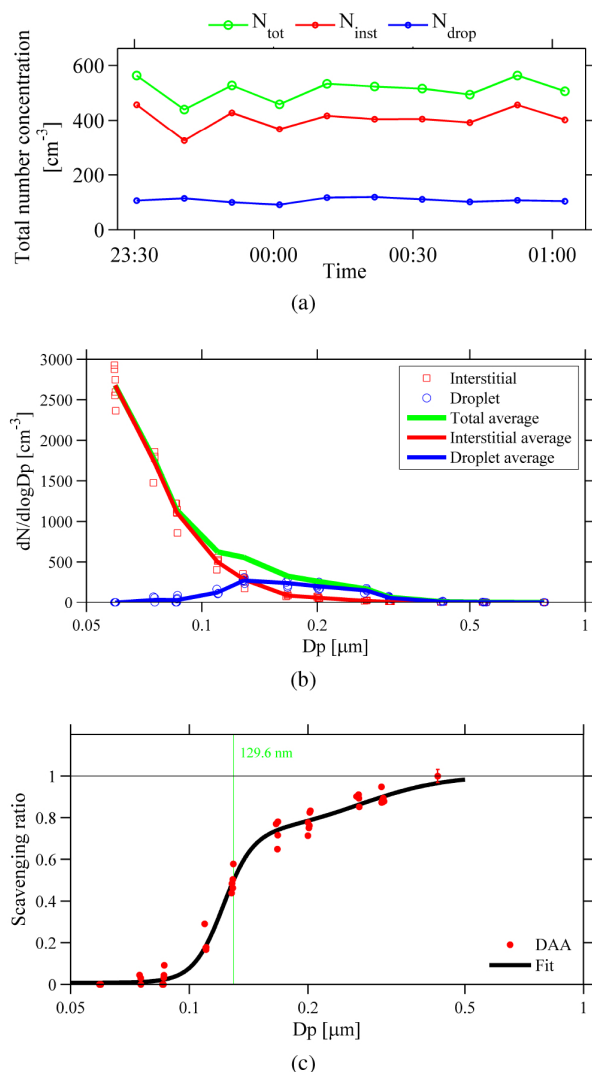
(a)

(b)

(c)

Fig. 4. (a) The total, interstitial and droplet number concentrations during the event, in the size range 49 to 563 nm. **(b)** Dry (residual) particle size distribution, $dN/d\log D_{p}$, of interstitial particles and droplets including averages (lines). **(c)** DAA scavenging ratio during the cloud event (red dots) with error bars indicating the estimated standard deviation in DAA counts during the event (smaller than the marker size for almost all data points), and a log-normal double-sigmoid fit (black line). The diameter for 50 % activation is 0.13 μm, indicated by the green line.

composition, because the interstitial aerosol can be expected to be at equilibrium with the surrounding air. As can be seen in Fig. 5, the rate of increase in ambient particle size with dry particle size decreases in the region around D_{50} (130 nm). This strongly indicates preferential cloud droplet nucleation scavenging of more hygroscopic particles, whereas the less hygroscopic particles remain as interstitial particles.

The settings of the DMA 2a–f of the DAA are based on dry particle size. Therefore, dry distributions can be obtained directly. To obtain the ambient particle size distribution, a function is fitted to the ambient particle diameter, D_{d}, as a function of dry (residual) particle diameter, D_{P}, for each measurement obtained. By differentiating $d\log D_{P}$ with respect to $d\log D_{d}$, the function $\frac{d\log D_{P}}{d\log D_{d}}$ is obtained, and the ambient particle size distribution is calculated from the dry (residual) particle size distribution as follows (Frank et al., 1998):

$$\frac{dN}{d\log D_{d}} = \frac{dN}{d\log D_{P}} \frac{d\log D_{P}}{d\log D_{d}}. \tag{16}$$

The ambient size distribution obtained (Fig. 5b) is another unique feature of the DAA and shows that interstitial particles below 1 μm are separated from the drop mode by a gap around the ambient particle diameter of 2 μm with a mean ambient particle diameter of 6 μm.

Another application of the DAA data products is the estimation of the solute concentration as a function of cloud droplet size. This can be achieved from the dry particle volume; measurements of its hygroscopic properties, for example, using a hygroscopic tandem differential mobility analyzer (H-TDMA); and the volume of the cloud droplet. Since we did not have access to H-TDMA data, we assumed approximately constant hygroscopic properties. This study concerns European continental air masses. For such air masses the volume fraction of soluble matter in dry particles of the size range between 0.1 and 0.5 μm was approximated to 0.5 ammonium sulfate and 0.5 insoluble material in approximate accordance with Kandler and Schütz (2007). In Fig. 5c it can be seen that the solute concentration depends strongly on the size of the dry (residual) particles. Particle size dependence of the dry particle soluble fraction usually varies by much less than ±0.25 (Kandler and Schütz, 2007), i.e., much smaller than the size dependence in the solute concentration, which was based on assumption of a size-independent particle soluble fraction. Limitations in vapor transport by diffusion prevent droplets formed on large particles from increasing in volume at the same relative rate as droplets formed on smaller particles.

5 Conclusions

The DAA was developed specifically for studying the interaction between aerosol particles and cloud/fog droplets. It collects droplets and interstitial particles under ambient conditions and can be used to determine the ambient particle size of individual droplets and the number and sizes of the dry (residual) particles after evaporation of the water. This gives a unique three-parameter data set (ambient particle diameter, dry (residual) particle diameter and number concentration).

The DAA inversion approach presented here employs basic corrections to the DAA raw data and different steps to convert the ambient particle charge distributions for certain
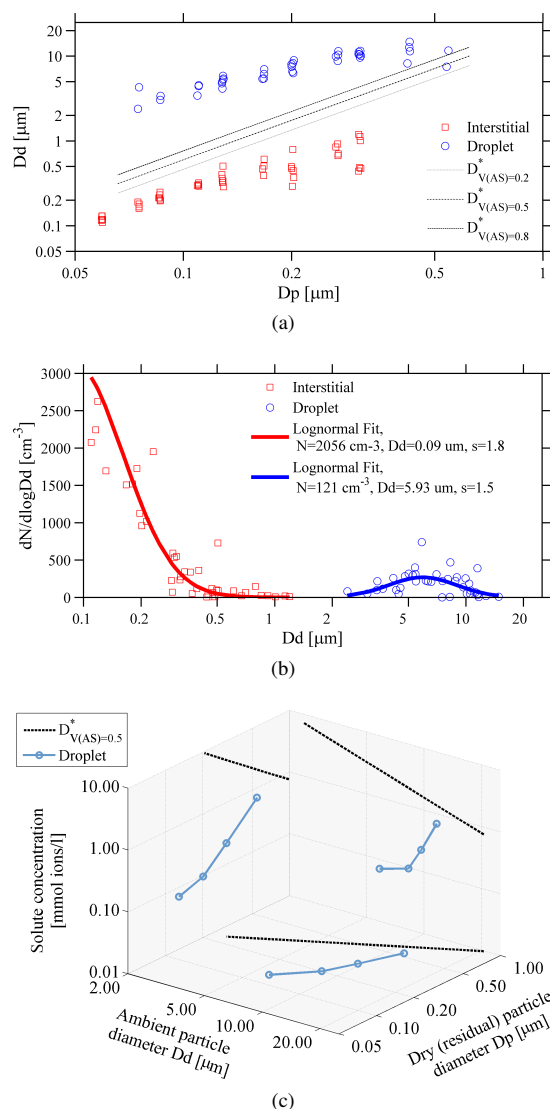
Fig. 5. (a) Ambient particle diameter, D_d, as a function of dry (residual) diameter, D_P, during the event. The three black lines show the critical diameter of activation $D^*_{V(AS)}$ for different volume fractions of ammonium sulfate in the particles. **(b)** Ambient particle size distribution, $dN/d\log D_d$, for interstitial particles and droplets during the event. The bold lines are log-normal fits to the data. **(c)** Estimated cloud droplet solute concentration as a function of the droplet size and dry (residue) particle size on 30 August 2010, at 23:51 UTC. The projections show droplet solute concentration as a function of interstitial particle diameter (left) and ambient particle diameter (right). The bottom projection shows the ambient particle diameter, D_d, as a function of dry (residual) particle diameter, D_P. The dashed lines show the limits of droplet activation for an ammonium sulfate volume fraction of 0.5 according to the Köhler theory in each projection.

measured dry particle diameters into an ambient particle size distribution. The components of the DAA, such as the DMAs (dimensions, flows, transfer function) and the CPCs, have been calibrated and characterized to provide the necessary input for data evaluation, ensuring reliable results.

The data can be evaluated with automatic fitting of the charge distribution. For particle number concentration of $dN/d\log D_p = 12.5\,\mathrm{cm}^{-3}$ ambient particle diameters down to $0.050\,\mu\mathrm{m}$ can be determined with an error of $\pm 0.005\,\mu\mathrm{m}$. The fitting routine is run automatically; however, manual screening of the results is necessary. In cases of low number concentrations in particular, manual fitting is sometimes needed to identify the interstitial particle and cloud droplet distributions. The estimated uncertainties in the basic DAA parameters, i.e., the diameters of ambient and dry particles and the number concentration, are 12 %, 6 % and $< 13\%$, respectively.

The inversion algorithm presented here was developed to evaluate long-term DAA data by using more automated data processing, making it possible to evaluate larger amounts of data. The presented data are part of long-term measurements made during 2010 on Mt. Brocken, performed with a version of the DAA designed for long-term measurements, with better time resolution than the previous version of the instrument. The data show the capability of the DAA when studying the influence of aerosol properties on clouds. The three-parameter DAA data set is presented in relation to thermodynamic activation with various aspects of the cloud-aerosol data set, such as the number concentration of interstitial particles and cloud droplets, the dry particle size distribution, droplet size distributions, scavenging ratios due to cloud droplet formation and size-dependent solute concentrations. Both the improved version of the DAA and the inversion algorithm will help to relate aerosol and cloud properties to facilitate investigations of cloud and fog formation.

References

Albrecht, B. A.: Aerosols, cloud microphysics, and fractional cloudiness, Science, 245, 1227–1230, 1989.

Anderson, T. L., Charlson, R. J., and Covert, D. S.: Calibration of a Counterflow Virtual Impactor at Aerodynamic Diam-

eters from 1 to 15 μm, Aerosol Sci. Technol., 19, 317–329, doi:10.1080/02786829308959639, 1993.

Belyaev, S. and Levin, L.: Techniques for collection of representative aerosol samples, J. Aerosol Sci., 5, 325–338, 1974.

Cederfelt, S. I., Martinsson, B. G., Svenningsson, B., Weidensohler, A., Frank, G., Hansson, H. C., Swietlicki, E., Wendish, M., Beswick, K. M., Bower, K. N., Gallagher, M. W., Pahl, S., Maser, R., and Schell, D.: Field validation of the droplet aerosol analyser, Atmos. Environ., 31, 2657–2670, 1997.

Draxler, R. and Rolph, G.: HYSPLIT (HYbrid Single-Particle Lagrangian Integrated Trajectory) Model access via NOAA ARL READY Website http://ready.arl.noaa.gov/HYSPLIT.php, NOAA Air Resources Laboratory, Silver Spring, MD, 2013.

European Environment Agency: Air quality in Europe, 2012 report, Tech. rep., European Environment Agency, 2012.

Frank, G., Martinsson, B. G., Cederfelt, S.-I., Berg, O. H., Swietlick, E., Wendisch, M., Yuskiewicz, B., Heitzenberg, J., Wiedensohler, A., Orsini, D., Stratmann, F., Lai, P., and Ricci, L.: Droplet formation and growth in polluted fogs, Contr. Atmos. Phys., 71, 65–85, 1998.

Frank, G. P., Cederfelt, S.-I., and Martinsson, B. G.: Characterisation of a unipolar charger for droplet aerosols of 0.1–20 μm in diameter, J. Aerosol Sci., 35, 117–134, 2004.

Frank, G. P., Berghof, M., Sjogren, S., and Martinsson, B.: A Droplet Aerosol Analyser (DAA) for Longterm Aerosol-Cloud Microphysics Measurements, in preparation, 2014.

Hoppel, W. A., Frick, G. M., and Fitzgerald, J.: Deducing droplet concentration and supersaturation in marine boundary layer clouds from surface aerosol measurements, J. Geophys. Res., 101, 26553–26565, 1996.

Kandler, K. and Schütz, L.: Climatology of the average water-soluble volume fraction of atmospheric aerosol, Atmos. Res., 83, 77–92, doi:10.1016/j.atmosres.2006.03.004, 2007.

Karlsson, M. N. A. and Martinsson, B. G.: Methods to measure and predict the transfer function size dependence of individual DMAs, J. Aerosol Sci., 34, 603–625, 2003.

Lawless, P. A.: Particle charging bounds, symmetry rrelation, and an analytic charging rate model for the continuum regime, J. Aerosol Sci., 27, 191–215, 1996.

Liou, K.-N. and Ou, S.-C.: The Role of Cloud Microphysical Processes in Climate:An Assessment From a One-Dimensional Perspective, J. Geophys. Res., 94, 8599–8607, 1989.

Lohmann, U. and Feichter, J.: Global indirect aerosol effects: a review, Atmos. Chem. Phys., 5, 715–737, doi:10.5194/acp-5-715-2005, 2005.

Martinsson, B. G.: Physical basis for a droplet aerosol analysing method, J. Aerosol Sci., 27, 997–1013, 1996.

Martinsson, B. G., Cederfelt, S. I., Svenningsson, B., Frank, G., Hansson, H. C., Swietlicki, E., Wiedensohler, A., Wendisch, M., Gallagher, M. W., Colvile, R. N., Beswick, K. M., Choularton, T. W., and Bower, K. N.: Experimental determination of the connection between cloud droplet size and its dry residue size, Atmos. Environ., 31, 2477–2490, 1997.

Martinsson, B. G., Frank, G. P., Cederfelt, S.-I., Swietlicki, E., Berg, O. H., Zhou, J., Bower, K. N., Bradbury, C., Birmili, W., Stratmann, F., Wendisch, M., Wiedensohler, A., and Yuskiewicz, B. A.: Droplet nucleation and growth in orographic clouds in relation to the aerosol population, Atmos. Res., 50, 289–315, 1999.

Martinsson, B. G., Frank, G., Cederfelt, S. I., Berg, O. H., Mentes, B., Papaspiropolos, G., Swietlicki, E., Zhou, J., Flynn, M., Bower, K. N., Choularton, T. W., Mäkelä, J., Virkkula, A., and v Dingenen, R.: Validation of very high cloud droplet number concentrations in air masses transported thousands of kilometres over the ocean, Tellus, 52, 801–814, 2000.

Martinsson, B. G., Karlsson, M. N. A., and Frank, G.: Metodology to Estimate the Transfer Function of Individual Differential Mobility Analyzers, Aerosol Sci. Technol., 35, 815–823, 2001.

Mertes, S., Lehmann, K., Nowak, A., Massling, A., and Wiedensohler, A.: Link between aerosolhygroscopic growth and droplet activation observed for hill-capped clouds at connected flow conditions during FEBUKO, Atmos. Environ., 39, 4247–4256, 2005.

Noone, K. J., Ogren, J. A., Heintzenberg, J., Charlson, R. J., and Covert, D. S.: Design and Calibration of a Counterflow Virtual Impactor for Sampling of Atmospheric Fog and Cloud Droplets, Aerosol Sci. Technol., 8, 235–244, doi:10.1080/02786828808959186, 1988.

Ogren, J. A., Heintzenberg, J., and Charlson, R. J.: In-situ sampling of clouds with a droplet to aerosol converter, Geophys. Res. Lett., 12, 121–124, doi:10.1029/GL012i003p00121, 1985.

Schwarzenboeck, A. and Heintzenberg, J.: Cut size minimization and cloud element break-up in a ground-based CVI, J. Aerosol Sci., 31, 477–489, 2000.

Sjogren, S., Frank, G. P., Berghof, M. I. A., and Martinsson, B. G.: Continuous stand-alone controllable aerosol/cloud droplet dryer for atmospheric sampling, Atmos. Meas. Tech., 6, 349–357, doi:10.5194/amt-6-349-2013, 2013.

Sorensen, C. M., Gebhart, J., O'Hern, T. J., and Rader, D. J.: Optical Measurement Techniques: Fundamentals and Applications, 269–312, John Wiley & Sons, Inc., doi:10.1002/9781118001684.ch13, 2011.

Spiegel, J. K., Zieger, P., Bukowiecki, N., Hammer, E., Weingartner, E., and Eugster, W.: Evaluating the capabilities and uncertainties of droplet measurements for the fog droplet spectrometer (FM-100), Atmos. Meas. Tech., 5, 2237–2260, doi:10.5194/amt-5-2237-2012, 2012.

Stevens, B. and Feingold, G.: Untangling aerosol effects on clouds and precipitation in a buffered system, Nature, 461, 607–613, 2009.

Stolzenburg, M. R.: An ultrafine aerosol size distribution measuring system., Ph.D. thesis, University of Minnesota, 1988.

Svenningsson, B., Hansson, H.-C., Martinsson, B. G., Wiedensohler, A., Swietlicki, E., Cederfelt, S.-I., Wendisch, M., Bower, K. N., Choularton, T. W., and Colvile, R. N.: Cloud droplet nucleation scavenging in relation to the size and hygroscopic behaviour of aerosol particles, Atmos. Environ., 31, 2463–2475, 1997.

Twomey, S.: Pollution and the planetary albedo, Atmos. Environ., 8, 1251–1256, 1974.

Warner, J.: A Reduction in Rainfall Associated with Smoke from Sugar-Cane Fires – An Inadvertent Weather Modification?, J. Appl. Meteorol., 7, 247–251, 1968.

Wiedensohler, A.: An approximation of the bipolar charge distribution for particles in the submicron size range, J. Aerosol Sci., 19, 387–389, 1988.

Paper III: Development of the Droplet Aerosol Analyser for long-term unattended in-cloud measurements of aerosol-cloud interactions

Paper III

Development of the Droplet Aerosol Analyser for long-term unattended in-cloud measurements of aerosol-cloud interactions

Göran P. Frank [1*], Maria I.A. Berghof [1], Staffan Sjogren [1,2], Bengt G. Martinsson [1]

[1] Div. of Nuclear Physics, Dept. of Physics, Lund University, Sweden
[2] Current affiliation: Institute of Aerosol and Sensor Technology, School of Engineering, University of Applied Sciences and Arts Northwestern Switzerland, Switzerland

Abstract

The Droplet Aerosol Analyser (DAA) is an instrument especially developed for in-cloud aerosol-cloud interaction studies. The instrument measures the ambient size of individual droplets and interstitial particles, the size of the dry residual particle after evaporation of the water vapour, and the number concentration of dry residual particles. This gives a unique three-parameter data-set (ambient diameter, dry residual particle diameter and number concentration), relating ambient size to dry size.

In this work, the DAA has been further developed in order to improve the time resolution and make it more suitable for long-term unattended measurements. The purpose is to use the DAA in long-term studies to investigate which factors are most important for determining the droplet number concentration, related to cloud dynamics and the properties of the aerosol present during cloud formation. We aim to study these relations for different types of clouds with varying cloud dynamics, different air masses and aerosol types (varying aerosol properties, such as pollution levels, origin, age, chemical composition, size distributions, etc.), at different locations. Here we present the design, properties, operation principle and calibrations to define the quality in the cloud and aerosol data produced.

1. Introduction

Clouds are an important factor in regulating the Earth's radiation budget and climate. They cool the Earth by reflecting incoming solar radiation, and warm by trapping outgoing infrared radiation. Clouds also affect the hydrological cycle and redistribute energy via transport of water vapour and latent heat in the atmosphere. Thus, it's of great importance to understand the factors controlling cloud properties (droplet size distribution, coverage, etc.).

A large variety of factors influence the formation of a cloud. Large and small scale meteorological conditions, such as large scale air motions, atmospheric layering, updraft velocity and turbulent mixing; influence the rate of cooling, cloud size and coverage; determine the type of cloud, etc. Aerosol properties, such as number concentration, chemical composition, size, and mixing state, influence the growth and activation of individual droplets, and affect cloud droplet concentrations, droplet diameters, etc. There are also intricate interactions between these factors.

An increased concentration of aerosol particles in the atmosphere, due to anthropogenic activity, thus has a significant influence on clouds. During polluted conditions activated droplet number concentrations of several thousand per cubic centimetre have been recorded

---

(Martinsson et al., 1999; Martinsson et al., 2000). Pollution can also lead to the formation of low-visibility fogs that consist of unactivated droplets (Frank et al., 1998). These examples from DAA measurements demonstrate the strong and complex effects on cloud microstructure of pollution. The indirect aerosol climate effects (e.g. Lohmann and Feichter, 2005; Stocker et al., 2013), describes changes in cloud properties induced by changes in aerosol concentration and properties. "Uncertainties in aerosol–cloud interactions and the associated radiative forcing remain large. As a result, uncertainties in aerosol forcing remain the dominant contributor to the overall uncertainty in net anthropogenic forcing" (Stocker et al., 2013).

In order to reduce the uncertainty, improved understanding of the processes involved is needed, as well as efficient ways of representing these processes in large-scale numerical models. A crucial process is the activation of aerosol particles to form cloud droplets. The major factors controlling the cloud droplet number concentration and the cloud droplet size distribution must be more accurately determined. Current climate models often use empirical links between aerosol mass and cloud droplet number concentrations. A goal for coming generations of climate models is to express the activation of aerosol particles to form cloud droplets, in terms of updraft velocity and the aerosol particle properties (number, size, composition and/or hygroscopicity, etc.). The aerosol indirect effects can thus be treated in a more physically based manner (Ghan and Schwartz, 2007). A number of possible parameterisations already exists, e.g. Abdul-Razzak and Ghan (2000), Nenes and Seinfeld (2003), Fountoukis and Nenes (2005), but lack in sufficient validation.

In order to improve the process understanding and to validate parameterisations, accurate and long-term in-situ and remote sensing observations for relevant quantities (aerosol, cloud, meteorological and environmental), are required at adequate spatial and temporal resolutions. Long-term measurements give the possibility to obtain results with high statistical confidence. In addition, more accurate laboratory studies are required. All these studies in turn rest on developments in instrumentation and measurement capabilities (Lohmann et al., 2007; Ghan and Schwartz, 2007; CCSP, 2009; Heintzenberg and Charlson, 2009).

The Droplet Aerosol Analyser (DAA) (Martinsson, 1996) is an instrument especially developed for in-cloud or in-fog studies of the interaction between aerosol particles, cloud/fog droplets and interstitial particles. The DAA measures the ambient size of individual droplets and interstitial particles, the size of the dry residual particle after evaporation of the water vapour, and the number concentration of dry residual particles. This gives a unique three-parameter data-set that connects ambient size to dry residual particle size and the number of particles and droplets/interstitial particles. This result cannot be obtained by any other currently existing instrument. Having access to these parameters, a number of related aerosol/cloud parameters, can be determined:

- Number size distribution of droplets and interstitial particles at ambient conditions
- Number size distribution of dry residual aerosol particles
- Connection between cloud droplet/interstitial particle size and their dry residue aerosol particle size
- Characterisation of the droplet activation as defined by the Köhler equation
- The size-dependent scavenging of particles due to activation
- Concentration of soluble matter in the individual droplets (solute concentration)

The DAA has until now been used in a number of field studies (Martinsson et al., 1997; Frank et al., 1998; Martinsson et al., 1999; Martinsson et al., 2000). Validations of parts of the instrumental technique have been published in Cederfelt et al. (1997) and Frank et al. (2004).

Here we present an improved version of the DAA, with higher time resolution, and automatic operation for long-term measurements. The instrument, measurement principle, data quality assurance methods, and measurement uncertainty analysis are presented in this article. Elsewhere Sjogren et al. (2013) describes an aerosol dryer of central importance to the DAA, and Berghof et al. (2014) presents the data acquisition and the data evaluation method.

The improved DAA was evaluated in long-term in-cloud field measurements at the cloud station at Mt. Brocken, Germany, September-October 2009 and June-October 2010.

2 The Droplet Aerosol Analyser (DAA)

The DAA is based on a concept where the aerosol is processed in several steps by aerosol charging mechanisms, diffusion drying, and electrostatic aerosol spectrometry, in order to obtain the desired ability to relate the ambient size to the dry residue size, see Fig. 1.

2.1 Instrument description

An important part of the instrument is placed outdoors, at ambient conditions, in order to obtain information on droplet size in the atmosphere, which is obtained by charging in a unipolar charger, where after the droplets and particles enter the dryer (Fig. 1 and Fig. 2). The constant relative humidity/supersaturation is required in order to obtain a constant diameter of the droplets and particles.
A whole air inlet samples droplets and interstitial particles, in-cloud or in-fog, see Fig. 2. A vane directs the inlet into the wind. The sample flow is 75.6 l/min. Three sampling heads are available for isokinetic sampling at wind speeds of 2, 5 and 10 m/s, respectively. The actual wind velocity is continuously measured and monitored, and deviations caused by non-isokinetic sampling are corrected for, following the description in Hinds (1999). The sampling heads are conical with 3.5° radius increase, up to a final diameter of 40 mm inner diameter to start the development of laminar flow in the sample head (White, 1994).

For the long-term unattended measurements, it was not possible to automatically change sampling head according to wind speed, and the 10 m/s head was therefore always in use.

The sampling head is connected to a 90° bend, 40 mm inner diameter, directing the flow vertically, to avoid sedimentation losses. The new DAA makes use of the same inlet as the earlier versions, and losses in the sampling head and bend, due to sedimentation and centrifugal acceleration, was estimated by Cederfelt et al. (1997). The estimation was based on computed particle trajectories. When using the 10 m/s sampling head, the maximum deviation of 20 µm droplets in the sampling head-bend combination, was found to be 10% of the tube radius, i.e. 2 mm. This leads to losses in the near-wall particle trajectories. However, the sample flow selected in the unipolar charger, 5.6 l/min, see below, is taken from a more central section (22-27% of the tube radius), and the conclusion was that droplets up to 20 µm can be sampled without significant losses. The performance of the DAA including the inlet has been verified in several field inter-comparisons (Cederfelt et al., 1997; Martinsson et al., 1999; Martinsson et al., 2000)

After the bend, the flow cross section is again increased, from 40 mm to 80 mm in diameter with conical increase in radius by 3.5°, see Fig. 2. In the lower part of the cone, the droplets and interstitial particles are charged (neutralised) in a bipolar charger. The charger provides bipolar charge equilibrium, and a low number of charges on the individual droplets and particles. More important, it provides a well-defined charge state before entering the

unipolar charger. The bipolar charger consists of strontium-90 (2x370 MBq, year 1997), radioactive sources, producing β- radiation that form ions in the air flow.

In the unipolar charger, see Fig. 2, the droplets and particles, still at their original (ambient) size, are positively charged according to their size (larger droplets/particles will acquire a higher charge).

The charging process is a combination of diffusion charging and field charging. Ions are produced in the ion-production region with a radioactive α-source (74 MBq, year 1992, curium-244 with half-life 18.1 years), and transported to the charging region by an electric field. The voltage on the centre electrode is +707 V, thus attracting negative ions. Positive ions are transported in radial direction towards the cylindrical perforated electrode, which has a voltage of +41.3 V. A fraction of the positive ions penetrate the perforated electrode and are transported in radial direction into the charging region and towards the grounded outer cylindrical charger housing. The electric field strength in the central part of the charging region, where the sample air is passing, is 20.75 V/cm. The power supplies used for the electrode voltages are manufactured by FuG Elektronik GmbH, Germany.

In order to keep the ion-production region and the electrodes dry, a small dry aerosol flow (ion source flow) is introduced via the central electrode, which in fact is a narrow tube. The flow is in the range 0.05-0.07 l/min. This flow is present close to the charging region of the sample flow, shielded from the ion source by a 20 l/min concentric excess flow at ambient condition. In-cloud tests confirm that this small, dry flow does not affect the droplet charging.

The relationship between diameter and charge rate is determined via calibration. The calibration method and calibrations are described in more detail in Frank et al. (2004). Due to radioactive decay of the α-source, the ion concentration in the charging region will decrease with time. This will lower the number of charges acquired by the droplets and particles. The change in charge rate was modelled by Frank et al. (2004), and the model is used to correct the calibration.

In the unipolar charging unit, the majority of the incoming flow of 75.6 l/min is removed as three excess flows. The removal is made isokinetic. The top excess flow of 20 l/min is removed in order to minimize the influence of the ion-production region as a flow obstacle. The two remaining excess flows are removed on the outer (30 l/min) and inner (20 l/min) side of the sample flow. Thus, the central part of the flow, passing through the charging region, is used as sample flow (5.6 l/min). The arrangement serves to obtain a similar flow velocity of the sample flow over the radial cross section and thus small variations in charging time, and also to minimize the effects of the above mentioned droplet/particle deviations in the inlet head and bend. The pump used for these three excess flows was a: Vacuubrand ME 16. The development of the charger and the calibration method has been described in more detail in Frank et al. (2004).

In the drying unit (dryer, Fig. 2), the droplets and particles are dried, while keeping their charge. This results in charged dry residual particles. The drying process is based on diffusion drying, and our goal is to reach below 20% relative humidity (RH) at the dryer outlet. This is well below 40% in RH, which is regarded as "dry conditions" in the harmonization paper on technical standards by Wiedensohler et al. (2012), i.e. changes in particle size due to hygroscopic growth remain negligible.

The drying unit follows directly after the unipolar charger. The charger is mounted directly on top of the dryer, and the sample slit of the charger is connected to the inlet slit of the dryer, in the same concentric geometry, thus avoiding impaction and sedimentation losses. The sample flow (5.6 l/min) is flowing downwards, residence time ~5.5 s, and two drying flows are flowing in the opposite direction, one on the inside and one on the outside. The flows are separated with Gore-Tex membranes mounted on fine metal nets. The membranes are particle tight, but not air tight. In order to minimize air leakage through the membranes,

the drying flows are arranged in closed loop, thus quickly adjusting their air pressure to the pressure in the sample flow.

The drying air is dried during passage through containers containing aluminium oxide. Two containers for each dry air flow are used, one at the time. Meanwhile, the aluminium oxide in the second container is regenerated, using a vacuum pump (Vacuubrand MV 2 NT), pumping at the pressure just below 1 hPa.

The drying unit was modified compared to earlier versions of the DAA, and the design, tests and calibrations has been described in Sjogren et al. (2013). The particle losses, with respect to diffusion, impaction, sedimentation and electrostatic forces, were found to be negligible.

During operation, the status of the dryer was continuously checked via measurement of the sample flow RH, and the flow through the drying containers was automatically switched when the RH was reaching above a pre-set threshold value.

The drying of highly charged droplets results in high charge levels compared to size of the shrinking droplets/particles, implying that the electrical charge limit has to be considered. This was investigated by Martinsson (1996), and the conclusion was that, provided the charging conditions are chosen with care, the risk of reaching the charge limit during a measurement is very low.

The dry aerosol is then transported from the outdoor part to the indoor part, where the size, number and charge level of the residue particles are classified by electrostatic aerosol spectrometry (differential mobility analysers, DMAs) and counted by condensation particle counters (CPCs) (Fig. 1 and Fig. 3). The aerosol enters Rack B (5.7 l/min) and is then split up in two parallel measurements sequences, in order to improve the time resolution. 3.2 l/min enters DMA 1a in Rack A (Fig. 3a), and 2.4 l/min enters DMA 1b in Rack B (Fig. 3b). A small flow (0.1 l/min) is used to constantly measure the relative humidity, in order to monitor the efficiency of the dryer.

The differential mobility analysers (DMAs) at the first level (DMA 1a and 1b) are stepped in voltage over the electrical mobilities of the dry residual particles. The dry particles carry the charge the droplets and interstitial particles acquired at original (ambient) size, and their electric mobility is thus related to their original size.

In the DMAs at the second level (DMA 2a-f), the dry diameter of the residual particles are measured, with bipolar recharging in-between, and the relation between ambient diameter and dry residual diameter can thus be established. This is explained in more detail in section 2.2.

In total eight DMAs are in use in the DAA. All are of the Vienna type, with inner diameter 50 mm and outer diameter 66 mm, but of various lengths, see Table 1. The DMAs were calibrated according to the procedures in Martinsson et al. (2001), and coefficients for broadening and losses were determined, see section 3 and Table 1.

All DMAs are operated with the sheath-excess flows in closed-loop, see Fig. 3. We have followed the recommendations by Wiedensohler et al. (2012) for closed-loop arrangement, except for the dryer in the loop. The aerosol dryer in the DAA has high efficiency, and is designed to dry the aerosol flow from a RH of 100% to a RH below 20%.Since there are no other sources for water vapour in the instrument, this will keep the RH in the DMAs, including the closed-loop components, below 20%.

After measurement of the electrical mobility of the dry residual particles at the DMA 1 level, the particles are recharged to equilibrium bipolar charge distribution. These bipolar chargers are placed directly after DMA 1a and DMA 1b respectively. The chargers are identical and consist of a small volume, containing krypton-85 radioactive sources (β^-, 555 MBq, year 2008 with half-life: 100 y). The performances of the chargers have been investigated in order to make sure that the highly charged residual particles acquire bipolar

charge equilibrium. Finally, the particles are counted in standard condensation particle counters (TSI CPC 7610).

To control the operation of the instrument, to monitor the performance, and to collect data, we have designed electronics hardware and computer software based on systems from National Instruments (NI). The central parts of the electronics hardware are the NI concept CompactRIO. The following modules are in use: NI cRIO-9014, NI 9401 digital input/output (2x), NI 9264 analog output (2x), NI 9205 analog input (2x), 9403 digital input/output, and 9265 analog output. A NI LabView program is used for the computer control and data collection system of the instrument.

A large number of sensors are in use in order to continuously produce data for the control system and to monitor the operation of the instrument. Some of these sensors are marked in Fig 3.

All flows are monitored, the more critical ones with high quality flow meters. The DMA sheath flows are monitored with Bronkhorst® mass flow meters, accuracy ±2%. Via measured temperature and in-DMA pressure, the corresponding sheath volume flow in the DMA is calculated.

The aerosol flows in to all DMAs are monitored with orifice/pressure drop aerosol flow meters. A small low-pressure drop orifice is introduced in the flow, with negligible aerosol particle losses, and the pressure drop (Δp) over the orifice is measured. Bernoulli obstruction theory (White, 1994) is used to relate the measured pressure drop to the aerosol volume flow (Q):

$$Q = k \cdot \sqrt{\frac{2 \cdot \Delta p}{\rho}}$$

where ρ is the density of the air. The constant k is determined for individual flow meters via calibration. The pressure drop is measured using a GE Druck LPM 5380, 0-10 hPa, differential pressure sensors.

The inlet excess flows (top, outer, inner), see Fig. 2, are measured with Bronkhorst® mass flow meters, accuracy ±2%, and the corresponding volume flows are calculated via atmospheric pressure and outdoor temperature. These flows are continuously regulated.

Other flows (ion source flow, water trap flow, dryer flows, see Fig. 2) are measured via pressure drop over a capillary tube, using the same Bernoulli obstruction theory mentioned above.

The absolute pressure is measured individually in each DMA, as well as in the room (atmospheric pressure) with MOTOROLA MPX5100 series sensors. The room temperature (close to the instrument) is monitored with a Pt100 sensor. Outdoor temperature and relative humidity is measured with a GREISINGER GHTU-MP sensor. Pressure and temperature are important parameters in order to calculate air density at certain points in the instrument. Outdoor relative humidity is also useful during data evaluation, since it provides a fast indication on when the measurement site was in-cloud.

Relative humidity in the aerosol flow reaching the indoor part (Fig. 3b) is important to measure in order to evaluate the dryer performance, to control the operation of the dryer, and to monitor the RH in the indoor part of the instrument to make sure that it is sufficiently low. Aerosol RH is measured by a Rotronic Hygromer relative humidity and temperature sensor.

To correct for inlet losses, wind velocity is continuously measured with a 3-cup anemometer placed nearby the inlet.

2.2 Operation principles

The operation principle of the DAA is such that the DMAs at the second level are set to fixed voltages, i.e. fixed particle residue diameters (and fixed particle electrical mobilities). The DMAs at the first level step over the charge states of the residual particles, which are related to the ambient (droplet) diameters. The scans thus results in a charge distribution for each selected dry residual particle diameter, and these charge distributions are related to the ambient (droplet) number size distributions determined by calibration of the unipolar charger. See example results in section 4. Two or more mathematical distributions are fitted to each measured charge distribution, in order to separate the interstitial cloud particles from the cloud droplets. From these fitted distributions it is possible to calculate the number of interstitial particles and number of cloud droplets, respectively, and via the average charge levels for each fitted distribution, determine average diameters for the interstitial particles and the cloud droplets.

In order to simplify the correction for multiply charged particles from the bipolar charger preceding the second DMA level, the electrical mobilities of the DMA 2a-f are separated by a factor of 2. The set-up routine is such that a largest dry residual diameter (in DMA 2a) is selected, e.g. 750 nm. The corresponding singly charged particle electrical mobility Z_0 is calculated, followed by the electrical mobilities to be selected in DMA 2 b-f, see Table 2. After one run over all voltage channels by DMA 1a and b, six new particle electrical mobilities are selected for DMA2a-f, all shifted by a factor of $\sqrt{2}$ for a new run over the DMA 1a and b voltages, see Table 2. During operation the DAA alternate between these two settings, where each run is evaluated separately to define the time resolution. During stable cloud conditions the alternate settings of the DMAs at level 2 serves to improve the size resolution in the measurements. The largest diameter measured is normally in the range 700-800 nm. Normally influence from multiply charged particles at diameters larger than that is negligible due to a strong declining gradient in number concentration in this size range (Berghof et al., 2014).

The number of positive (i.e. detectable) elementary charges on the particles at the first level can be in the range from one up to a few hundred, depending on the ambient diameters. Interstitial particles obtain a low number of charges, and the high charge levels are acquired by large cloud droplets. Table 2 shows the charge levels from the unipolar charger studied for the different dry particles sizes defined by the DMAs at level 2. The voltages of the two DMAs at level 1 are set in a way that when singly charged particles is measured for the smallest dry size, the sizes having the same mobility with 2, 4, 8, 16 and 32 elementary charges are measured simultaneously thus allowing for accurate multiple charge correction.

2.3 Time resolution

A drawback with the first version of the DAA was that rather long time was required to obtain one complete cloud measurement. It was operated in stepping mode, where switching of the DMA 1 voltage was followed by a 15 s waiting time before the data acquisition system started to record particles detected by the CPCs for 15 to 30 s depending on particle number concentrations at the measurement site. Scanning methodology has been developed where the DMA voltage is ramped and counts from the particle detector is recorded more or less continuously in order to obtain high time resolution (Wang and Flagan, 1990). The method to ramp the DMA voltage is, in contrast to one-dimensional particle size distribution measurements, not suitable for the DAA because this instrument is based on two levels of DMAs with the first level having varying voltage and the second level at fixed voltage. At

low charge levels from the unipolar charger (interstitial particles) ramping of the DMA 1 voltage would mean that a large part of the measurement time would be spent measuring in between discrete charge states of singly, doubly etc. charged particles. In order to avoid this obvious waste of time, we introduced what we call targeted scanning mode data acquisition. This method combines the stepping and scanning DMA methods. As in the first version of the DAA, the DMA 1 voltages are stepped directly to the targeted value (i.e. without ramping) as described above, but the data recording method from scanning mode is used. This way the time required for the sampling to adjust to a change in DMA 1 voltage can be directly observed in the acquired data. As a result the effective measurement time could be improved. The DMA 1 voltages were kept constant for 30 s before changing to the next voltage. Data collection started 15 s after the voltage was changed and continued until 6 s after the voltage change, thus 21 s measurement time and 9 s without particle counting, implying that 70% of the time was used for measurements.

Further steps to improve the time resolution were connected with improving the count-rate of the DAA. Increasing the aerosol flow-rate is a straightforward way that however not is a viable option because the entire DAA part operated at ambient conditions would need to be redesigned. Instead the charge distribution of the unipolar charger in relation to the resolution of the DMAs was considered. The DMA resolution is strongly connected with the ratio of the aerosol (Q_a) and sheath air (Q_s) flow-rates. This ratio also strongly affects the count-rate of a DMA. The charge distribution from the unipolar charger is broad (Frank et al., 2004). Increasing the width of the DMA transfer functions at level 2 (Level 1 DMAs were already in version 1 broad ($Q_a/Q_s = 0.22$).) by increasing Q_a/Q_s from 0.15 to 0.25 would significantly increase the count-rates while only marginally broadening the DAA charge distributions, because is the DMA penetration is proportional to Q_a/Q_s when Q_s is changed.

Further steps to improve the time resolution includes reducing the number of DMA 1 measurement steps. One simple improvement was to remove five steps in a range for very high electrical mobility (i.e. highly charged) where particles was never observed in the first version of the DAA. The electrical mobility for adjacent measured dry sizes (level 2) is shifted by a factor of 2, thus spanning a factor of 32 for the six sizes. Using a single DMA at level 1 would spread the voltage for e.g. singly charged particles by the same factor 32, implying that part of the measurement time some sizes were measured for fractions of one elementary charge. At the other end of the spectrum some of the sizes were measured for unrealistically high charge levels. Using two DMAs at level 1 compared to only one in version 1 of the DAA significantly reduces this problem because their voltages can be run independently. However, we still need to consider correction for multiple charges at the second level. In order to fulfil both these requirements DMA 1a was stepped from the lowest to the highest voltage. The lowest voltage needed for DMA1a corresponds to the fifth lowest DMA 1b in the correction for multiple charging. Therefore these two voltages are the starting points of the scan. When the last (largest particle size) singly charged under DMA 1b is measured, four voltage steps remain for DMA 1a. While these steps are running, the four DMA 1b steps that were skipped in the beginning are undertaken to complete all the steps of both DMAs at level 1. This way scanning of regions where no particles/droplets are available (i.e. when the charge is less than one elementary charge or unrealistically large droplets (high charge level)) was reduced.

The number of measurements per DAA run was this way reduced from 29 to 20, a reduction by more than 30%. Altogether these changes in data acquisition, flow settings, DMA arrangement and measurement pattern reduced the time for a complete measurement from 15 to 22 min. to 10 min. This measurement time was quite a conservative choice. Most measurements were taken with ample counting statistics. Further reduction of the measurement time can be undertaken without loss in statistical quality, and there is also room

for reduction of the waiting time between measurements at two voltages. With the improvements described here, 5 min for completion of one DAA cloud measurement is feasible.

2.4 Long-term measurements

The development of the second version of the DAA aimed at the already described improvements of the time resolution in the measurements and to improve the capacity for long-term automatic operation, and thus the capacity to produce comprehensive DAA-based datasets on the connection between aerosol and cloud properties. The major steps taken to improve the long-term capacity were to re-design the aerosol dryer and to implement closed loop operation for the sheath air of all eight DMAs.

The dryer of the first version of the DAA used aluminium oxide beads as the drying agent. This agent had to be regenerated every day to ensure optimal drying performance. In order to obtain automatic operation, the dryer was rebuilt by removing the aluminium beads, mounting Gore-Tex^{TM} membranes around the aerosol flow region and introducing dry air flows surrounding the aerosol flow that removed water vapour that penetrated the membranes (Sjogren et al., 2013). This way the drying could run continuously without human interference.

Operation of DMAs with the sheath air in a closed loop enhances stability in the operation (Jokinen and Mäkelä, 1997) compared to feeding and removing air separately, which is highly desirable for DMA systems in long-term operation.

High-quality needle valves are used as critical orifices for the aerosol flow-rate behind each of the six CPCs (Figure 3a and b), thus controlling the aerosol flow-rate through the DMAs at level 2 as well as at level 1.

Set points of the sheath flows of all DMAs are calculated from the measured aerosol flows, in order to keep the DMA flow ratios constant, and continuously computer controlled via speed control of the sheath flow pumps. Also inlet flows, ion source flow for the unipolar charger, and dryer flows are computer controlled to keep the flows at the set points.

Approximately 125 parameters, set points and measured values, are monitored at 1 second time resolution, and used for the quality check (Sec. 3.3). In addition, the instrument can be remotely controlled via internet. However, this was not possible during the field experiments 2009 and 2010 due to lack of internet connection.

3   Data quality assurance

3.1 Calibrations

Before the DAA was ready for field experiments a large number of different kinds of calibrations were undertaken in order to characterize the instrument. The calibrations concerned both sizing and quantifications of number concentrations, including calibrations of the eight DMAs with respect to geometrical dimensions and transfer function, and the six CPCs used as particle detectors with respect to counting characteristics. Calibrations were also undertaker for the unipolar charger for the relation between ambient droplet size and number of elementary charges obtained in the charger. Also the chargers used to obtain bipolar charge equilibrium between DMA levels 1 and 2 were checked. The capacity of aerosol dryer was investigated. The high voltage supplies (FuG Elektronik GmbH, Germany) for the DMAs and the two used for the unipolar charger were calibrated with respect to the

relation between the steering signal from the computer and the output voltage of the power supply, and with respect to the relation between the monitoring signal and the output voltage. The sensors used to measure and monitor the aerosol flow-rates of the eight DMAs were calibrated with respect to the relation between the voltage from pressure drop sensors and volume flow-rate for different temperatures and pressures. Mass flow meters used to monitor the sheath air flow-rate of the eight DMAs were calibrated, and the volume flow-rates of these sensors were obtained based on temperature and pressure measurements. Below follows short descriptions of some of these calibrations.

3.1.1 DMA calibration

The properties of a DMA can be expressed by geometrical dimensions and its transfer function. The DAA contains eight DMAs which all are copies of the Vienna type with a cylindrical outer electrode concentrically placed around a central electrode. The outer electrode of all the used DMAs has nominally inner diameter of 33 mm and the central rod nominal diameter is 25 mm. The nominal length of the region where the electrical field of DMAs is acting on the measured aerosol either is 110, 280 or 500 mm for the different DMAs. Due to uncertainties in the geometrical dimensions of the DMAs, the DMAs were calibrated with latex spheres of diameters 100 ± 3 nm and 300 ± 6 nm. The results are summarized by the effective length (Table 1), which is the length obtained from the calibration assuming that the actual diameters of the DMA electrodes coincide with the nominal diameters. The deviations of the effective from nominal length are small, ranging from 0 to 5%. This effective length together with the nominal radii, the sheath air flow-rate and the voltage determines the electrical mobility of the particles in the DMA measurement flow (or exit aerosol flow).

The properties of the DMA transfer function (TF) include losses of particles in the instrument and the width in terms of particle electrical mobility in the measurement flow. Ideally aerosol passes a DMA without losses and the relative full width at half maximum of the triangularly shaped electrical mobility distribution in the measurement flow, is defined by the ratio of the aerosol flow-rate (Q_a) to the sheath air flow-rate (Q_s). It is common that DMAs deviate from the ideal TF due to imperfections in the design or construction (Birmili et al., 1997; Martinsson et al. 2001) or due to Brownian motion (diffusion) of small particles (Stolzenburg, 1988; Karlsson and Martinsson, 2003). Deviations from the ideal TF affect quantification from DMA-based measurements. Losses in the instrument, of course, affect all measurements. Broadening of the TF normally is of little quantitative consequence in measurements with only one level of DMAs, such as size distribution measurements. However, when DMAs are used at two (or more) levels the combined penetration of the two DMA levels is affected by TF broadening. The TF of the DMAs were investigated based on the methodology of Martinsson et al. (2001), where the TF of each individual DMA can be determined. The results are expressed by two parameters: the loss parameter (λ) and the broadening parameter (μ). The loss parameter or, the penetration of the DMAs was found to be 93% or higher for all DMAs except DMA 2d with the penetration 82% (Table 1). Several of the DMAs also deviated from unity in the broadening parameter, ranging from 0.87 to 1. Such deviations from unity of λ and μ are quite common (Birmili et al., 1997; Martinsson et al., 2001; Karlsson and Martinsson, 2003). The effective length is used to set the DMA voltages, and the broadening and loss parameters are used in the data evaluation to quantify the results obtained from DAA measurements.

3.1.2 Particle detectors

Particle detectors are placed downstream of all the six DMAs at level 2 (Figure 1). These detectors, CPC from TSI, model 7610 were calibrated for the three aerosol flow-rates used in the DAA: 0.8, 1.1 and 1.3 l/min (Table 1). In a first test the TSI 7610 were calibrated against a TSI model 3025 with a lower detectable diameter of 0.003 µm in order to find out at how far down in particle size the detection efficiency remains constant before it starts to decrease. It was found that one of the TSI 7610 started to drop off in efficiency at 0.04 µm diameter and the remainder at 0.02 µm. Thus all the TSI 7610 CPCs have high detection efficiency for the smallest dry particle size ever investigated with the DAA (0.042 µm). The TSI 3025 CPC measurements are strongly dependent on the balance between different flows, making quantification by this instrument sensitive for small internal imbalances. The TSI 7610 do not suffer from this problem at the expense of a larger cut-off diameter with respect to detection. Therefore TSI 3025 was not used in the second test where the quantification of six TSI 7610 was compared in the size range 0.08 to 0.3 µm at the three flow-rates mentioned above. The six CPCs demonstrated excellent agreement deviating by less than 2% from each other.

3.1.3 Other calibrations

The calibration of the DAA unipolar charger (Figure 2) with respect to the number of elementary charges as a function of droplet size has been reported elsewhere (Frank et al., 2004). Correction for ageing of the radioactive source used for charge production in the charger was undertaken based on a model by Frank et al. (2004), where the non-dimensional charging time of the charger with the aged radioactive source was obtained. This was used to obtain new charge level – droplet diameter relations based on a combined field- and diffusion charging model for the continuum regime by Lawless (1996).

 The DAA aerosol dryer placed immediately after the unipolar charger (Figure 2). Charged cloud and interstitial particles passes directly from the charger into the space between two concentric Gore-Tex^{TM} tubes reinforced by stainless steel mesh tubes. Inside the inner and outside the outer Gore-Tex^{TM} flows of dry air in opposite direction to the aerosol flow are used to remove water vapour penetrating the membranes. The relative humidity after the dryer reached below 30% more than 70% of the time during a four month measurement campaign and losses of particles larger than 0.03 µm in the dryer was very low. The characteristics and properties of the DAA dryer are described in detail by Sjogren et al. (2013).

3.2 Performance validation during operation

During operation, regular checks, both automatic and manual, are made to evaluate the performance of the instrument. Our goal was to operate the DAA up to one month, maybe longer, without on-site maintenance. During the operation 2009 and 2010, we did on-site maintenance and field calibrations once per month. During these on-site visits, overview performance checks and maintenance, calibrations of all flow meters were checked with a Sensidyne Gilibrator, as well as a few tests were made. One of the most important tests was the scanning test, in order to test sheath flows and voltages of the DMAs. DMA 2a-c were set to sample the same diameter, and DMA 1a made a scan over this size. The same procedure was made for DMA 2d-f and DMA 1b, but for another diameter. Nearly identical scan results should be obtained for a well performing instrument. A second test was a tightness test of the DMAs. The closed-loops in all DMAs were turned off and on, continuously measuring the

aerosol flow. If no leaks, the aerosol flow should stay at a constant level. Varying aerosol flows imply leaks.

3.3 Quality check of the data

Quality check of the DAA data (screening) is performed on the raw data before the data evaluation starts. A first screening is of course based on time periods of interest to the scientific questions related to the experiments, e.g. finding interesting events (in-cloud or out of cloud), removing data from periods influenced by local pollution, etc.

The quality checks of the DAA functionality include DMA and unipolar charger performance, inlet flow stabilities and dryer capacity (aerosol RH). Most measured sensor parameters together with results from field calibrations and performance validations are used for the screening. The variation of aerosol and sheath air flow, high voltage and pressure of each DMA during one scan (10 min) is restricted to be within four standard deviations. The relative humidity of the aerosol flow is restricted to be lower than 20%.

3.4 Measurement uncertainty analysis

Uncertainties in the obtained three-parameter data-set: ambient diameter of cloud droplets and interstitial particles (D_d), diameter of the dry residual particles (D_p) and number of particles/droplets (N) can be related to stochastic errors (or variability), and to systematic errors. The sensitivity to stochastic errors in the raw data set was estimated by Berghof et al. (2015), and found to be less than 1.1 % for D_p and less than 6 % for D_d (expressed as one relative standard deviation). For the number of particles/droplets (expressed as dN/dlogD_p), the sensitivity was strongly dependent on the ambient diameter (Berghof et al., 2015), with highest uncertainties for the smallest and largest ambient diameters.

Systematic errors are minimized by thorough calibrations, as described in section 3.1. In addition, earlier field measurements, with the previous DAA version, have shown good agreement with other parallel measurements for several parameters. Good agreement have been found with dry aerosol size distributions (measured by Differential Mobility Particle Sizing, DMPS/SMPS), and in comparable cases with ambient size distribution and liquid water concentration (measured by Forward Scattering Spectrometer Probe, FSSP, and similar instruments) (Martinsson et al., 1997; Cederfelt et al., 1997; Frank et al., 1998; Martinsson et al., 1999; Martinsson et al., 2000).

4. Discussion

We have in the previous sections described the DAA design, its operation principles, calibrations undertaken in the laboratory, quality control during operation, screening methods and the estimated uncertainties in the measurements. Data from one DAA run is shown in Figure 4. The charge distribution obtained from the unipolar charger, used to charge droplets at ambient conditions, is shown for six dry particle sizes (0.077, 0.113, 0.171, 0.273, 0.428 and 0.776 µm). These spectra are fitted by an automated routine presented elsewhere (Berghof et al., 2014). The smallest particle size counts are almost exclusively obtained for very few charges, singly charged being most frequent. The electrical mobility step in the charge distribution is $\sqrt{2}$, thus causing the minimum between singly and doubly charged particles. The average charge is smaller than one elementary charge (Figure 4). Although we

only detect positively charged residual particles the distribution can contain negatively charged or neutral particles for the smallest ambient diameters, because the aerosol entering the unipolar charger is bipolarly charged. This average charge corresponds to droplet diameter 0.19 µm, which is an interstitial aerosol particle. As the dry residue size increases the charge distribution moves over towards higher charge levels. This reflects two different processes. Firstly, the interstitial droplets are at equilibrium with the surrounding air. Therefore the ambient sizes of interstitial particles are larger for larger dry residues, unless the chemical composition very strongly depends on particle size. Secondly, we see a strong broadening of the charge distributions of larger particles, in particular the 0.171 µm dry residue, and a minimum opens up in the distribution. This minimum is connected with cloud droplet activation. The droplets recorded with charge levels smaller than that of the minimum are interstitial particles bound to equilibrium, whereas those above are activated cloud droplets.

The spectrum fitting routine (Berghof et al., 2014) results in one ambient size for interstitial particles and one for activated cloud droplets, when available (Figure 4), and their respective number concentrations for each dry residue size. The resulting three-dimensional dataset from Figure 4 (dry diameter, ambient diameter and number concentration) is shown in Figure 5, where the faint lines and symbols are projections showing dry particle size distributions (projection b), droplet size Vs. number concentration (projection a) and the relation between dry and ambient particle/droplet size (projection c). The dry particle size distributions from interstitial and cloud droplet residues are directly obtained from this kind of projections because of the stepping method used in the DAA is based on fixed particle sizes. As can be seen, the droplet size projection is more complicated because the droplet size difference between droplet sizes from two different dry residue sizes varies. Therefore some additional methodology needs to be applied to obtain the droplet size distribution (Frank et al., 1998).

The plane describing the relation between dry and ambient size also contains important information. Together with the projections of interstitial and cloud droplets, three lines show the critical diameter of cloud droplet activation for three particle compositions of ammonium sulphate and insoluble material (20, 50 and 80% ammonium sulphate). It is clear that the smallest interstitial particle sizes essentially runs parallel to and at ambient diameter below the critical diameters, thus displaying similar hygroscopic properties (Martinsson et al., 1999). The largest residue size of the interstitial aerosol tends to bend off from the trend of the smaller sizes towards smaller ambient diameters. This tendency is usually stronger than in this example (Martinsson et el., 1997; Martinsson et al., 1999; Martinsson et al., 2000; Berghof et al., 2015). This behaviour is consistent with that more hygroscopic particles form cloud droplets and the less hygroscopic particles remain in the interstitial aerosol in this dry residue size range. Turning to the cloud droplets we see that those formed on the smallest residues are well above the critical diameter of activation. For larger dry residue sizes the curve bends towards and in this example passes over to the region for unactivated droplets. Although these latter droplets in thermo-dynamical sense are unactivated they should be regarded as cloud droplets, because of their size and stability compared to the smaller droplets that formed on smaller particles in the same cloud. The curves of interstitial and cloud droplets bend in a similar way. However, the reason for this relation to the limit of activation is altogether different from that of the interstitial aerosol. The growth-rate of cloud droplets in the initial phase is limited by vapour transport, causing inverse diameter dependence. As a result droplets formed on small particles take up more water in relation to their size, making the droplet size distribution narrow in relation to the width of the distribution of the dry particles serving as cloud condensation nuclei. Another effect of this dependence is a strong droplet size dependence of the solute concentration affecting cloud chemistry. DAA measurements

have shown that the solute concentration can differ by a factor 100 between cloud droplets separated by 2 µm in ambient size (Martinsson et al., 1999).

The new version of the DAA was used in a field study during five months at Mt Brocken in Germany. Altogether 560 h of cloud measurements that passed the data screening were obtained. The particle number concentration in the diameter range 0.1 – 0.7 µm showed large variability ranging from 5 to 1300 cm^{-3}, and from cloud dynamical point of view the updraft velocity during cloud formation was estimated to cover the range 0.05 to 0.8 m/s during the campaign. The resulting cloud droplet number concentrations were in the range 5 – 900 cm^{-3} (Berghof et al., 2015). Parameterizations of the cloud droplet number concentration were undertaken in relation to particle number concentration, size distribution and updraft velocity during cloud formation. The parameterizations were related to regimes defined based on the ratio (w/N) between the updraft velocity and the particle number concentration (Reutter et al., 2009). It was found that in the aerosol-limited regime (w/N > 10^{-3} cm^3 m s^{-1}) the cloud droplet number concentration could be parameterized without significant contribution form the updraft velocity in the cloud formation. The tendency of roll-off (Leaitch et al., 1992), i.e. deviation from linear dependence between cloud droplet and particle number concentrations, was found to increase with decreasing w/N ratio as the regime shifted from aerosol limited towards updraft velocity limited (Berghof et al., 2015).

5. Conclusions

The droplet aerosol analyser (DAA) is based on cloud and aerosol processing in several steps in order to obtain connected ambient cloud droplet size and dry residue size, permitting studies of cloud droplet nucleation scavenging based on thermo-dynamical criteria. The first version of the DAA was developed for short measurement campaigns with daily management by an operator. The second version of the instrument was developed with the aim to obtain suitability for unattended long-term operation and improved time resolution. The main changes made to obtain the former was by rebuilding an aerosol dryer for continuous operation based on the use of Gore-Tex^{TM} membranes surrounding the aerosol flow channel and dry air flows removing water vapour penetrating the membranes from the aerosol flow, and by increasing the DMA flow stability by introducing closed-loop arrangements for all eight DMAs of the DAA. The time resolution was improved by changing the data acquisition to what we call targeted scanning mode data acquisition, where the voltage is stepped to a targeted value without ramping and the data from the particle detectors are collected almost continuously. This way time-wasting connected with discrete charge levels and DMAs operated in two levels of the DAA could be avoided. The sampling time in relation to delays between voltage change and change in the count rates in the particle detectors could thus be optimized.

Further improvements was obtained by rearranging the stepping patterns of the DMAs and by changing the ratio of the aerosol flow-rate to the sheath air flow-rate of the DMAs and that way adapting the resolution of the DMAs to other parts of the DAA, thus obtaining sufficient counting statistics in a shorter period of time. This methodology has the potential to reduce the time resolution to 5 min to carry out one complete DAA cloud characterization, a factor of 3 to 5 reduction compared to the first version of the DAA. These improvements are presented together with methods to control data quality, i.e. calibrations in the laboratory, instrument tests during field measurements, data logging and screening of the data based on the logged parameters.

The second version of the DAA was used in a five month measurement campaign at Mt Brocken in Germany 2010. Examples of results obtained are shown. The DAA produced high-quality data in unattended operation, with maintenance needed only once per month.

Acknowledgements

References

CCSP 2009: Atmospheric Aerosol Properties and Climate Impacts, A Report by the U.S. Climate Change Science Program and the Subcommittee on Global Change Research. [Mian Chin, Ralph A. Kahn, and Stephen E. Schwartz (eds.)]. National Aeronautics and Space Administration, Washington, D.C., USA, 128 pp, 2009. Available at: http://www.climatescience.gov/Library/sap/sap2-3/final-report/default.htm

Berghof, M.I.A., Frank, G.P., Sjogren, S. and Martinsson, B.G.: Inversion of droplet aerosol analyzer data for long-term aerosol–cloud interaction measurements, Atmos. Meas. Tech., 7, 877-886, 2014

Berghof, M.I.A., Svenningsson, B., Frank, G.P., Sjogren, S., and Martinsson, B.G.: DAA Field Study on Cloud Droplet Activation Related to Aerosol and Updraft Regimes, 2015. In preparation.

Birmili, W., Stratmann, F., Wiedensohler, A., Covert, D., Russell, L. M., & Berg, O., Determination of differential mobility analyzer transfer functions using identical instruments in series. Aerosol Sci. and Technol., 27, 215–223, 1997.

Cederfelt, S-I, Martinsson, B.G., Svenningsson, B., Frank, G., Hansson, H-C, Swietlicki, E., Wiedensohler, A., Wendisch, M., Beswick, K.M., Bower, K.N., Gallagher, M.W., Pahl, S., Maser, R. and Schell, D.: Field validation of the droplet aerosol analyser, Atmos. Environ. 31, 2657-2670, 1997

Frank, G., Martinsson, B.G., Cederfelt, S-I, Berg, O.H., Swietlicki, E., Wendisch, M., Yuskiewics, B., Heintzenberg, J., Wiedensohler, A., Orsini, D., Stratmann, F., Laj, P. and Ricci, L.: Droplet formation and growth in polluted fogs, Contr. Atmos. Phys. 71, 65-85, 1998

Frank, G.P., Cederfelt, S-I and Martinsson, B.G.: Characterisation of a unipolar charger for droplet aerosols of 0.1-20 µm in diameter, J. Aerosol Sci., 35, 117-134, 2004

Ghan, S.J. and Schwartz, S.E.: Aerosol properties and processes – A path from field and laboratory measurements to global climate models, B. Am. Meteorol. Soc., 88, 7, 1059-1083, 2007.

Heintzenberg, J., and Charlson, R.J. (editors): Clouds in the perturbed climate system: their relationship to energy balance, atmospheric dynamics, and precipitation, Strüngmann Forum Reports, MIT Press, 2009

Hinds, W.C.: Aerosol Technology: properties, behaviour, and measurement of airborne particles, 2nd ed., John Wiley & Sons, Inc., 1998

Jokinen V. and Mäkelä J. M.: Closed-loop arrangement with critical orifice for DMA sheath/excess flow system. J. Aerosol Sci., 28, 643-648, 1997.

Karlsson M.N.A. and B.G. Martinsson: Methods to measure and predict the transfer function size dependence of individual DMAs, J. Aerosol Sci. 34, 603-626, 2003

Leaitch W. R., G. A. Isaac, J. W. Strapp, C. M. Banic, and H. A. Wiebe. The relationship between cloud droplet number concentrations and anthropogenic pollution: Observations and climatic implications. J Geophys. Res., 97(D2): 2463–2474, 1992.

Lohmann, U, and Feichter, J.: Global indirect aerosol effects: a review, Atmos. Chem. Phys., 5, 715-737, 2005.

Lohmann, U., Quaas, J., Kinne, S. and Feichter, J.: Different approaches for constraining global climate models of the anthropogenic indirect aerosol effect, B. Am. Meteorol. Soc., 88, 2, 243-249, 2007.

Martinsson, B.G.: Physical basis for a droplet aerosol analysing method, J. Aerosol Sci., 27, 7, 997 – 1013, 1996.

Martinsson B.G., Cederfelt, S-I., Svenningsson, B., Frank, G., Hansson, H-C., Swietlicki, E., Wiedensohler, A., Wendisch, M., Gallagher, M. W., Colvile, R. N., Beswick, K.M., Choularton, T.W. and Bower, K.N.: Experimental determination of the connection between cloud droplet size and its dry residue size, Atmos. Environ. 31, 2477-2490, 1997

Martinsson, B.G., Frank, G., Cederfelt, S-I, Berg, O.H., Swietlicki, E., Zhou, J., Bower, K.N., Bradbury, C., Birmili, W., Stratmann, F., Wendisch, M., Wiedensohler, A. and Yuskiewics, B.: Droplet nucleation and growth in orographic clouds related to aerosol population, Atmos. Res. 50, 289-315, 1999

Martinsson, B.G., Frank, G., Cederfelt, S-I, Berg, O.H., Mentes, B., Papaspiropoulos, G., Swietlicki, E., Zhou, J., Flynn, M., Bower, K.N., Choularton, T.W., Mäkelä, J., Virkkula A. and Van Dingenen, R.: Validation of very high cloud droplet number concentrations in air masses transported thousands of kilometres over the ocean, Tellus 52B, 801-814, 2000

Martinsson, B.G., Karlsson, M.N.A. and Frank G.: Methodology to Estimate the Transfer Function of Individual Differential Mobility Analyzers, Aerosol Sci. Tech., 35: 815–823, 2001Sjogren, S., Frank, G.P., Berghof, M.I.A., and Martinsson, B.G.: Continuous stand-alone controllable aerosol/cloud droplet dryer for atmospheric sampling, Atmos. Meas. Tech., 6, 349-357, 2001

Reutter P., Su, H., Trentmann, J., Simmel, M., Rose, D., Gunthe, S. S., Wernli, H., Andreae, M. O., and Pöschl, U.: Aerosol- and updraftlimited regimes of cloud droplet formation: influence of particle number, size and hygroscopicity on the activation of cloud condensation nuclei (ccn). Atmos. Chem. Phys., 9(18), 7067–7080, 2009.

Stocker, T.F., D. Qin, G.-K. Plattner, L.V. Alexander, S.K. Allen, N.L. Bindoff, F.-M. Bréon, J.A. Church, U. Cubasch, S. Emori, P. Forster, P. Friedlingstein, N. Gillett, J.M. Gregory, D.L. Hartmann, E. Jansen, B. Kirtman, R. Knutti, K. Krishna Kumar, P. Lemke, J. Marotzke, V. Masson-Delmotte, G.A. Meehl, I.I. Mokhov, S. Piao, V. Ramaswamy, D. Randall, M. Rhein, M. Rojas, C. Sabine, D. Shindell, L.D. Talley, D.G. Vaughan and S.-P. Xie, 2013: Technical Summary. In: Climate Change 2013: The Physical Science Basis. Contribution of Working Group I to the Fifth Assessment Report of the Intergovernmental Panel on Climate Change [Stocker, T.F., D. Qin, G.-K. Plattner, M. Tignor, S.K. Allen, J. Boschung, A. Nauels, Y. Xia, V. Bex and P.M. Midgley (eds.)]. Cambridge University Press, Cambridge, United Kingdom and New York, NY, USA.

Stolzenburg, M. R., An ultrafine aerosol size distribution measuring system. Ph.D. thesis, University of Minnesota, Minneapolis, MN, 1988.

Wiedensohler, A. Birmili, W., Nowak, A., Sonntag, A., Weinhold, K., Merkel, M., Wehner, B., Tuch, T., Pfeifer, S., Fiebig, M., Fjäraa, A. M., Asmi, E., Sellegri, K., Depuy, R., Venzac, H., Villani, P., Laj, P., Aalto, P., Ogren, J. A., Swietlicki, E., Roldin, P., Williams, P., Quincey, P., Hüglin, C., Fierz-Schmidhauser, R., Gysel, M., Weingartner, E., Riccobono, F., Santos, S., Grüning, C., Faloon, K., Beddows, D., Harrison, R. M.,

Monahan, C., Jennings, S. G., O'Dowd, C. D., Marinoni, A., Horn, H.-G., Keck, L. Jiang, J., Scheckman, J., McMurry, P. H., Deng, Z., Zhao, C. S., Moerman, M., Henzing, B., de Leeuw, G., Löschau, G. and Bastian, S.: Mobility particle size spectrometers: harmonization of technical standards and data structure to facilitate high quality long-term observations of atmospheric particle number size distributions, Atmos. Meas. Tech., 5, 657-685, 2012

Wang S.H. and Flagan R.C., Scanning Electrical Mobility Spectrometer, Aersosol Sci. Technol. 13, 230-240, 1990.

White, F.M.: Fluid Mechanics, 3rd ed., McGraw-Hill Inc., 1994

Table 1. The DMAs of the DAA.

DMA	U (V)[a]	Q_a (l/min)	Q_s (l/min)	L_e (mm)[b]	D (µm)	λ[c]	μ[d]
1a	10 – 9800	3.2	14.3	274	-	0.98	0.87
1b	6 – 4700	2.4	10.7	108	-	0.99	0.89
2a	5000/3500[e]	1.3	5.2	475	0.75/0.56[e]	0.97	1.0
2b	2100/1500[e]	1.1	4.4	492	0.43/0.33[e]	0.99	0.90
2c	3500/2500[e]	0.8	3.2	110	0.26/0.21[e]	0.95	0.94
2d	1700/1200[e]	0.8	3.2	110	0.16/0.13[e]	0.82	1.0
2e	880/620[e]	0.8	3.2	109	0.11/0.089[e]	0.93	1.0
2f	430/310[e]	0.8	3.2	110	0.073/0.060[e]	0.94	1.0

[a] Typical voltages and dry particle diameters, changes with conditions

[b] Effective length of the DMAs assuming standard Vienna type DMA radii

[c] DMA loss parameter (Ideal DMA: $\lambda = 1$)

[d] DMA broadening parameter (Ideal DMA: $\mu = 1$)

[e] Settings for alternate runs of dry particle sizes

Table 2. DMA settings of the DAA.

	Run 1		Run 2	
DMA 1a voltages (V)	17 – 12288		12 – 8689	
DMA 1b voltages (V)	8.1 – 5850		5.7 – 4137	
	DMA 2 Mobility	DMA 1 charge levels	DMA 2 Mobility	DMA 1 charge levels
DMA 2a	Z_0	2 - 1448	$\sqrt{2} \cdot Z_0$	2 - 1448
DMA 2b	$2\,Z_0$	1 – 724	$\sqrt{2} \cdot 2\,Z_0$	1 – 724
DMA 2c	$4\,Z_0$	1 – 362	$\sqrt{2} \cdot 4\,Z_0$	1 – 362
DMA 2d	$8\,Z_0$	1 – 724	$\sqrt{2} \cdot 8\,Z_0$	1 – 724
DMA 2e	$16\,Z_0$	1 – 362	$\sqrt{2} \cdot 16\,Z_0$	1 – 362
DMA 2f	$32\,Z_0$	1 – 181	$\sqrt{2} \cdot 32\,Z_0$	1 – 181

Figure captions

Figure 1. The principle of the DAA. Droplets and particles are processed in several steps by aerosol charging mechanisms in bipolar (BiCh) and unipolar chargers (UniCh), diffusion drying (Dryer), electrostatic aerosol spectrometry (DMA), and counted in condensation particle counters (CPC) in order to obtain the desired relationships.

Figure 2. The outdoor part of the DAA at ambient conditions.

Figure 3a. Indoor part of the DAA, Rack A.

Figure 3b. Indoor part of the DAA, Rack B.

Figure 4. Data (charge distributions) from one DAA run (2010-08-23, 06:17-06:26 UTC)

Figure 5. The resulting three-dimensional dataset from Figure 4 (dry diameter, ambient diameter and number concentration)
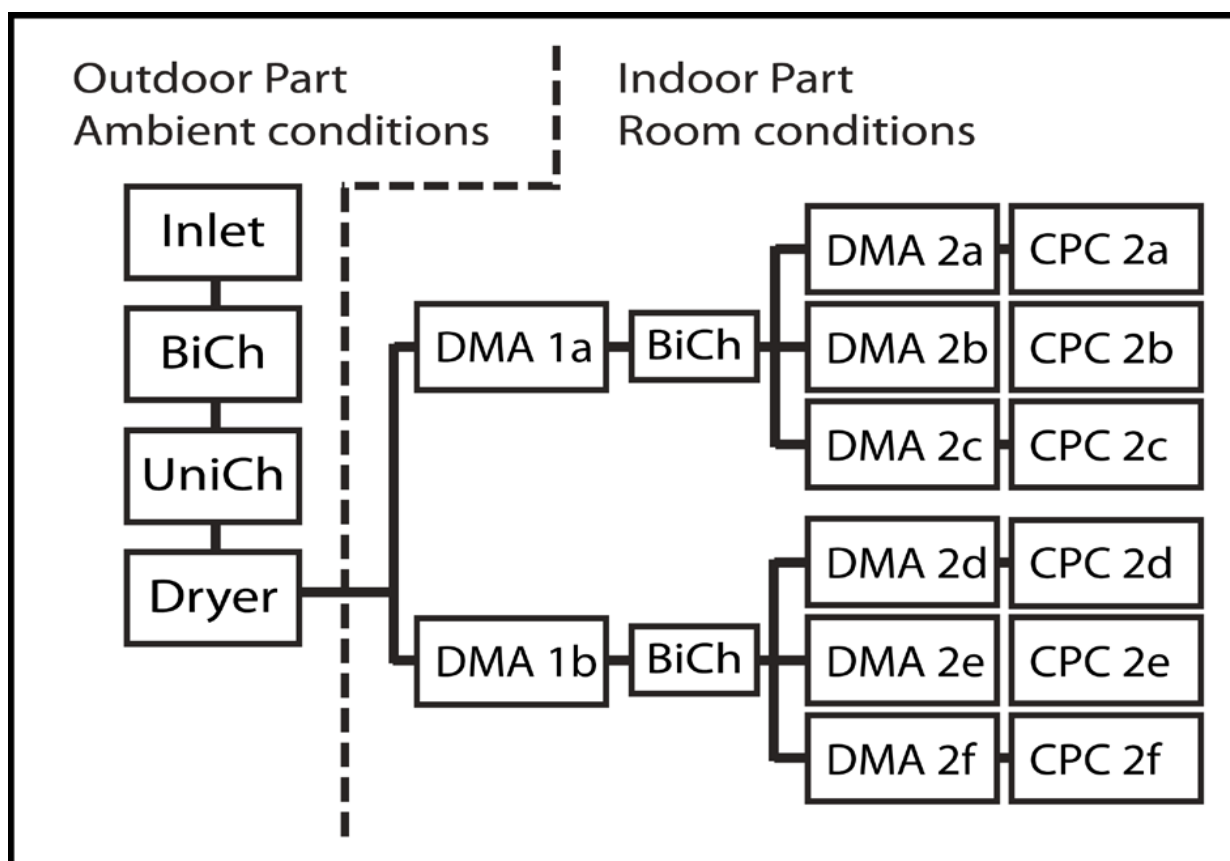
Figure 1. The principle of the DAA. Droplets and particles are processed in several steps by aerosol charging mechanisms in bipolar (BiCh) and unipolar chargers (UniCh), diffusion drying (Dryer), electrostatic aerosol spectrometry (DMA), and counted in condensation particle counters (CPC) in order to obtain the desired relationships.

Figure 2

75 l/min

Wind vane

Radioactive sources
are marked in red

Inlet excess
flow: Top
20 l/min

Bipolar charger

Water trap
flow
0.5 l/min

Water trap

Unipolar charger

Outer
30 l/min

Inlet
excess
flows:

Ion source flow (dry)
0.05-0.07 l/min

Inner
20 l/min

Inner
Outer } dryer air out

Dryer

Outer
Inner } dryer air in

Dry residual
aerosol out

To inlet in
indoor part
(in Rack B)

Figure 2. The outdoor part of the DAA at ambient conditions.

Aerosol in
(from Rack B)
3.2 l/min

Bipolar charger

DMA
1a

Sheat air: 14.3 l/min

Pp

HEFD

1.3 l/min

1.1 l/min

0.8 l/min

DMA
2a

HEFD

5.2 l/min

Pp

DMA
2b

HEFD

4.4 l/min

Pp

DMA
2c

HEFD

3.2 l/min

Pp

CPC

CPC

CPC

To aerosol
flow pump
(Vacuubrand
ME 4 NT)
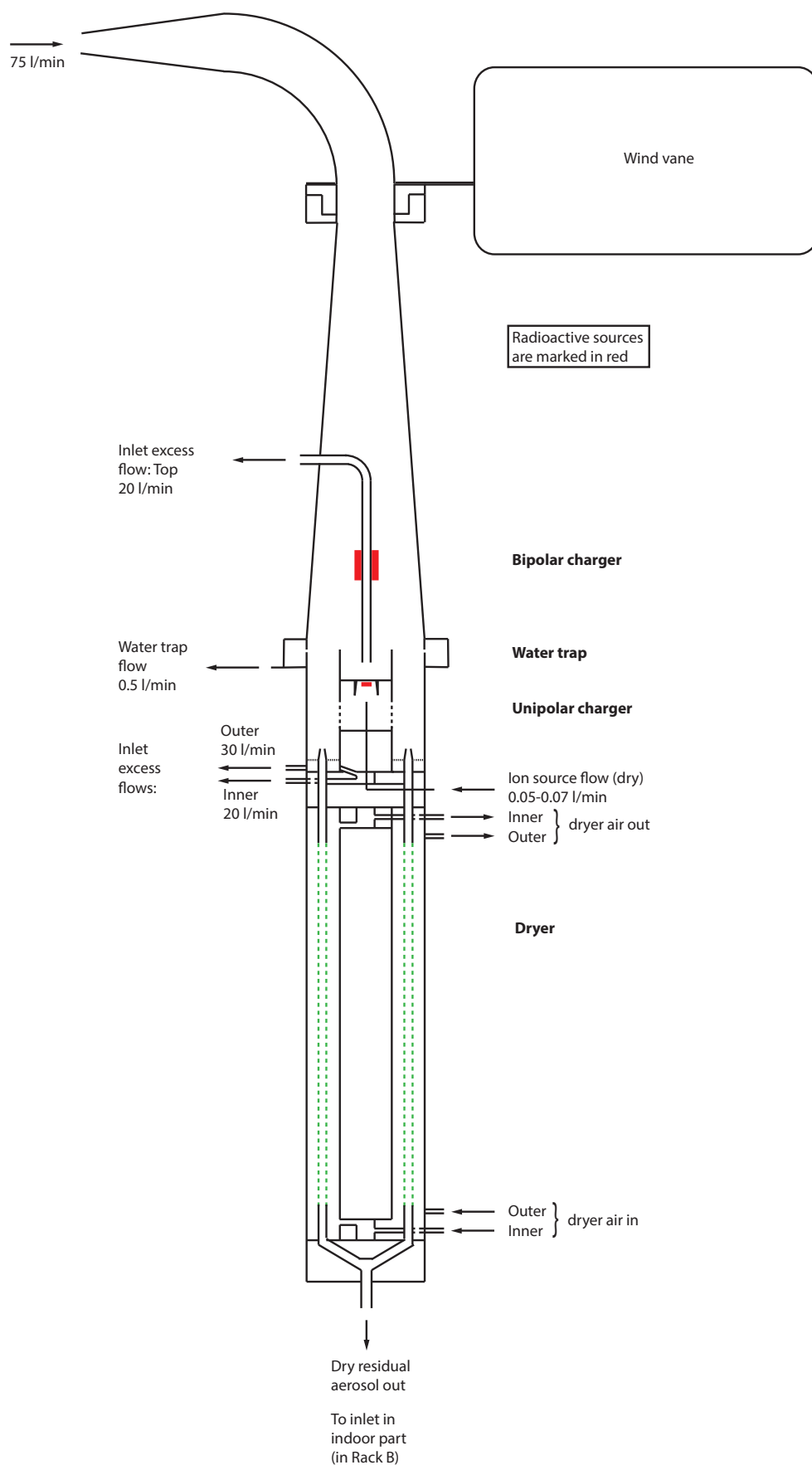
Abbreviations and symbols (Fig. 3):

DMA	Differential Mobility Analyser	
CPC	Condensation Particle Counter	
p	pressure sensor	
Δp	differential pressure sensor	
RH	relative humidity sensor	
T	temperature sensor	
Pp	Pump	
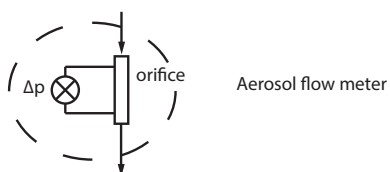
Needle valve

2-way valve

3-way valve

Mass flow meter (Bronkhorst)

Filter

HEFD   Heat exchanger & flow damper
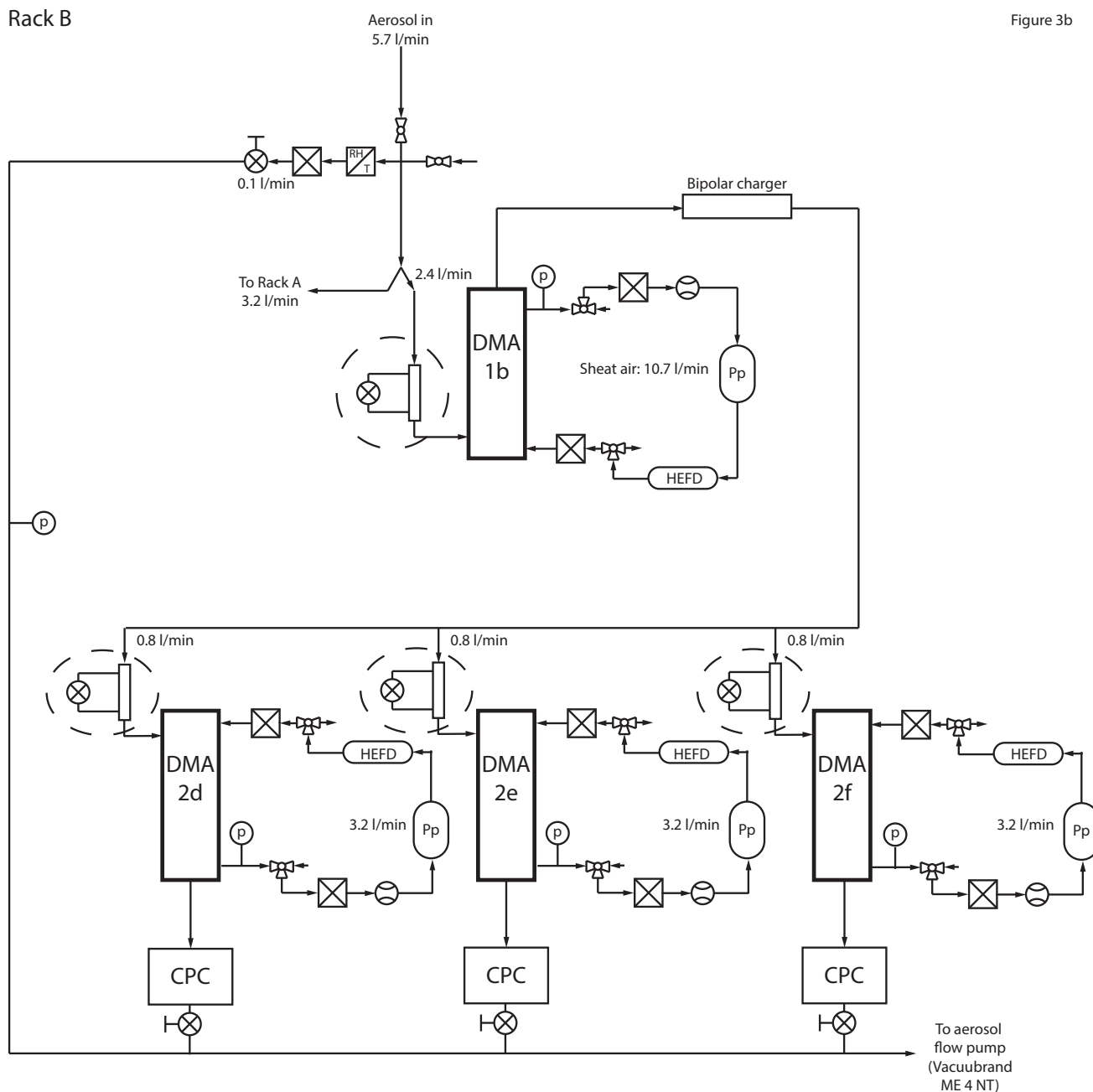
Δp orifice   Aerosol flow meter

Figure 3a. Indoor part of the DAA, Rack A

Figure 3b. Indoor part of the DAA, Rack B
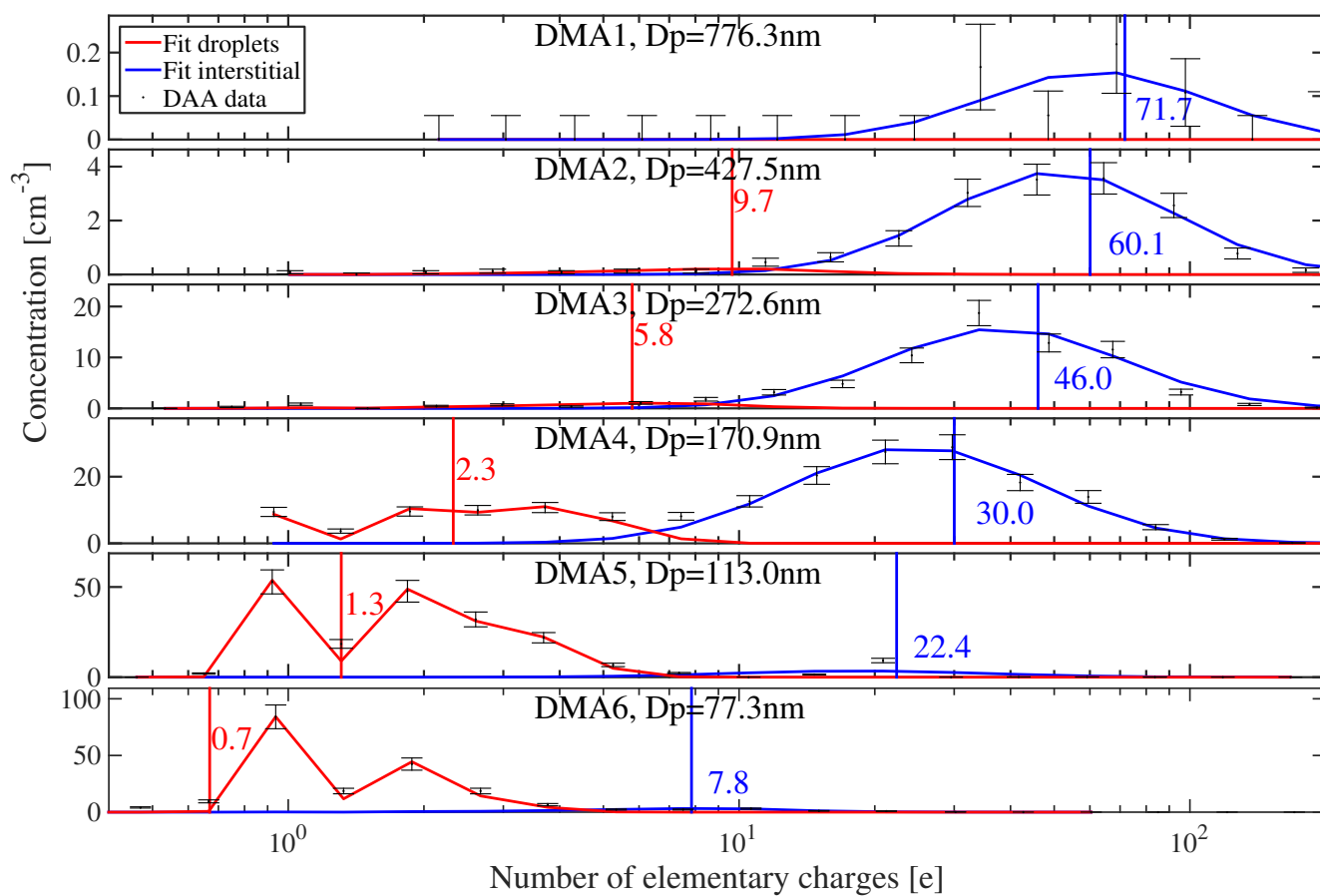
Figure 4. Data (charge distributions) from one DAA run (2010-08-23, 06:17-06:26 UTC)
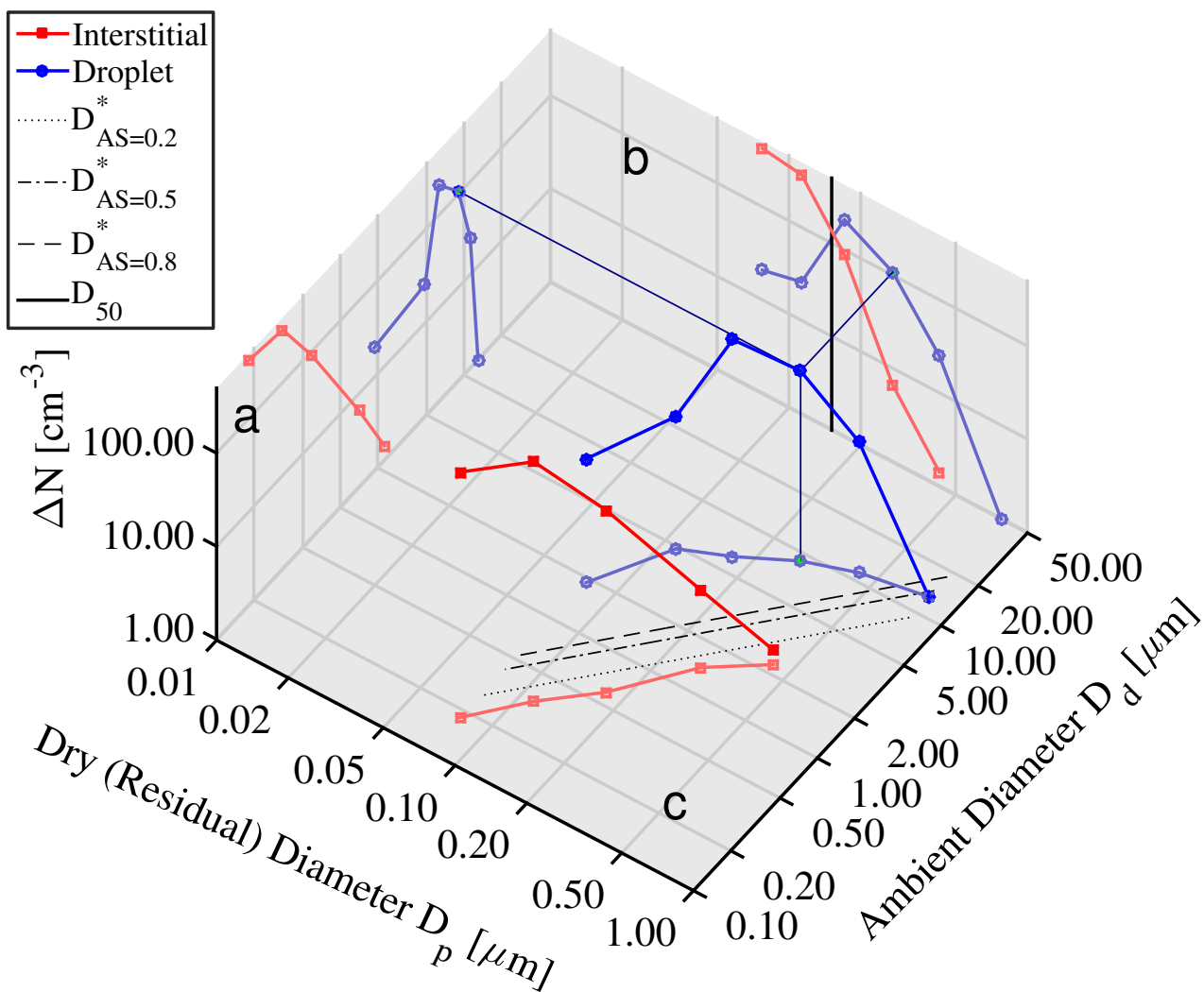
Figure 5. The resulting three-dimensional dataset (dry diameter, ambient diameter and number concentration)

Paper IV: DAA Field Study on Cloud Droplet Activation Related to Aerosol Updraft Regimes

Paper IV

DAA Field Study on Cloud Droplet Activation Related to Aerosol Updraft Regimes

By M. I. A. Berghof[1][*], B. Svenningsson[1], G. P. Frank[1], S. Sjogren[2], and B. G. Martinsson[1]

[1]*Division of Nuclear Physics, Lund University, Lund, Sweden;* [2]*University of Applied Sciences Northwestern Switzerland, Brugg-Windisch, Switzerland*

(Unsubmitted Manuscript)

ABSTRACT

Aerosol particles acting as cloud or ice nuclei can induce a change in cloud properties and thus indirectly induce a change in planetary albedo, which is considered the major reason of changes in planetary albedo associated with global warming.

Because of the complexity of the interaction between aerosols and clouds, uncertainties in cloud parametrization remain the major cause of discrepancies between cloud observations and simulations.

Aerosol-cloud interaction measurements have been performed between June and October 2010 at Mt. Brocken summit ($51.80°$ N, $10.62°$ E, 1142 m a.s.l.) in Central Germany. The cloud droplet number concentration $N_{d,tot}$ has been parameterized using total number concentration N_{tot}, horizontal wind speed at Mt. Brocken summit U, and a factor describing the shape of the sizedistribution, the number-to-volume ratio $R(0.1)$. The droplet activation was determined regarding to the ratio between updraft velocity and particle number concentration (w/N_{tot}). As expected, $N_{d,tot}$ is mainly limited by aerosol number and less by updraft velocity according. $N_{d,tot}$ showed an almost linear relation with total number concentration N_{tot} up to around $N_{tot} \sim 500 \text{ cm}^{-3}$ (($N_{d,tot} \propto N_{tot}^{0.96}$). Above 500 cm^{-3} $N_{d,tot}$ does not respond to the same extend to an increase in N_{tot} ('roll-off').

Keywords: DAA, aerosol-cloud interaction, cloud, droplet activation

1. Introduction

The quantification of the radiative forcing (RF) induced by the interaction between aerosols and clouds (aerosol-cloud interactions) is one of the challenges in climate science (Rosenfeld et al., 2014). The magnitude of the anthropogenic RF is important for estimating climate sensitivity. Aerosol particles can act as cloud condensation nuclei (CCN) or ice nuclei (IN). Thus, by influencing the microphysical and radiative properties of clouds, aerosol particles can affect the climate system indirectly (Twomey, 1974; 1977; Albrecht, 1989; Hu and Stamnes, 1993). Assuming a constant global cloud amount, an increase in cloud albedo would have a global cooling effect. A stronger cooling effect of the aerosols, would correspond to a higher climate sensitivity, which would partly or completely offset the climate impact of CO_2. Thus, the quantification of the anthropogenic RF and climate sensitivity is important for quantifying risks and probabilities, and the development of adaption strategies.

According to Modini et al. (2015) is the relation between cloud droplet number $N_{d,tot}$ and total aerosol number N_{tot} dependent on cloud dynamics and the size and composition of the aerosol.

Physically based parameterizations use updraft velocity, aerosol size distribution and chemical composition, to calculate the activation of aerosol particles into cloud droplets (Boucher et al., 1995; Abdul-Razzak et al., 1998; Nenes and Seinfeld, 2003; Petters and Kreidenweis, 2007; Kumar et al., 2009). Those are all based on Köhler-theory (Köhler, 1936). The closure between measured and predicted CCN show overall good agreement (Henning et al., 2002; Dusek et al., 2006; Jurányi et al., 2010). However, the relation between CCN number and cloud droplet number $N_{d,tot}$ depends on the maximum supersaturation S_{max} reached in the cloud, which is not easy to quantify.

There exist a number of simple parameterizations of $N_{d,tot}$ as a function of N_{tot} (Martin et al., 1994; O'Dowd et al., 1999; McFarquhar and Heymsfield, 2001; Twohy et al., 2005; Lu et al., 2007; Hegg et al., 2012), for stratiform clouds and cumuli mainly. Based on cloud parcel model studies (Reutter et al., 2009) suggests a set of regimes for droplet activation

---

depending on the ratio between updraft velocity w [m/s] and aerosol number concentration N_{tot} [cm^{-3}] at cloud base. The number of cloud droplets was found to be limited either by the number of aerosol particles ($w/N_{\text{tot}} \gtrsim 10^{-3}\,\mathrm{m\,s^{-1}\,cm^{-3}}$), or the updraft velocity ($w/N_{\text{tot}} \lesssim 10^{-4}\,\mathrm{m\,s^{-1}\,cm^{-3}}$), or both ($10^{-4}\,\mathrm{m\,s^{-1}\,cm^{-3}} \lesssim w/N_{\text{tot}} \lesssim 10^{-3}\,\mathrm{m\,s^{-1}\,cm^{-3}}$). Thus, the aim of this study is to determine the droplet activation regime and to develop simple parameterizations of the cloud droplet number concentration, that are easy to implement in global circulation models (GCM).

2. Measurement Site

The cloud investigations presented in this work have been performed at Mt. Brocken (51.80° N, 10.62° E, 1142 m a.s.l.) in the Harz region of central Germany between June and October 2010. Mt. Brocken is the highest peak of the Harz mountain range. The top of Mt. Brocken is a small plateau above the tree line, its wind field is relatively uninfluenced by the surrounding subpeaks Heinrichshöhe (1040 m), Königsberg (1034 m) and Kleiner Brocken (1018 m). It is dominated by westerly/southwesterly winds representing predominant low tropospheric wind (Acker et al., 1998; Adrian and Fiedler, 1991). Due to its steep slopes at all of its edges, the summit plateau is situated in the upper boundary layer (ABL) or even free troposphere (Beyrich et al., 1996). Since 1991 Mt. Brocken is used as a platform for cloud measurements (Möller et al., 1994; Acker et al., 1995; 1998; 2001; Plessow et al., 2001; Acker et al., 2002). Mt. Brocken has is exposed within the surrounding lowlands and has a high occurrence of clouds (Acker et al., 1998). Acker et al. (2002) estimated that between May and October 1998 during daytime around 58 % of all low clouds have their cloud base below the Mt. Brocken summit, with Stratus clouds dominating (65 %) before Cumulus clouds (27 %) and Stratocumulus clouds (8 %). Also different cloud types were found to differ in cloud base, with a higher cloudbase for convective clouds (900 to 1200 m a.s.l.) and a lower cloudbase for stratiform clouds (700 to 900 m a.s.l.).

In the measurement hut, instruments were mounted on the roof around 4 m above the ground. In close proximity of the hut on Mt. Brocken plateau, there is a meteorological station distance $d=$ 96 m, direction 114°), a hotel ($d=$ 140 m, 296 − 334°) and a trainstation building ($d=$ 80 m, 10 − 58°) with tracks ($d=$ 90 m, 10 − 85°) of the steam train bringing tourists up and down the Mountain during daytime (see Fig. 1(a)). There is a small road with restricted motorized traffic and transport only to and from weather station and hotel (very few cars per day).

To monitor clouds the Droplet Aerosol Analyzer (DAA) was mounted in the measurement hut with its outdoor part on top of the roof, together with the Gerber Particle Volume Monitor (PVM 100), detecting the liquid water content of clouds (LWC). Commercial instruments measured wind direction,

Table 1. DAA dry residue diameters measured.

Set	D_p [nm]					
	DMA 2a	DMA 2b	DMA 2c	DMA 2d	DMA 2e	DMA 2f
1	776	427	272	170	112	78
2	548	313	205	131	88	61

horizontal wind velocity (ultrasonic anemometer), temperature and humidity.

At the foot of Mt. Brocken an automatic weather station was equipped with a Vaisala CT25K Laser Ceilometer continuously measuring the cloud base height (CBH). Its location was 4.44 km and 146° in horizontal direction (Southeast), and 530 m below the measurement hut at 612 m a.s.l. at Schierke (see straight red line in Fig. 1(b) and 1(c)).

3. Instrumentation

The Droplet Aerosol Analyzer (DAA) measures cloud microphysical properties and is described in more detail by Frank et al. (2015). It determines the droplet and interstitial particle ambient size (D_{d}) and number concentration (N) for a certain diameter of the dry residue (D_{p}) with a time resolution of 10 min. Under operation two sets of six different dry residue diameters D_{p} in the range between 61 nm and 776 nm were chosen (Table 1).

From this three-dimensional DAA data set (N, D_{p}, D_{d}) it is possible to divide the ambient aerosol into cloud droplets and interstitial particles, as described in more detail by **?**. Even though cloud droplets formed on large dry particles might not have been activated according to Köhlers theory, they are regarded as cloud droplets, since they are larger than the activated droplets formed on smaller nuclei. Further parameters can be estimated, for example the critical diameter of activation (D_{50}), at which 50 % of the aerosol particles are activated.

A schematic of the DAA is shown in Fig. 2. The DAA consists of an outdoor and an indoor part. The outdoor part consists of an isokinetic inlet, directed towards the wind by a wind vane, a charging unit, and a dryer. Cloud droplets entering the inlet pass a bipolar charger (BiCh) to achieve a well defined charge state. In the following unipolar charger (UniCh) the droplets acquire a charge level dependent on their size, while still at ambient conditions (Frank et al., 2004). After passing the dryer (Sjogren et al., 2013) the dry aerosol enters the indoor part.

Still charged according to their ambient size, the particles enter the first differential mobility analyzers (DMA 1a and 1b) where the particles are selected according to their electrical mobility. The following combination of Bipolar Charger (BiCh), DMA 2 and Condensation Particle Counter (CPC), gives the electrical mobility of the singly charged droplet residuals for a given dry diameter. By knowing the dry particle diameter and the electric mobility of the residual particles in DMA 2, their charge state downstream of the unipolar charger can be calcu-
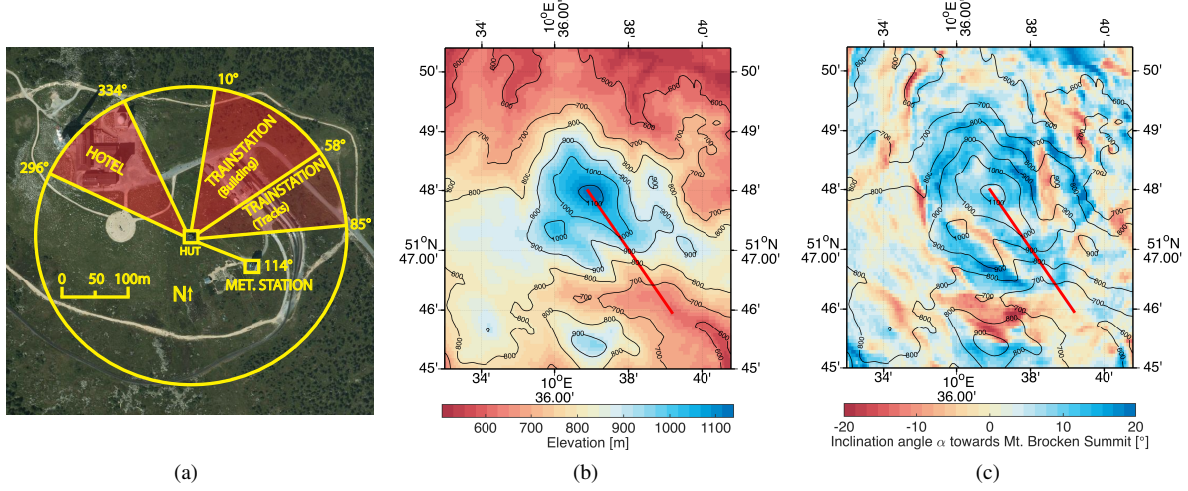
Fig. 1. (a) Measurement site at summit of Mt. Brocken with meteorological station, hotel, train station and tracks marked. Certain wind directions are restricted, due to possible contamination by local sources (marked with red). (b) Topographic map of Mt. Brocken with contour lines in 100 m intervals. The red line indicates the direction and distance between Mt. Brocken summit and the location of the Celiometer at the foot of Mt. Brocken. (c) Inclination angle α of Mt. Brocken slope.
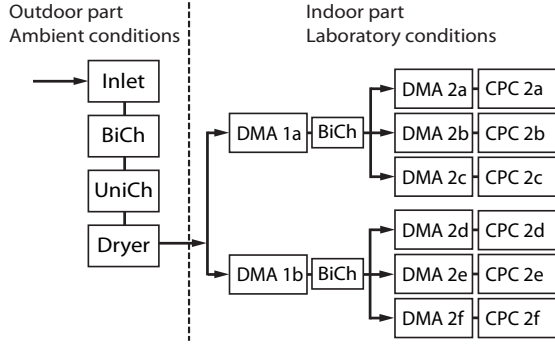

Fig. 2. The principle of the DAA. Droplets and particles are processed in several steps by aerosol charging mechanisms in bipolar (BiCh) and unipolar chargers (UniCh), diffusion drying (Dryer), electrostatic aerosol spectrometry (DMA), and counting in condensation particle counters (CPC) in order to obtain the desired relationships.

lated. The arithmetic mean charge is then related to the ambient particle diameter via the calibration of the unipolar charger. The ion source in the unipolar charger is an α-source (Cm-244, 75 MBq) with a half-life of 18.1 years. Since the last calibration in 2000 by Frank et al. (2004) the ion concentration has decreased due to radioactive decay and the relation between arithmetic mean charge level q and mean ambient diameter D_d [μm] has changed. A new calibration curve was estimated using the field-diffusion charging model for the continuum regime by Lawless (1996). Together with the half-life of the α-source and previous measured relation between q and Dd the dimensionless charging time τ of the calibration data from 1996 and 2000 was estimated. In order to estimate the change in τ due to the

decay, the ion current model developed by Frank et al. (2004) was used. The relation between arithmetic mean charge level q and mean ambient diameter D_d was then estimated for the predicted τ using the field-diffusion charging model and a pressure reduced ion mobility Tammet (1998). A fit to the modeled relation between q and Dd for for average pressure and temperature at Mt. Brocken during the measurement campaign is used here

$$D_d(q_a) = -3.91 + (6.59 + 0.67q_a)^{0.72}. \quad (1)$$

Since ten years passed between the last calibration of the unipolar charger and the measurements presented here, the estimated mean ambient diameter D_d of this dataset has to be treated with care. Previous results obtained with the DAA show good agreement when comparing interstitial and residue size distribtion, total cloud droplet number concentration, cloud droplet size distribution and cloud liquid water content LWC with other instruments (Differential Mobility Spectrometer (DMPS), Fast Forward Scattering Probe (FSSP) and Particulate Volume Monitor (PVM), Cederfelt et al. (1997)). In this dataset the estimated LWC is no well reproduced suggesting that the ambient diameter is underestimated by a factor of 1.5 to 2.

During operation of the DAA, the voltages of the DMAs 2a...f are fixed, while the voltages of DMA 1a and 1b are varied over different charge levels from the unipolar charger. The mobility step between each DMA 2a...f is set to two. The mobility step in DMA 1a and 1b is set to $\sqrt{2}$ so as to coincide with the DMA 2 mobility of singly, doubly, quadruply, etc., charged particles from the unipolar charger. This allows for efficient detection of small particles, carrying few elementary charges. For each DMA 1a and 1b voltage, a set of six measurements from DMA 2a...f are obtained.

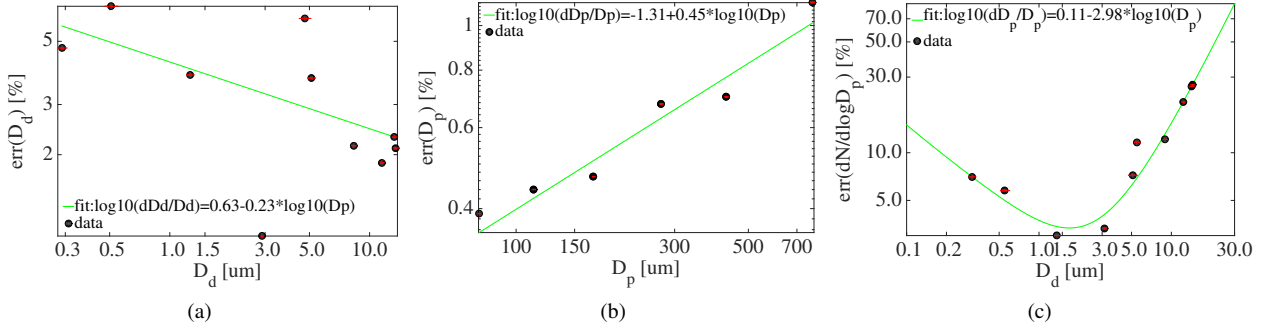The Gerber Particle Volume Monitor (PVM 100) monitored

Fig. 3.   Uncertainty intervals calculated and fitted (green lines) for (a) ambient diameter Dd, (b) dry diameter D_{p}, (c) number concentration $dN/dlogD_{\mathrm{p}}$

the liquid water content of clouds (LWC) by measuring the forward scattering of laser light by cloud water droplets in the open air along a 40 cm path (5 s sampling rate). The PVM measures in situ and real time the integrated volume of suspended water droplets. The LWC detection limit of the PVM 100 is 0.002 $\frac{\mathrm{g}}{\mathrm{m}^3}$ with an average uncertainty of less than 0.009 $\frac{\mathrm{g}}{\mathrm{m}^3}$ under operation Acker et al. (1998).

The Ceilometer (Vaisala CT25K) continuously monitored the Cloud base hight above Schierke. It detects backscattering of laser light caused by clouds in vertical direction resulting in a backscatter profile. Up to three cloud bases can be detected with a time resolution of 15 s and a vertical resolution of 30 m (Vaisala, 1999).

An ultrasonic anemometer was mounted on the roof top of the measurement hut at Mt. Brocken. It measured the 3-dimensional wind speed. The average of the horizontal component of the windvector and its direction over one DAA scan is used here.

4. DAA Data Inversion

Since measurements have been performed continuous for several month, only cloud data of restricted quality regarding DAA instrument performance are selected for further evaluation (see also Frank et al. (2015)). The variation of aerosol and sheath air flow, high voltage and pressure of each DMA during one scan (10 min) is restricted to be within four standard deviations of its variation during the whole measurement campaign. Also the relative humidity of the aerosol flow is restricted to be lower than 20 %. In a next step cloud data are selected with help of LWC data. For LWC higher than the detection limit ($> 0.002 \frac{\mathrm{g}}{\mathrm{cm}^3}$) it is assumed to be cloudy at Mt. Brocken. Since high variation of LWC during one scan makes the data interpretation difficult, the standard deviation during one scan was restricted to be smaller than 1.7 % of the average during one scan. DAA scans measured during cloud and also 40 min (4 scans) before and after are selected for further evaluation.

Some of the buildings at Mt. Brocken containing restaurants and also the train are assumed to contribute as local aerosol particle sources. Therefore during day time (7 to 19 UTC) only

Table 2. The standard deviation σ of the data variation during one DAA scan of Temperature T, pressure p, DMA high voltage U_{HV}, sheath air Q_{sh} and aerosol flow Q_{ae} used to estimate the uncertainty in the calculated DAA dataset.

Set	$\sigma[\%]$							
	DMA 2a	DMA 2b	DMA 2c	DMA 2d	DMA 2e	DMA 2f	DMA 1a	DMA 1b
T [K]	0.75	0.75	0.75	0.75	0.75	0.75	0.75	0.75
p [hPa]	0.1	0.15	0.1	0.1	0.1	0.1	0.1	0.1
U_{HV} [V]	0.8	0.6	0.2	0.2	0.3	0.3	3	3
Q_{sh} [lpm]	2.1	1.6	1.7	1.5	1.4	1.4	3.2	1.8
Q_{ae} [lpm]	2.1	1.6	1.7	1.5	1.4	1.4	3.2	1.8

data that during one DAA scan had no wind direction from hotel (140 m, 296 to 334°), station and tracks train station (80 m, 10 to 85°) are selected. During night time (19 to 7 UTC) only hotel and station building (80 m, 10 to 58°) were restricted wind directions.

In order to obtain the three-parameter dataset (N, D_p, D_{d}), the DAA raw data have to be inverted. The inversion routine used was presented by Berghof et al. (2014) and consists of several steps. First the raw data are corrected for losses in the DMAs and multiple charging in the bipolar charger between the first and second level DMAs. The concentration is corrected for standard pressure (1013 hPa) and temperature (293.15 K). In the second step a function is fitted to the charge distribution, obtained from the corrected DAA raw data, for a certain dry diameter D_{p}. The fit function used is a model, that calculates the charge distribution obtained for ambient particles of concentration N and diameter D_{d} that enter the unipolar charger and pass through the DAA system. In a last step, the concentration obtained is corrected for isocinetic sampling speed for the used inlet with the actual wind speed.

The sensitivity of the obtained three-parameter dataset (N, D_{p}, D_{d}) to the variation within the raw data was estimated according to Moffat (1988). The standarddeviation σ of the variation during one DAA scan of Temperature T, pressure p, DMA highvoltage U_{HV}, sheath air Q_{sh} and aerosol flow Q_{ae} was es-

timated and used to estimate the uncetrainty in the calculated DAA dataset (Table 2). The estimated uncertainty for D_p was less than 1.1 %, for the ambient diameter less than 6 %, and for $\frac{dN}{dlogD_\mathrm{p}}$ dependent on the ambient diameter (see Fig. 3).

5. Cloud Base Height

At Schierke (612 m a.s.l.), 530 m below and 4.44 km in horizontal direction southeast from the Mt. Brocken summit (see straight red line in Fig. 1(a)), a Ceilometer detected cloudbase height with a time resolution of 15 s and vertical resolution of 30 m. In order to account for the different location of the cloud base measurements, winddirection, wind speed and trigonometry was used to estimate the difference in time of both measurements. The lowermost detected cloudbase height was averaged over one DAA scan for cloudbase height below Mt. Brocken summit ($\overline{CBH}_{<1142\ \mathrm{m}}$) and for all cloudbase heights ($\overline{CBH}_\mathrm{tot}$). The resulting data were divided into three groups by comparing the cloudbase detected below Mt. Brocken with CBH_all:

Lowlevel clouds, unbroken: closed cloud layer detected below Mt. Brocken, $\overline{CBH}_{<1142\ \mathrm{m}}+\sigma(CBH_{<1142\ \mathrm{m}})\leqslant CBH_\mathrm{all}$

Lowlevel clouds, broken: gaps in the cloud layer detected below Mt. Brocken, $\overline{CBH}_{<1142\ \mathrm{m}}+\sigma(CBH_{<1142\ \mathrm{m}})<CBH_\mathrm{all}$

orographic clouds: no cloud layer detected below Mt. Brocken, but LWC data indicate cloud occurrence at Mt. Brocken

The Harz mountain range has a horizontal length between 40 and 80 km and does affect the planetary boundary layer significantly Gopalakrishnan et al. (2000). Thus all clouds measured at the Mt. Brocken experience an orographic influence of the underlying terrain.

6. Back trajectories

In order to analyze source and transport of air masses arriving at Mt. Brocken summit (51.80° N, 10.62° E, 1142 m a.s.l.), 48-h back trajectories have been computed for cloud periods using the NOAA HYSPLIT model (Draxler and Rolph, 2013). The back trajectories started at 1242 m a.s.l. or 100 m over Mt. Brocken summit using the velocity field from archived meteorological data (GDAS1).

The Potential Source Contribution Function (**PSCF**, Hopke et al. (1995)) can be used to identify geographical regions that contribute to observed air pollution at a site. Here **PSCF** is calculated to identify sources that contribute to pollution and cloud properties observed at Mt. Brocken. A 1°x1° grid is used here for calculation of conditional probability for each grid cell **PSCF**$_{i,j}$ by relating the number of back trajectory datapoints corresponding to a set criterion $\mathbf{m}_{i,j}$ to the total number of back trajectory datapoints $\mathbf{n}_{i,j}$ in each cell

$$PSCF_{\mathbf{i,j}} = \frac{m_{\mathbf{i,j}}}{n_{\mathbf{i,j}}}. \qquad (2)$$

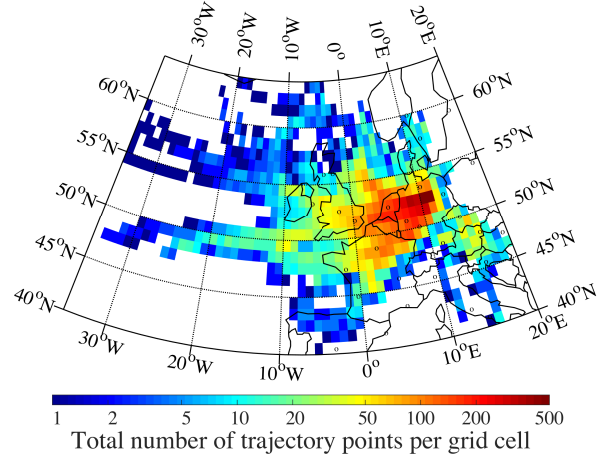The total number of trajectory datapoints in all grid cells over

Fig. 4. The total number of back-trajectory datapoints ($\mathbf{n}_{i,j}$) for each cell shows the coverage of trajectories during cloud events.

Europe ($\mathbf{n}_{i,j}$) shows the coverage of the trajectories during the campaign (see Fig. 4).

In order to account for overestimating of the $PSCF$ an arbitrary weight is used based on the standard error of counting. For a grid cell with a low number of trajectory datapoints the $PSCF$ might be overestimated, for example with $PSCF_{\mathbf{i,j}} = \frac{m_{\mathbf{i,j}}}{n_{\mathbf{i,j}}} = \frac{1}{1}$ a high source contribution is estimated. For grid cells with an error larger than w_thresh the weighting factor $\mathbf{w}_{i,j}$ is multiplied with **PSCF**

$$\mathbf{w}_{i,j} = \left(\frac{1}{\mathrm{w_{thresh}} - 1}\right)\left(\frac{\sqrt{\mathbf{n}_{i,j}}}{\mathbf{n}_{i,j}} - 1\right) + \mathrm{w_{min}}. \qquad (3)$$

Here an arbitrary error threshold of $\mathrm{w_{thresh}} = 0.2$ and a minimum weight of $\mathrm{w_{min}} = 0.2$ is used.

7. Results

7.1. Overview

During the measurement campaign at Mt. Brocken, 23.4 days of cloud data met the conditions of the data quality check, 77 % have been evaluated and are presented in this article. A general overview over the campaign is presented in Fig. 7 and Table 3. Due to restrictions of the wind direction, the dominating sector the wind was coming from was between west and south.

The DAA estimates the number concentration ΔN and ambient particle diameter D_d for a measured dry diameter D_p. It is possible to detect several ambient diameters and corresponding concentration for each measured dry diameter. Thus, both a direct relation between D_d and D_p can be obtained, and interstitial aerosol and droplets can be distinguished.

Droplets and interstitial aerosol particles are distinguished by two assumptions. The first assumption is, that with an arbitrary volume fraction of ammonium sulfate of $V(AS) = 0.8$ in the particles, particles larger than the diameter of activation
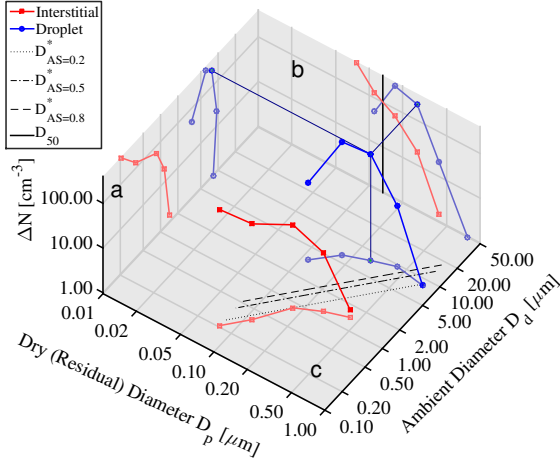
Fig. 5. Concentration in each measured size interval ΔN of droplets and residual particles as a function of ambient particle D_{d} and dry particle diameter D_{p} on September 14, 2010, 02:05 to 2:15 UTC. The three black lines in the D_p-D_d plane indicate the the critical diameter of activation according to Köhler's theory for different volume fractions of ammonium sulfate in the particles, $D^*_{V(AS)}$. The projections in paler colors show the distribution of ambient particles (left, D_d-ΔN plane), the distribution of dry (residual) particles (right, D_p-ΔN plane) and ambient particle diameter D_d as a function of dry (residual) particle diameter D_p (bottom, D_p-D_d plane).

Table 3. overview over meteorological variables, aerosol and cloud properties during the measurement campaign at Mt. Brocken.

Variable	mean	std	p(0.1)	p(0.9)
$U[\mathrm{m}]$	9.60	3.42	5.24	14.77
$T[^\circ\mathrm{C}]$	8.59	2.15	5.78	11.31
$LWC[\frac{\mathrm{g}}{\mathrm{cm}^3}]$	0.35	0.14	0.18	0.52
f_{act} (*)	0.61	0.15	0.41	0.81
$D_{50}[\mu\mathrm{m}]$	0.151	0.034	0.115	0.193
$N_{\mathrm{tot}}[\mathrm{cm}^{-3}]$ (*)	337.44	287.54	52.14	739.73
$N_{\mathrm{tot}}[\mathrm{cm}^{-3}]$ (**)	190.14	171.20	27.26	404.30
$N_{\mathrm{i,tot}}[\mathrm{cm}^{-3}]$ (*)	131.36	136.52	18.68	308.67
$N_{\mathrm{d,tot}}[\mathrm{cm}^{-3}]$ (*)	206.45	182.09	30.08	431.30
(*) $D_{\mathrm{p}} = 0.1...0.7 \mu\mathrm{m}$				
(**) $D_{\mathrm{p}} = 0.2...0.7 \mu\mathrm{m}$				

$D^*_{V(AS)=0.8}$, are activated according to Köhler's theory and are regarded as droplets. The second assumption is, that the droplet diameter does not decrease with increasing dry diameter, while taking measurement uncertainty into account (see Fig. 3). The second assumption is important for cloud droplets that formed on the largest dry particles. These droplets might not be activated according to Köhler's theory and would be mistaken as residual particles.

The DAA data are number concentration N, droplet number concentration N_{d}, interstitial number concentration N_{i}, and ambient size D_{d}, for each measured dry diameter D_{p} (see Fig. 5).
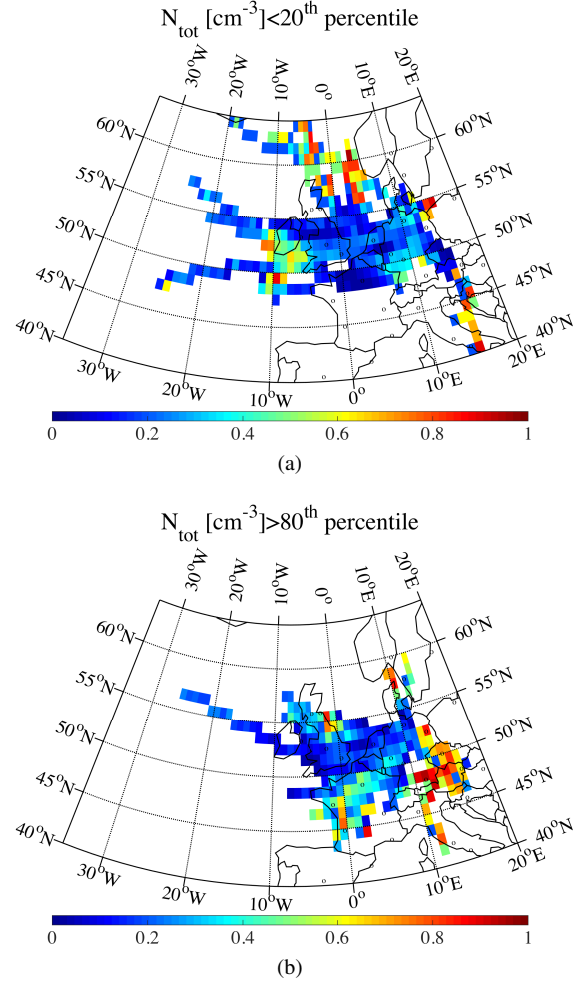

(a)

(b)

Fig. 6. (a) Potential Source Contribution Function for low N_{tot} ($N_{\mathrm{tot}} < 20$th percentile). (b) Potential Source Contribution Function for high N_{tot} ($N_{\mathrm{tot}} > 80$th percentile).

As presented in Figure 5, there is a distinct gap between interstitial aerosol and cloud droplets in the distribution of ambient particles, at around 2 μm (D_d-ΔN plane (a)). Cloud droplets formed on dry particles in the size range between 0.11 μm to 0.77 μm and their ambient diameter ranged from 3.5 μm to 9.5 μm (see D_p-D_d plane (c) in Fig. 5). Cloud droplets that formed on the largest dry particles might not be activated according to Köhler's theory (indicated by the three black lines in the D_p-D_d plane (c)), but according to the above assumptions they are regarded as cloud droplets here.

Parameters that can be derived from the DAA data are, e.g., total number concentration N_{tot}, total droplet number concentration $N_{\mathrm{d,tot}}$, and total interstitial number concentration $N_{\mathrm{i,tot}}$. The total and interstitial number concentration N_{tot} are both calculated for the size range between 0.1 μm to 0.7 μm. The total droplet number concentration $N_{\mathrm{d,tot}}$ is calculated over the total size range measured, which depends on the DAA set mea-
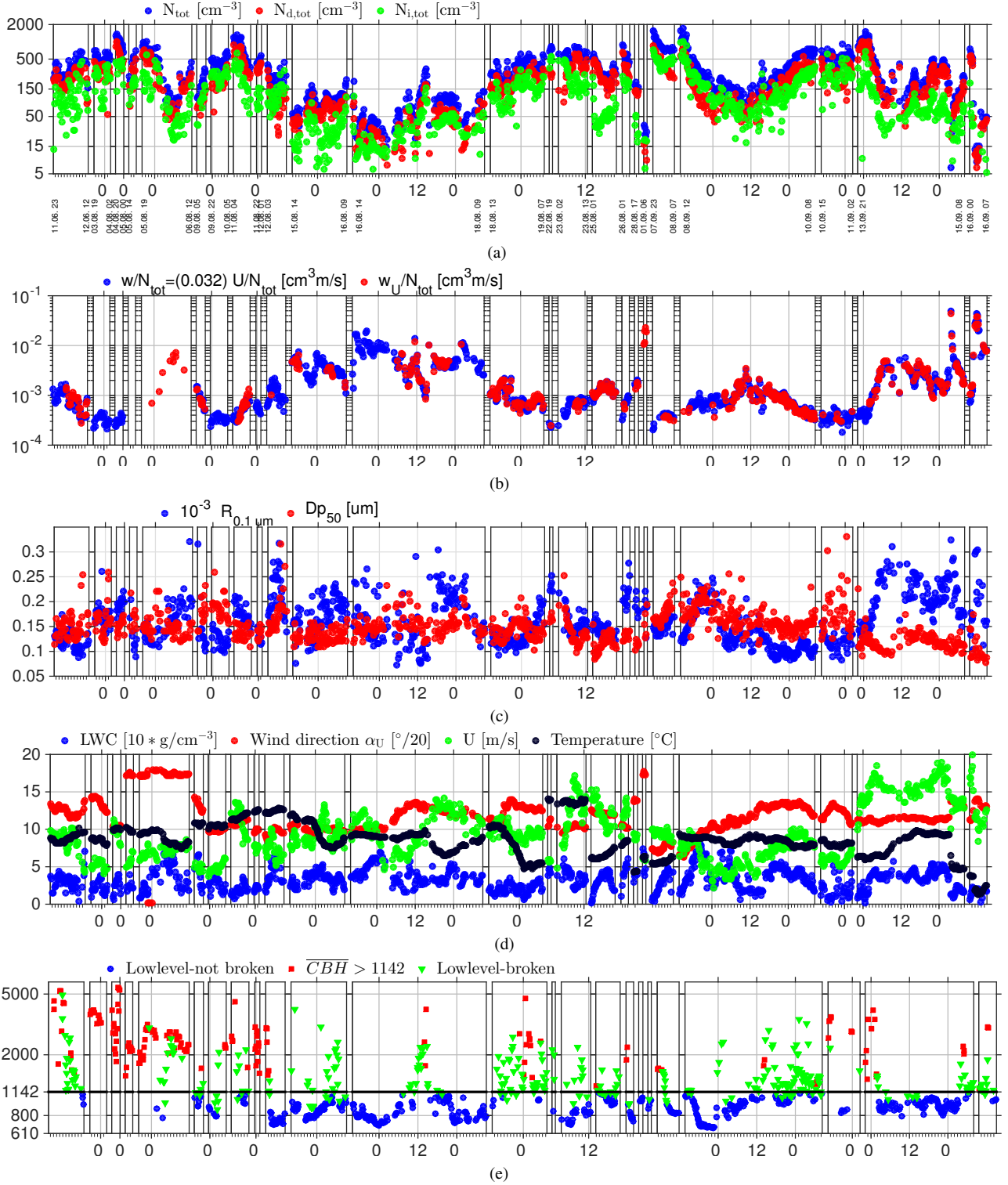
Fig. 7. Measurement campaign overview from June 1 until September 16, 2010. Temporal variation of the (a) total aerosol number concentration N_{tot} (blue), total droplet number concentration $N_{\text{d,tot}}$ (red), and total interstitial aerosol number concentration $N_{i,tot}$ (green), with vertical start and end date (*dd.mm HH*) for each cloud event; (b) estimated w/N_{tot}-ratio (red) and prediction w/N_{tot} using horizontal wind speed for wind direction between 145° to 286° (blue); (c) aerosol size distribution shape $R_{0.1\ \mu m}$ (blue), and diameter of 50 % activation D_{50} (red); (d) liquid water content LWC [g/cm^3] and meteorological parameters (horizontal wind speed U [m/s], wind direction, and temperature T); (e) average of the Lowest cloud base height over each DAA scan, as detected by the Ceilometer at the foot of Mt. Brocken. Note that in case of cloud measured at Mt. Brocken summit (1142 m a.s.l.) and broken cloud layer below Mt. Brocken, the average cloud base height can be higher than Mt. Brocken summit.

sured (see Table 1). The temporal variation during the cloud events is presented in Figure 7(a).

From the distribution of dry (residual) particles (right, D_p-ΔN plane in Fig. 5) further parameters can be estimated, for example the critical diameter of 50 % activation (D_{50}) and the shape of the dry size distribution expressed by $R_{0.1\ \mu m}$. The number-to-volume concentration ratio $R(D_c)$ (Kivekäs et al., 2008) is defined as the ratio between the number concentration N_{tot} of particles with a dry diameter D_p larger than D_c and the total volume concentration V_{tot}

$$R(D_c) = \frac{N_{tot}(D_p > D_c)}{V_{tot}}\ [1/\mu m^3]. \qquad (4)$$

The variation of D_{50} and $R_{0.1\ \mu m}$ is presented in Figure 7(c).

A higher $R_{0.1\ \mu m}$ indicates a higher number concentration of particles around 0.1 µm compared to 0.7 µm, which can be identified in the last period of the evaluated data (14.09. to 15.09.2010). At the same time D_{50} is decreasing. During this time period the wind direction is stable around 220° with high wind speed, as can be seen in Figure 7(d). The lowermost detected cloud base height is used in this study as indicator for a closed or broken cloud layer for low-level clouds and to detect orographic type clouds (see Fig. 7(e)). Below 900 m a.s.l. the major part of the low-level clouds were unbroken. This agrees well with previous results from Möller et al. (1996), where stratiform clouds have been detected mainly between 700 and 800 m a.s.l.. The height of the lowest cloudbase between 14.09. and 15.09.2010 is below Mt. Brocken summit and most of the period unbroken. An overview over meteorological variables, aerosol and cloud properties during the campaign are given in Table 3.

In order to identify areas that contribute to the observed high or low total number concentrations at Mt. Brocken the Potential Source Contribution Function (**PSCF**; Hopke et al. (1995), Crawford et al. (2007)) was used (see Fig. 6(b) and 6(a)). They show that low total aerosol number concentration N_{tot} occurred mainly under marine influenced airmasses from west and north. High N_{tot} occurred mainly under airmasses from southwest, south and east of Mt. Brocken, these source regions were classified as polluted continental European background (Asmi et al., 2011).

7.2. Droplet Activation Regime

Reutter et al. (2009) suggests three distinctly different regimes of cloud condensation nucleus (CCN) activation and droplet formation depending on the ratio between updraft velocity w [m/s] and aerosol number concentration N_{tot} [cm^{-3}] at the cloud base. For $w/N_{tot} \gtrsim 10^{-3}\ \mathrm{m\,s^{-1}\,cm^{-3}}$ the droplet activation is aerosol-limited and the number of cloud droplets is directly proportional to N_{tot} and independent of w. For $w/N_{tot} \lesssim 10^{-4}\ \mathrm{m\,s^{-1}\,cm^{-3}}$ the updraft velocity is limiting the droplet activation and $N_{d,tot}$ is directly proportional to w and independent of N_{tot}. For the transition regime, $10^{-4}\ \mathrm{m\,s^{-1}\,cm^{-3}} \lesssim w/N_{tot} \lesssim 10^{-3}\ \mathrm{m\,s^{-1}\,cm^{-3}}$, $N_{d,tot}$ is non-linear proportional to both w and N_{tot}.
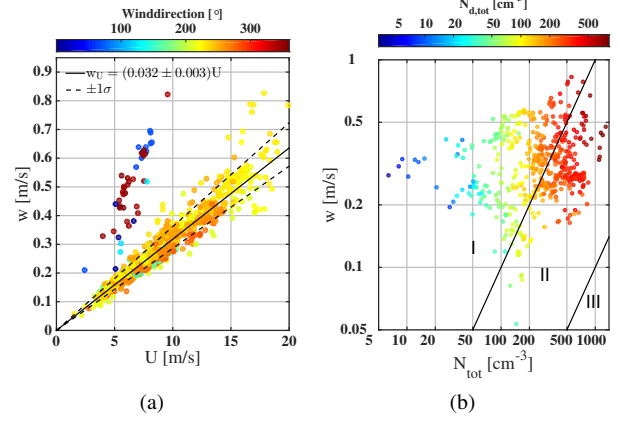

(a)　　　　　　　　　(b)

Fig. 8. (a) Relation between horizontal wind speed U [m/s], measured at top of Mt. Brocken, and estimated updraft velocity w [m/s], at cloud base. Color indicates winddirection. (b) Relation between estimated updraft velocity at cloud base w [m/s] and N_{tot} [cm^{-3}] with cloud droplet number $N_{d,tot}$ [cm^{-3}] as color code. The black lines mark the approximate boarders between the three droplet activation regimes according to Reutter et al. (2009) into (I) aerosol-limited regime ($w/N_{tot} \gtrsim 10^{-3}\ \mathrm{m\,s^{-1}\,cm^{-3}}$), (II) transitional regime ($10^{-4}\ \mathrm{m\,s^{-1}\,cm^{-3}} \lesssim w/N_{tot} \lesssim 10^{-3}\ \mathrm{m\,s^{-1}\,cm^{-3}}$), and (III) updraft-limited regime ($w/N_{tot} \lesssim 10^{-4}\ \mathrm{m\,s^{-1}\,cm^{-3}}$).

In order to estimate the updraft velocity at the cloud base the same approach as in (Hoyle et al., 2015) is used here. The inclination angle of the slope towards Mt. Brocken summit is up to 20° (see Fig. 1(c)), and even though there are surrounding sub-peaks, they are supposed not to influence the wind field at Mt. Brocken (Acker et al., 1998). The updraft velocity at cloud base (w_U) is estimated using horizontal wind speed at Mt. Brocken summit (U) and the inclination angle of the hill slope (α) at cloud base:

$$w_U = \tan(\alpha)U \qquad (5)$$

with the assumption that the flow lines for the updraft strictly follow the terrain with neither convergence nor divergence. The inclination angle of the flow lines at the cloud base (α) was calculated by matching CBH and wind direction with topographical data. The estimated w_U shows that, for a given vertical wind speed U higher updrafts are reached for cases with northerly winds (between 342° to 128°, see Fig. 8(a)). Those could be due to a steeper slope towards the north, but could also be artifacts caused by the location of the Celiometer relative to Mt. Brocken summit. The ratio between w and U is almost constant for wind direction between 145° to 287°, probably due to little variation in inclination angle α. Thus, the average relation $w = 0.032 \cdot U$ (see Fig. 8(a)) is used from here on to estimate the updraft velocity w for wind direction between 145° and 287°. With both approximate updraft velocity w and total

number concentration N_{tot} the droplet activation can be characterized (see Fig. 8(b)).

In this dataset droplet activation is most likely characterized by the aerosol limited or transitional regime.Therefore as non-linear approach a power-law dependence for the prediction of total cloud droplet number concentration ($N_{\text{d,tot}}$) is used. A multiple linear regression model was run performing iteratively reweighted least squares multivariate regression. The variables included are: total number concentration N_{tot}, horizontal wind speed measured at Mt. Brocken U [m/s], and the number-to-volume concentration ratio $R(\text{D}_c)$ in order to express the shape of the aerosol number size distribution. The estimated relation for the whole dataset is giving by

$$N_{\text{d,tot}}^{model} = 0.27 \, N_{\text{tot}}^{0.97} \, w^{0.37} \, R_{0.1 \, \mu m}^{-0.17}. \tag{6}$$

The comparison between measured and predicted cloud droplet number gives a correlation coefficient of R^2=0.89. The standard deviation of the difference between parameterized and measured $N_{\text{d,tot}}$ was 32 %, with a maximum standard deviation of 54 %. Even though no information about chemical composition of the particles is used in the model, the error in prediction of cloud droplet number is low.

The obtained relation shows that the droplet number concentration is most sensitive to the variation in total number concentration (Fig. 9(a)). When the total number concentration in the model is varied, but average w or $R_{0.1 \, \mu m}$ are used respectively, the predicted cloud droplet number is still reasonable (green and red dots, respectively, in Fig. 9(a)). When the variability of N_{tot} is neglected, the predicted cloud droplet number differs strongly from the measured $N_{\text{d,tot}}$.

For a constant wind speed U and shape of the aerosol size distribution (R), the resulting model would indicate that a doubling of the total number concentration of aerosol particles would almost lead to a doubling of cloud droplet number (1.95 ± 0.01) which is higher than the values suggested by Feingold et al. (2001) of 1.3 to 1.7 using linear regression of numerical model output.

The relation between cloud droplet number and total aerosol is presumably positive and almost linear up to a certain total aerosol level, depending on cloud dynamics and the size and composition of the aerosol (Modini et al., 2015). Some previous results have shown a 'roll-off' of activated cloud droplet number at different total aerosol concentrations, where an increase in N_{tot} does not lead to a proportional increase in $N_{d,tot}$ ((Leaitch et al., 1992; Glantz and Noone, 2000; Bower et al., 2000)). Other studies have not observed a 'roll-off' (Hegg et al., 2012). The power-law form used here (see eq. 6) suggests a 'roll-off' if the exponent of N_{tot} is smaller than one.

When the droplet activation regime (w/N_{tot}) is examined (see Fig. 9(b)), the observed 'roll-off' could be explained by a stronger dependence on the updraft velocity. In the updraft-limited regime, $N_{d,tot}$ is linear dependent on w and weak dependent on N_{tot}, resulting in low maximum supersaturation S_{max} (Reutter et al., 2009). When the aerosol concentration is
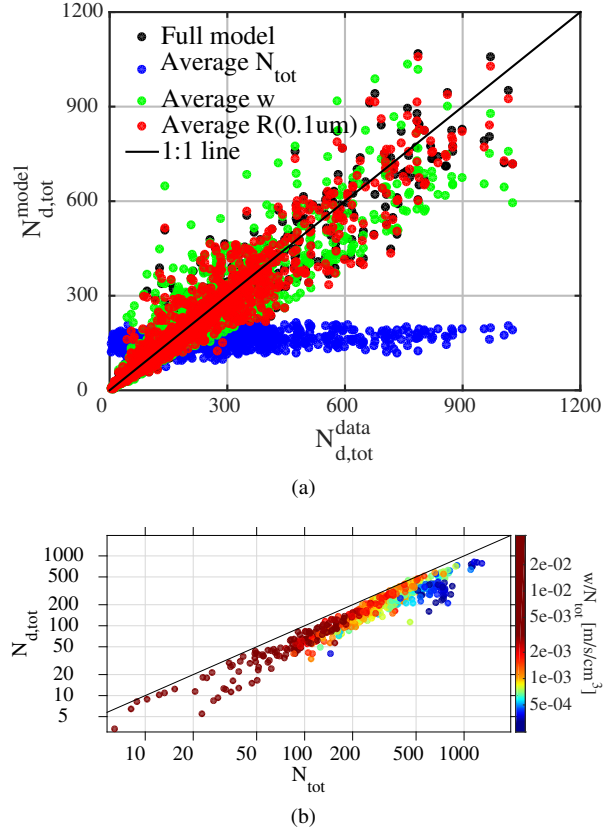

(a)

(b)

Fig. 9. (a) Sensitivity of modeled droplet number concentration $N_{\text{d,tot}}^{model}$ when excluding the variation in aerosol properties (N_{tot}, U and $R_{0.1 \, \mu m}$) and horizontal wind speed w measured at Mt. Brocken summit and using average instead. (b) Total number of cloud droplets $N_{\text{d,tot}}$ as function of total number number of particles N_{tot} with w/N_{tot}-ratio indicating cloud droplet activation regime according to Reutter et al. (2009) as color code.

high enough, the aerosol particles compete for water vapor to the benefit of the more CCN active larger aerosols (water vapor depletion, Ghan et al. (1997)). This would lead to larger D_{50} (Reutter et al., 2009) and the observed 'roll-off'.

This hypothesis was tested by dividing the data into three overlapping w/N_{tot}-intervals. The relation $N_{\text{d,tot}} \sim N_{\text{tot}}^{C_N} \, w^{C_w} \, R_{0.1 \, \mu m}^{C_R}$ was estimated for each interval performing iteratively reweighted least squares multivariate regression. The relative sensitivity of $N_{\text{d,tot}}$ against w, N_{tot} and $R_{0.1 \, \mu m}$ can be derived from the above relation to $\partial N_{\text{d,tot}}/\partial w = C_w$, $\partial N_{\text{d,tot}}/\partial N_{\text{tot}} = C_N$, and $\partial N_{\text{d,tot}}/\partial R_{0.1 \, \mu m} = C_R$ respectively. Thus, for increasing w/N_{tot}-ratio the relative sensitivity of $N_{\text{d,tot}}$ against w and $R_{0.1 \, \mu m}$ decreases while the relative sensitivity of $N_{\text{d,tot}}$ against N_{tot} increases (see Fig. 10(a) and Table 4).

The 'roll-off'-onset shifts towards higher N_{tot} when going towards the aerosol limited regime (for increasing w/N_{tot}-ratio), which supports the idea of w/N_{tot}-ratio dependent 'roll-

off' at different total aerosol level (see Fig. 10(b)). For the same N_{tot}, higher updraft velocities w and higher maximum supersaturation S_{max} would be expected in the aerosol limited regime compared to the transitional regime. Thus for for increasing w/N_{tot}-ratio (going from the transitional to the aerosol limited regime), water vapor depletion would occur at higher total aerosol concentrations N_{tot}, which could explain the difference in N_{tot}-onset of the 'roll-off'.

In order to investigate the importance of updraft velocity in each w/N_{tot}-interval, N_{tot} only or both N_{tot} and w were included in the model. In the w/N_{tot}-interval between $1 \cdot 10^{-3}$ and $5 \cdot 10^{-2}$ (II) including w does not improve the fit in terms of R^2 (see Table 5). In interval I the droplet activation is less dependent on updraft velocity compared to the transitional regime (II). An explanation could be, that in the aerosol limited regime the updraft velocity creates sufficiently high maximum supersaturation S_{max} to activate a major fraction of the total aerosol into cloud droplets.

8. Conclusion

Long-time cloud investigations have been performed at Mt. Brocken (51.80° N, 10.62° E, 1142 m a.s.l.) in the Harz region of central Germany between June and October 2010. Different types of orographic influenced clouds have been studied.

In order to asses the suggested cloud droplet regimes by Reutter et al. (2009), updraft velocity has been determined according to Hoyle et al. (2015). Cloud droplet formation was observed mainly in the aerosol limited and transitional-regime.

The relation between cloud droplet number concentration $N_{d,tot}$ and total number concentration N_{tot}, updraft velocity w_{pred}, and size distribution shape $R_{0.1\ \mu m}$ has been determined for three overlapping w/N_{tot}-intervals.

As expected in this regimes, the cloud droplet number shows an almost linear increase with increasing total aerosol number.

For increasing w/N_{tot}-ratio (from the transitional regime towards aerosol limited regime) the relative sensitivity of $N_{d,tot}$ against w and $R_{0.1\ \mu m}$ decreases, while the relative sensitivity of $N_{d,tot}$ against N_{tot} increases. This is in accordance with (Reutter et al., 2009).

For the same N_{tot}, higher updraft velocities w and higher maximum supersaturation S_{max} would be expected in the aerosol limited regime compared to the transitional regime. In the aerosol limited regime including w in the model ($N_{d,tot} \sim N_{tot}^{C_N} w^{C_w}$) does not improve the fit in terms of R^2. Thus the maximum supersaturation S_{max} seems to be sufficiently high to activate a major fraction of the total aerosol into cloud droplets.

Some previous measurements of the relation between cloud droplet number and total aerosol number show a 'roll-off', where an increase in N_{tot} does not lead to a proportional increase in $N_{d,tot}$, at different total aerosol levels (Leaitch et al., 1992; Glantz and Noone, 2000; Bower et al., 2000) or not at all (Hegg et al., 2012). The relation between cloud droplet number
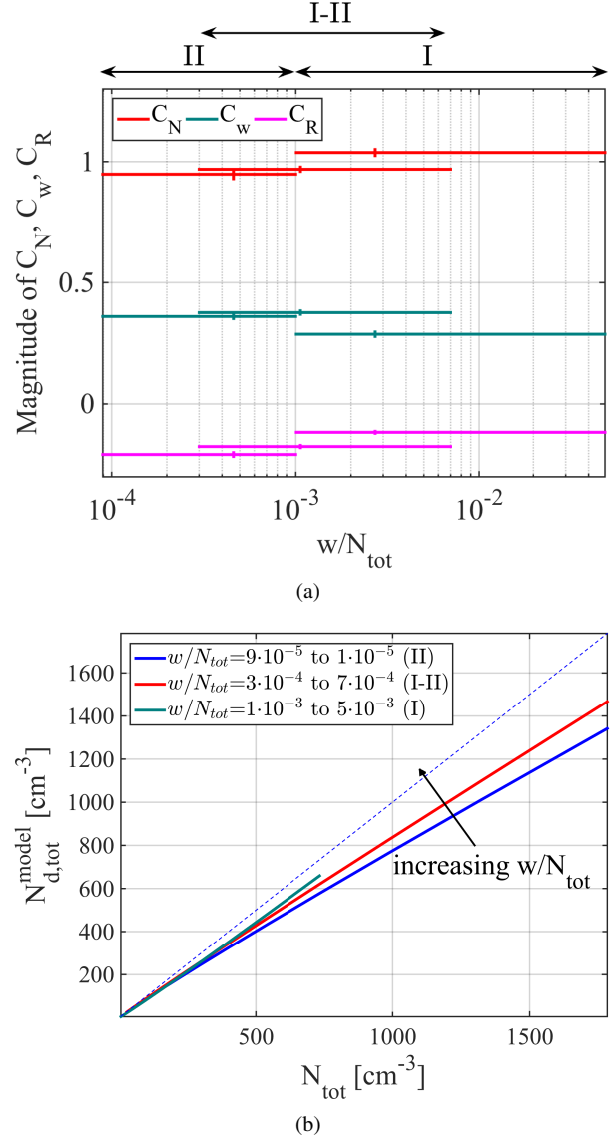
(a)

(b)

Fig. 10. (a) w/N_{tot}-ratio dependency of the coefficients of each parameter used in the modeled droplet number concentration $N_{d,tot}^{model}$. (b) Total number of cloud droplets $N_{d,tot}$ as function of total number number of particles N_{tot} for different w/N_{tot}-intervals using a constant $R_{0.1\ \mu m} = 300\ \mu m\ -3$.

and total aerosol depends on cloud dynamics and the size and composition of the aerosol (Modini et al., 2015).

The onset of 'roll-off' shifted towards higher total number concentration for increasing w/N_{tot}-ratio.

An explanation could be higher updraft velocities w and higher maximum supersaturation S_{max} in the aerosol limited regime compared to the transitional regime (for the same N_{tot}). Thus for for increasing w/N_{tot}-ratio (going from the transitional to the aerosol limited regime), water vapor depletion would occur at higher total aerosol concentrations N_{tot}, which could explain the difference in N_{tot}-onset of the 'roll-off'.

[h]

Table 4. Exponents of the relation $N_{\mathrm{d,tot}} \sim N_{\mathrm{tot}}^{C_N}\, w^{C_w}\, R_{0.1\ \mu\mathrm{m}}^{C_R}$ estimated for each w/N_{tot}-interval using a multiple linear regression model. Averages of D_{50}, LWC and $R_{0.1\ \mu\mathrm{m}}$ for N_{tot} between 64 cm^{-3} and 561 cm^{-3}. I, I-II, and II according to Figure 10(a).

	w/N_{tot}-interval	C_N	C_w	C_R	R^2	D_{50} [μm]	LWC [$\frac{\mathrm{g}}{\mathrm{cm^3}}$]	$R_{0.1\ \mu\mathrm{m}}$ [m^{-3}]
II	$[9{\cdot}10^{-5}$ to $1{\cdot}10^{-3}]$	0.95	0.36	-0.21	0.85	0.158	0.234	143
I-II	$[3{\cdot}10^{-4}$ to $7{\cdot}10^{-3}]$	0.97	0.38	-0.18	0.93	0.144	0.287	153
I	$[1{\cdot}10^{-3}$ to $5{\cdot}10^{-2}]$	1.04	0.29	-0.12	0.95	0.134	0.325	169

[h]

Table 5. Exponents of the relation $N_{\mathrm{d,tot}} \sim N_{\mathrm{tot}}^{C1_N}$ and $N_{\mathrm{d,tot}} \sim N_{\mathrm{tot}}^{C2_N}\, U^{C2_w}$ estimated for each interval using a multiple linear regression model. I, I-II, and II according to Figure 10(a), n is the number of data points in the interval.

	n	w/N_{tot}-interval	$C1_N$	R^2	$C2_N$	$C2_w$	R^2
II	663	$[9{\cdot}10^{-5}$ to $1{\cdot}10^{-3}]$	1.07	0.79	0.93	0.36	0.84
I-II	987	$[3{\cdot}10^{-4}$ to $7{\cdot}10^{-3}]$	1.01	0.91	0.99	0.31	0.93
I	513	$[1{\cdot}10^{-3}$ to $5{\cdot}10^{-2}]$	1.09	0.95	1.05	0.22	0.95

Thus, when predicting cloud droplet number and size and the change in radiative properties of clouds induced by a change in total aerosol concentration it is important to know the regime of droplet activation. Care has to be taken when using cloud parameterizations for other regimes than the one they have been determined in.

References

H. Abdul-Razzak, S. J. Ghan, and C. Rivera-Carpio. A parameterization of aerosol activation 1. Single aerosol type. *JGR*, 103:6123–6132, 1998.

K. Acker, D. Möller, W. Wieprecht, and St Nauman. Mt. brocken, a site for a cloud chemistry measurement programme in central europe. *Water, Air, and Soil Pollution*, 85(4):1979–1984, 1995.

K. Acker, D. Möller, W. Wieprecht, D. Kalaß, and R. Auel. Investigations of ground-based clouds at the mt. brocken. *Fresenius' Journal of Analytical Chemistry*, 361(1):59–64, 1998.

K. Acker, D. Möller, W. Wieprecht, R. Auel, D. Kalaß, and W. Tscherwenka. Nitrous and nitric acid measurements inside and outside of clouds at mt. brocken. *Water, Air, and Soil Pollution*, 130(1-4):331–336, 2001.

K. Acker, S. Mertes, D. Möller, W. Wieprecht, and R. Auel. Case study of cloud physical and chemical processes in low clouds at mt. brocken. *Atmospheric Research*, 64(14):41 – 51, 2002. ISSN 0169-8095. 2nd International Conference on Fog and Fog Collection.

G. Adrian and F. Fiedler. Simulation of unstationary wind and temperature fields over complex terrain and comparison with observations. *Beitr. Phys. Atmosph.*, 64:27–48, 1991.

B. A. Albrecht. Aerosols, cloud microphysics, and fractional cloudiness. *Science*, 245(4923):1227–1230, 1989.

A. Asmi, A. Wiedensohler, P. Laj, A.-M. Fjaeraa, K. Sellegri, W. Birmili, E. Weingartner, U. Baltensperger, V. Zdimal, N. Zikova, J.-P. Putaud, A. Marinoni, P. Tunved, H.-C. Hansson, M. Fiebig, N. Kivekäs, H. Lihavainen, E. Asmi, V. Ulevicius, P. P. Aalto, E. Swietlicki, A. Kristensson, N. Mihalopoulos, N. Kalivitis, I. Kalapov, G. Kiss, G. de Leeuw, B. Henzing, R. M. Harrison, D. Beddows, C. O'Dowd, S. G. Jennings, H. Flentje, K. Weinhold, F. Meinhardt, L. Ries, and M. Kulmala. Number size distributions and seasonality of submicron particles in europe 20082009. *Atmospheric Chemistry and Physics*, 11(11):5505–5538, 2011.

M. I. A. Berghof, G. P. Frank, S. Sjogren, and B. G. Martinsson. Inversion of droplet aerosol analyzer data for long-term aerosol-cloud interaction measurements. *Atmospheric Measurement Techniques*, 7 (4):877–886, 2014.

F. Beyrich, K. Acker, A. Kalaß, O. Klemm, D. Möller, E. Schaller, J. Werhahn, and U. Weisensee. Boundary layer structure and photochemical pollution in the Harz Mountains - An observational study. *Atmospheric Environment*, 30(8):1271 – 1281, 1996. ISSN 1352-2310.

O. Boucher, H. Le Treut, and M. B. Baker. Precipitation and radiation modeling in a general circulation model: Introduction of cloud microphysical processes. *Journal of Geophysical Research: Atmospheres (1984–2012)*, 100(D8):16395–16414, 1995.

K. N. Bower, T. W. Choularton, M. W. Gallagher, K. M. Beswick, M. J. Flynn, A. G. Allen, B. M. Davison, J. D. James, L. Robertson, R. M. Harrison, C. N. Hewitt, J. N. Cape, G. G. McFadyen, C. Milford, M. A Sutton, B. G. Martinsson, G. Frank, E. Swietlicki, J. Zhou, O. H. Berg, B. Mentes, G. Papaspiropoulos, H.-C. Hansson, C. Leck, M. Kulmala, P. Aalto, M. Vkev, A. Berner, M. Bizjak, S. Fuzzi, P. Laj, M.-C. Facchini, G. Orsi, L. Ricci, M. Nielsen, B. J. Allan, H. Coe, G. McFiggans, J. M. C. Plane, J. L. Collett, K. F. Moore, and D. E. Sherman. Ace-2 hillcloud. an overview of the ace-2 ground-based cloud experiment. *Tellus B*, 52(2):750–778, 2000. ISSN 1600-0889.

S.-I. Cederfelt, B.G. Martinsson, B. Svenningsson, A. Wiedensohler, G. Frank, H.-C. Hansson, E. Swietlicki, M. Wendish, K. M. Beswick, K. N. Bower, M. W. Gallagher, S. Pahl, R. Maser, and D. Schell. Field validation of the droplet aerosol analyser. *Atmospheric Environment*, 31(16):2657 – 2670, 1997. ISSN 1352-2310. The Great Dun Fell Cloud Experiment 1993, Eurotrac sub-project Ground-based Cloud Experiment (GCE).

J. Crawford, S. Chambers, D. D. Cohen, L. Dyer, T. Wang, and W. Zahorowski. Receptor modelling using positive matrix factorisation, back trajectories and radon-222. *Atmospheric Environment*, 41(32): 6823 – 6837, 2007. ISSN 1352-2310.

R. R. Draxler and G. D. Rolph. Hysplit (hybrid single-particle lagrangian integrated trajectory) model access via noaa arl ready web-

12

site (http://ready.arl.noaa.gov/hysplit.php). NOAA Air Resources Laboratory, Silver Spring, MD, 2013.

U. Dusek, G. P. Frank, L. Hildebrandt, J. Curtius, J. Schneider, S. Walter, D. Chand, F. Drewnick, S. Hings, D. Jung, S. Borrmann, and M. O. Andreae. Size matters more than chemistry for cloud-nucleating ability of aerosol particles. *Science*, 312(5778):1375–1378, 2006.

G. Feingold, L. A. Remer, J. Ramaprasad, and Y. J. Kaufman. Analysis of smoke impact on clouds in brazilian biomass burning regions: An extension of twomey's approach. *Journal of Geophysical Research: Atmospheres*, 106(D19):22907–22922, 2001. ISSN 2156-2202.

G. P. Frank, S.-I. Cederfelt, and B. G. Martinsson. Characterisation of a unipolar charger for droplet aerosols of 0.1-20 μm in diameter. *Journal of Aerosol Science*, 35(1):117 – 134, 2004.

G. P. Frank, M. I. A. Berghof, S. Sjogren, and B. G. Martinsson. A droplet aerosol analyser (daa) for longterm aerosol-cloud microphysics measurements. In preparation., 2015.

S. J. Ghan, L. R. Leung, R. C. Easter, and H. Abdul-Razzak. Prediction of cloud droplet number in a general circulation model. *Journal of Geophysical Research: Atmospheres*, 102(D18):21777–21794, 1997. ISSN 2156-2202.

P. Glantz and K. J. Noone. A physically-based algorithm for estimating the relationship between aerosol mass and cloud droplet number. *Tellus B*, 52(5):1216–1231, 2000.

S. G. Gopalakrishnan, S. Baidya Roy, and R. Avissar. An evaluation of the scale at which topographical features affect the convective boundary layer using large eddy simulations. *Journal of Atmospheric Sciences*, 57:334–351, January 2000.

D. A. Hegg, D. S. Covert, H. H. Jonsson, and R. K. Woods. A simple relationship between cloud drop number concentration and precursor aerosol concentration for the regions of earth's large marine stratocumulus decks. *Atmospheric Chemistry and Physics*, 12(3):1229–1238, 2012.

S. Henning, E. Weingartner, S. Schmidt, M. Wendisch, H. W. Gäggeler, and U. Baltensperger. Size-dependent aerosol activation at the high-alpine site jungfraujoch (3580 m asl). *Tellus B*, 54(1):82–95, 2002.

P. K. Hopke, L. A. Barrie, S.-M. Li, M.-D. Cheng, C. Li, and Y. Xie. Possible sources and preferred pathways for biogenic and non-sea-salt sulfur for the high arctic. *Journal of Geophysical Research: Atmospheres*, 100(D8):16595–16603, 1995. ISSN 2156-2202.

C. R. Hoyle, C. S. Webster, H. E. Rieder, E. Hammer, M. Gysel, N. Bukowiecki, E. Weingartner, M. Steinbacher, and U. Baltensperger. Chemical and physical influences on aerosol activation in liquid clouds: an empirical study based on observations from the jungfraujoch, switzerland. *Atmospheric Chemistry and Physics Discussions*, 15(11):15469–15510, 2015.

Y. X. Hu and K. Stamnes. An accurate parameterization of the radiative properties of water clouds suitable for use in climate models. *Journal of climate*, 6(4):728–742, 1993.

Z. Jurányi, M. Gysel, E. Weingartner, P. F. DeCarlo, L. Kammermann, and U. Baltensperger. Measured and modelled cloud condensation nuclei number concentration at the high alpine site jungfraujoch. *Atmos. Chem. Phys*, 10(16):7891–7906, 2010.

N. Kivekäs, V.-M. Kerminen, T. Anttila, H. Korhonen, H. Lihavainen, M. Komppula, and M. Kulmala. Parameterization of cloud droplet activation using a simplified treatment of the aerosol number size distribution. *Journal of Geophysical Research: Atmospheres*, 113(D15): 2008. ISSN 2156-2202. D15207.

H. Köhler. The nucleus and the growth of hygroscopic ddroplet. *Transaction of the Faraday Society*, 32:1152–1161, 1936.

P. Kumar, I. N. Sokolik, and A. Nenes. Parameterization of cloud droplet formation for global and regional models: including adsorption activation from insoluble ccn. *Atmospheric Chemistry and Physics*, 9(7):2517–2532, 2009.

P. A. Lawless. Particle charging bounds, symmetry rrelation, and an analytic charging rate model for the continuum regime. *Lournal of Aerosol Science*, 27:191–215, 1996.

W. R. Leaitch, G. A. Isaac, J. W. Strapp, C. M. Banic, and H. A. Wiebe. The relationship between cloud droplet number concentrations and anthropogenic pollution: Observations and climatic implications. *Journal of Geophysical Research: Atmospheres*, 97(D2): 2463–2474, 1992. ISSN 2156-2202.

M.-L. Lu, W. C. Conant, H. H. Jonsson, V. Varutbangkul, R. C. Flagan, and J. H. Seinfeld. The marine stratus/stratocumulus experiment (mase): Aerosol-cloud relationships in marine stratocumulus. *Journal of Geophysical Research: Atmospheres (1984–2012)*, 112(D10), 2007.

G. M. Martin, D. W. Johnson, and A. Spice. The measurement and parameterization of effective radius of droplets in warm stratocumulus clouds. *Journal of Atmospheric Sciences*, 51:1823–1842, July 1994.

G. M. McFarquhar and A. J. Heymsfield. Parameterizations of indoex microphysical measurements and calculations of cloud susceptibility: Applications for climate studies. *Journal of Geophysical Research: Atmospheres (1984–2012)*, 106(D22):28675–28698, 2001.

R. L. Modini, A. A. Frossard, L. Ahlm, L. M. Russell, C. E. Corrigan, G. C. Roberts, L. N. Hawkins, J. C. Schroder, A. K. Bertram, R. Zhao, A. K. Y. Lee, J. P. D. Abbatt, J. Lin, A. Nenes, Z. Wang, A. Wonaschütz, A. Sorooshian, K. J. Noone, H. Jonsson, J. H. Seinfeld, D. Toom-Sauntry, A. M. Macdonald, and W. R. Leaitch. Primary marine aerosol-cloud interactions off the coast of california. *Journal of Geophysical Research: Atmospheres*, 120(9):4282–4303, 2015. ISSN 2169-8996. 2014JD022963.

R. J. Moffat. Describing the uncertainties in experimental results. *Experimental Thermal and Fluid Science*, 1(1):3 – 17, 1988. ISSN 0894-1777.

D. Möller, K. Acker, and W. Wieprecht. Cloud chemistry at mt. brocken/harz. In *Proc. 6th Europ. Symp. Physico-Chemical Behavior of Air Pollutants, Rep. EUR*, volume 15609, pages 968–974, 1994.

D. Möller, K. Acker, and W. Wieprecht. A relationship between liquid water content and chemical composition in clouds. *Atmospheric Research*, 41(34):321 – 335, 1996. ISSN 0169-8095. Cloud-Aerosol Interactions.

A. Nenes and J. H. Seinfeld. Parameterization of cloud droplet formation in global climate models. *Journal of Geophysical Research: Atmospheres (1984–2012)*, 108(D14), 2003.

C. D. O'Dowd, J. A. Lowe, M. H. Smith, and A. D. Kaye. The relative importance of non-sea-salt sulphate and sea-salt aerosol to the marine cloud condensation nuclei population: An improved multicomponent aerosol-cloud droplet parametrization. *Quarterly Journal of the Royal Meteorological Society*, 125(556):1295–1313, 1999.

M. D. Petters and S. M. Kreidenweis. A single parameter representation of hygroscopic growth and cloud condensation nucleus activity. *Atmospheric Chemistry and Physics*, 7(8):1961–1971, 2007.

K. Plessow, K. Acker, H. Heinrichs, and D. Möller. Time study of trace elements and major ions during two cloud events at the mt. brocken. *Atmospheric Environment*, 35(2):367–378, 2001.

P. Reutter, H. Su, J. Trentmann, M. Simmel, D. Rose, S. S. Gunthe, H. Wernli, M. O. Andreae, and U. Pöschl. Aerosol- and updraft-limited regimes of cloud droplet formation: influence of particle number, size and hygroscopicity on the activation of cloud condensation nuclei (ccn). *Atmospheric Chemistry and Physics*, 9(18):7067–7080, 2009.

D. Rosenfeld, S. Sherwood, R. Wood, and L. Donner. Climate effects of aerosol-cloud interactions. *Science*, 343(6169):379–380, 2014.

S. Sjogren, G. P. Frank, M. I. A. Berghof, and B. G. Martinsson. Continuous stand-alone controllable aerosol/cloud droplet dryer for atmospheric sampling. *Atmospheric Measurement Techniques*, 6(2): 349–357, 2013.

H. Tammet. Reduction of air ion mobility to standard conditions. *Journal of Geophysical Research: Atmospheres*, 103(D12):13933–13937, 1998. ISSN 2156-2202.

C. H. Twohy, J. R. Anderson, and P. A. Crozier. Nitrogenated organic aerosols as cloud condensation nuclei. *Geophysical Research Letters*, 32(19):n/a–n/a, 2005. ISSN 1944-8007. L19805.

S. Twomey. Pollution and the planetary albedo. *Atmospheric Environment (1967)*, 8(12):1251 – 1256, 1974.

S. Twomey. The influence of pollution on the shortwave albedo of clouds. *Journal of Atmospheric Sciences*, 34:1149–1154, July 1977.

Vaisala. *Ceilometer CT25 User's Guide*. Vaisala, Helsinki, Finland, 1999. version CT25K-U059en-2.1.